

UNCLASSIFIED

---

---

AD 259 233

*Reproduced  
by the*

ARMED SERVICES TECHNICAL INFORMATION AGENCY  
ARLINGTON HALL STATION  
ARLINGTON 12, VIRGINIA



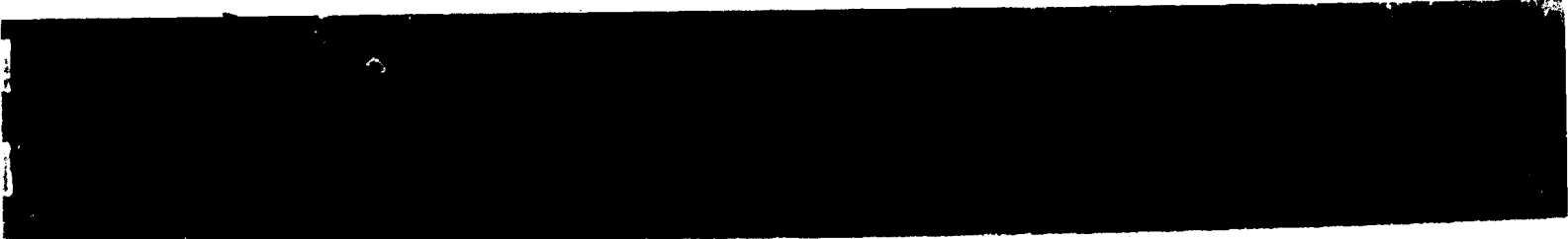
---

---

UNCLASSIFIED

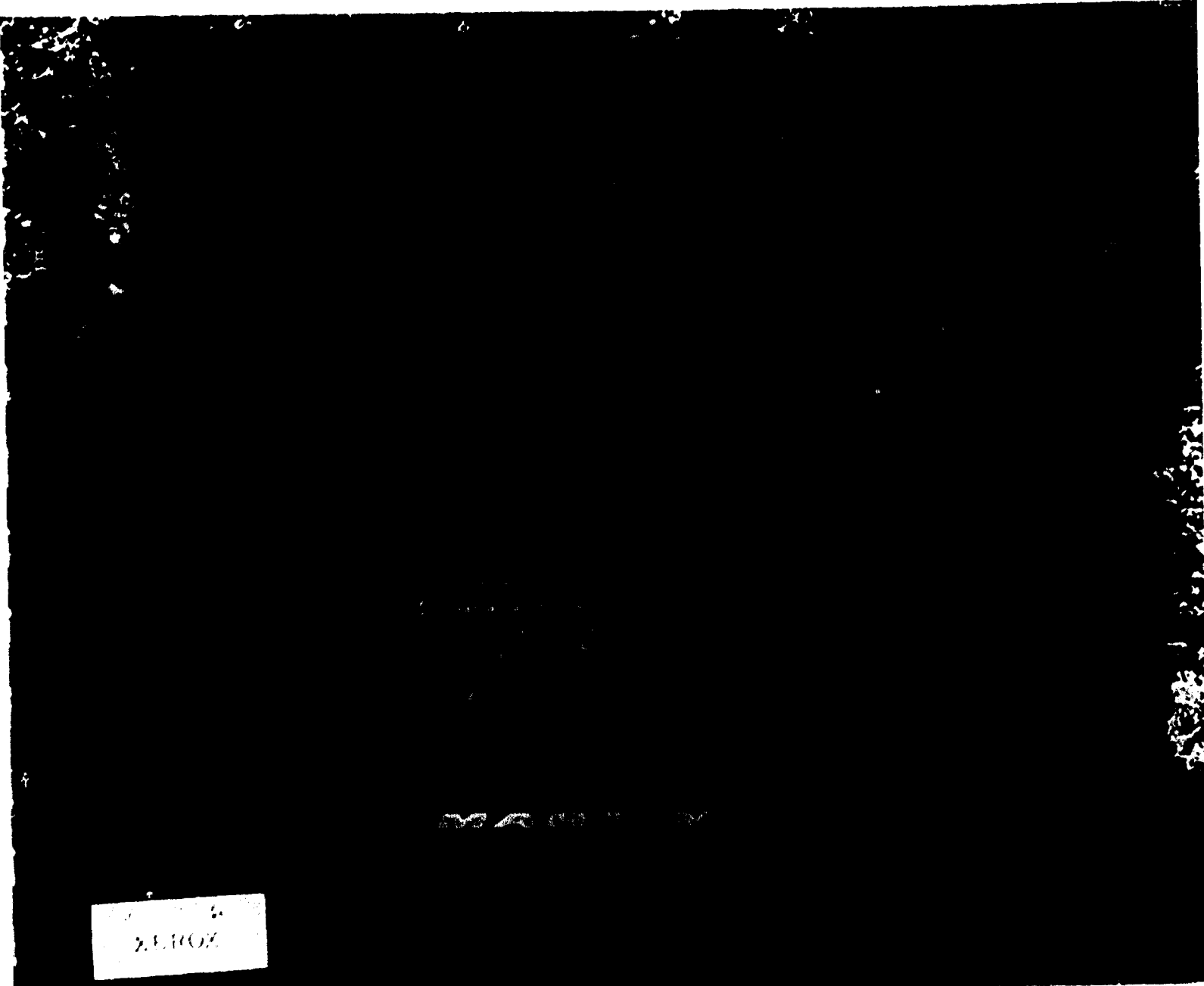
Best Available Copy

NOTICE: When government or other drawings, specifications or other data are used for any purpose other than in connection with a definitely related government procurement operation, the U. S. Government thereby incurs no responsibility, nor any obligation whatsoever; and the fact that the Government may have formulated, furnished, or in any way supplied the said drawings, specifications, or other data is not to be regarded by implication or otherwise as in any manner licensing the holder or any other person or corporation, or conveying any rights or permission to manufacture, use or sell any patented invention that may in any way be related thereto.



259233

PRELIMINARY DESIGN FOR  
SATELLITE GUIDANCE SUBSYSTEM



XEROX

**Best  
Available  
Copy**

**DYNAMIC ANALYSIS**  
**and**  
**PRELIMINARY DESIGN FOR**  
**SATELLITE GUIDANCE SUBSYSTEM**

**JUNE 1961**

**ER 11647**

Contract AF 33(616)-6040  
Supplemental Agreement 4(61-425)  
Task No 50824  
Project No 1/630-5216

**MARTIN**

### FOREWORD

This final engineering report was prepared by The Martin Company (Baltimore) in fulfillment of Supplemental Agreement No. 4(61-425) to United States Air Force Contract No. AF33(616)-6040, Task No. 50824, which was administered by the Guidance Laboratory at the Wright Air Development Division.

### ABSTRACT

A self-contained guidance and control system for a hypothetical, unmanned one-year mission in space is presented. System operation is based on the use of altitude measurements to define the in-plane orbit parameters and preselected star occultation time measurements to define the orbit plane orientation parameters. Overall system operation is presented and system errors are evaluated, using an IBM 7090 computer program.

A detailed description of each of the subsystems is given and the reliability of these systems is predicted for the one-year mission, using component failure rate data. From this study, it is shown that the system could be instrumented using state-of-the-art hardware. Preliminary missions analysis indicates that the system would have considerable utility in manned satellite missions requiring exit from orbit and rendezvous with earth-based target points.

## CONTENTS

	Page
Foreword . . . . .	ii
Abstract . . . . .	iii
Symbols . . . . .	vii
Summary . . . . .	viii
I. Introduction . . . . .	1-1
II. System Requirements . . . . .	II-2
III. Recommended System . . . . .	III-1
A. Self-Contained Guidance and Control . . . . .	III-1
B. System Operation . . . . .	III-2
C. Development of a Computer Program . . . . .	III-15
D. Control Laws . . . . .	III-17
IV. Subsystem Description . . . . .	IV-1
A. Radar Altimeter . . . . .	IV-1
B. IR Horizon Sensor . . . . .	IV-33
C. Occultoscope Star Tracker . . . . .	IV-51
D. The Computer . . . . .	IV-65
E. Basic Electrical Power . . . . .	IV-83
F. Attitude Control System . . . . .	IV-95
V. Error Analysis . . . . .	V-1
A. Propagation of Launch Errors . . . . .	V-1
B. System Errors . . . . .	V-5
C. Compounded System Error Analysis . . . . .	V-9

CONTENTS (continued)

	Page
VI. Reliability Analysis . . . . .	VI-1
A. Radar . . . . .	VI-1
B. IR System . . . . .	VI-4
C. Occultoscope Star Tracker . . . . .	VI-7
D. Power System . . . . .	VI-9
E. Control Stabilization System . . . . .	VI-14
F. Computer . . . . .	VI-16
G. Predicted System Reliability . . . . .	VI-18
VII. Satellite Synchronization Study Development Plan . . . . .	VII-1
A. Radar Altimeter . . . . .	VII-1
B. Computer . . . . .	VII-2
C. IR Horizon Scanner . . . . .	VII-2
D. Electrical Power Supply . . . . .	VII-4
E. Attitude Control System . . . . .	VII-4
VIII. Mission Analysis . . . . .	VIII-1
IX. Conclusions and Recommendations . . . . .	IX-1
X. References . . . . .	X-1

## SYMBOLS

$P_T$	= Peak power transmitted, watts
$P_R$	= Peak power received, watts
R	= Radius of earth, meters
h	= Altitude of satellite, naut mi
$\tau$	= Duration (width) of transmitted pulse, sec
$f_r$	= Pulse repetition frequency, pps
d	= Duty cycle, ratio
NF (or $F_N$ )	= Noise figure
$G_0$	= Antenna gain over isotropic, db
B	= Receiver bandwidth, cps
$\lambda$	= Wave length, cm
$\delta$	= Propagation and degradation losses, db
$\frac{S}{N}$	= Signal-to-noise ratio
T	= Time constant, seconds
$\phi$	= Angle of incidence (from vertical), degree
$\sigma$	= Radar cross section, per unit area
$A_E$	= Effective area, meters

viii

## SUMMARY

The findings of this final Engineering Report may be summarized within the framework of three major areas of preliminary system design, which have been analyzed as follows:

### Feasibility

A self-contained guidance and control system (of the type considered in this report is feasible using hardware which is well within the state of the art of present hardware design. In considering the various subsystems which make up the guidance and control system, only a few of the components can presently be purchased as "on-the-shelf" items. However, it is apparent that equipment which cannot be purchased readily does not represent design problems requiring major advances in the present art of equipment design. The computer, for example (though nonexistent), is a derivative of a currently available computer and has already been partially designed.

### Performance

System accuracy, based largely on an IBM 7090 program, has been estimated. The mathematical model for this program has assumed a spherical nonrotating earth and a fixed error due to the fact that the occulting surface (earth plus the atmosphere) is not circular. In addition, this fixed error has ignored statistical fluctuations in the atmosphere at the time of measurement of occultation. This fixed error is believed to be a reasonable value however, and it is not felt that the overall system error would change appreciably by a more sophisticated approach to this problem.

In summary, it seems reasonable to conclude that the overall system accuracy would yield future predicted position accuracies of one nautical mile if the orbital elements are averaged over several orbit passes. Perturbations on the orbit, due to earth model uncertainties are not included in this estimate of system accuracy.

### Reliability

The overall system reliability has been found to be so low that a one-year mission (of the type considered throughout this report) is impractical. The principal problem arises from the fact that the attitude control system must be on continuously during an unmanned mission, hence, the attitude sensors and the thrust nozzles which torque the vehicle are continuously in operation. From the failure rate data that has been made available, these devices simply will not operate for one year in the system design considered here. Redundancy has been explored only briefly for two basic reasons:

- (1) It is felt that the mission used throughout the report to evaluate the system cannot be considered realistic; however, the system (in its present configuration) could be used on alternate manned missions with success. These alternate manned missions would result in greatly enhanced reliability, since most of the subsystems could be turned off until they are needed. For these manned missions, reliability (even for extended periods of operation in space) would not be a severe problem.
- (2) Simplicity in design has been adhered to wherever possible in the present system. It is felt that this approach is one way of achieving a reliable system design.

## I. INTRODUCTION

This document is the final report in a series of engineering studies conducted at The Martin Company under the provisions of Contract AF 33(616)-8040. In general, these engineering studies have been concerned with an evaluation of possible unmanned satellite guidance and control techniques.

Work previously completed under the contract has considered, in detail, the various alternatives in devising a guidance and control system for orbiting vehicles. This work has included the analysis of guidance and control laws based on all known techniques within the two broad categories of guidance and control systems, i.e., the system must either be self contained or it must include ground-based elements in the guidance and control loops. There are many obvious advantages to a completely self-contained guidance and control system for most satellite missions, and late in 1960 it was decided to pursue this course in developing the guidance and control concept.

In order to study a self-contained guidance and control system it was necessary to establish a mission for the orbiting vehicle and the associated subsystems. This hypothetical mission then establishes an accuracy and mission time basis for studying the system. The mission geometry selected is shown in Fig. 1-1. There are four orbit planes, each containing four satellites, with the orbit planes symmetrically located with respect to the earth. The proposed inclination of the orbit planes is 54.736 degrees, and the orbits are near circular at an altitude of approximately 5600 naut mi. This arrangement permits simultaneous viewing from the earth of at least three of the satellites at any given time. Such a system would have utility, for example, as a navigational aid, and for present purposes of study only, this has been assumed to be the mission for the system of orbiting vehicles. This mission requires relatively severe guidance and control system accuracies, and the mission time, here assumed to be one year, places a substantial emphasis on system reliability in a completely automatic system. This hypothetical mission should not be construed as the principal recommended usage for the system.

The self-contained guidance concept is formulated about two principle sensing devices:

- (1) Celestial sightings which are interpreted by the system as time measurements when certain preselected stars are occulted by the earth.
- (2) Conventional electromagnetic ranging techniques which are interpreted by the system as radial distance measurements at preselected points in time.

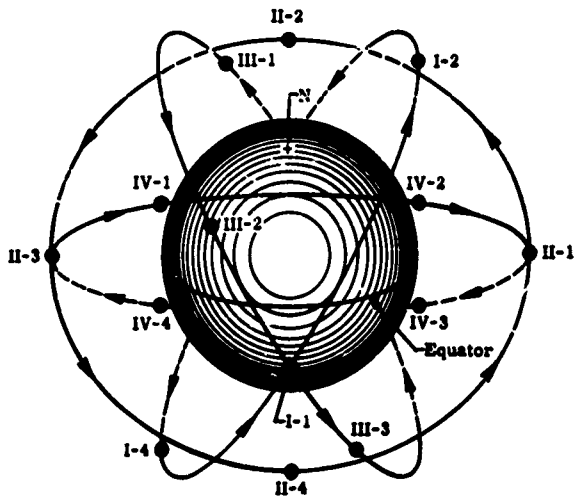
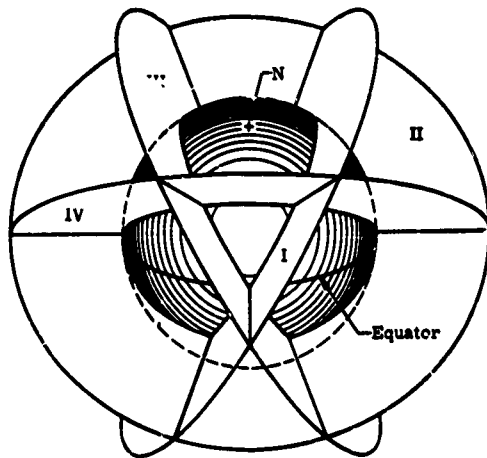


Fig. I-1. Three-Dimensional Orbit Pattern

A combination of the data from (1) and (2) above enables a direct solution for the trajectory of the vehicle in terms of the orbital elements. As used here, these elements include the period of the orbit, the eccentricity, the magnitude and orientation of the semimajor axis, the argument of perigee and the longitude of the ascending node. Once this information is available aboard the vehicle, comparisons can be made with preselected orbit parameters. The error signals which result from these comparisons are used to force the vehicle to fly a preselected course. Ideally the preselected course is a circular orbit in the pattern shown in Fig. I-1.

It should be noted that the assumed mission implies numerous problem areas which are not directly associated with the guidance and control problem. As an example, the data link between the orbiting vehicle and surface-based craft would be an important consideration in the design of an orbiting navigational aid system. Such problems are beyond the scope of this final engineering study, and emphasis has been placed solely on the guidance and control problem. In particular, it is desirable that the degree of hardware feasibility of the self-contained guidance and control system be established.



## II. SYSTEM REQUIREMENTS

The requirements for the total system are specified with reference to the hypothetical mission of one year duration in a circular orbit of approximately 5600-naut mi altitude. During this period, all subsystems aboard the vehicle must operate automatically for selected intervals of time from a programmed sequence of events.

In addition to those requirements noted in Table II-1, the general requirement exists for the system to operate in a space environment approximately 6000 naut mi above the earth for the one-year period of the mission. It is possible to speculate at great length on possible problems introduced by the phenomena of charged particle radiation in such an environment. However, in view of the relatively meager amount of information available, it would seem presumptuous to attempt to assess the long term effects of such radiation at this time.

**TABLE II-1**  
**System Requirements**

<u>Subsystem</u>	<u>Period of Operation</u>	<u>Performance Requirements</u>	<u>Comments</u>												
1. Radar altimeter	Intermittent operation for a small portion of each orbit period. Total operation time is approximately 200 hr.	Must measure altitude in the range of 5000 to 6500 naut mi. Accuracy requirements are $\pm 1.0$ mile	Accuracy expected to deteriorate with time. If accuracy is degraded as much as $\pm 2.0$ miles, then radar does not improve overall orbit prediction, based on occultation technique alone.												
2. IR system	Continuous operation for one year.	Must provide error signals for torquing vehicle to local vertical in pitch and roll. Accuracy requirement is $\pm 0.1^\circ$ . Variable field of view required in optical system.	Accuracy expected to deteriorate with time. Maximum error after one-year operation is to be no greater than $1.0^\circ$ .												
3. Computer	On continuously, but computing only a small fraction of the time.	Storage of preselected star positions; digital computation of orbital elements from altitude, occultation (time) inputs. Computation of vehicle attitude correcting maneuvers. Initiation of various on-off functions.	Some deterioration of accuracy with time expected. Not expected to cause total mission failure from standpoint of accuracy degradation.												
4. Power system	Continuous operation for one year but peak loading only when radar is on, i.e., a small fraction of each day.	<table border="0"> <tr> <td><u>Continuous</u></td> <td><u>Intermittent</u></td> </tr> <tr> <td>69 watts</td> <td>235 w/1.5 min</td> </tr> <tr> <td></td> <td>+ 95 w/2 min</td> </tr> <tr> <td></td> <td>+ 85 w/1.5 min</td> </tr> <tr> <td></td> <td>+ 65 w/0.5 min</td> </tr> <tr> <td></td> <td>+ 5 w/2.0 min</td> </tr> </table>	<u>Continuous</u>	<u>Intermittent</u>	69 watts	235 w/1.5 min		+ 95 w/2 min		+ 85 w/1.5 min		+ 65 w/0.5 min		+ 5 w/2.0 min	Nonoriented silicon solar cell system and radioisotope system considered. Solar cell system attractive from weight standpoint. Radioisotope system attractive from reliability standpoint.
<u>Continuous</u>	<u>Intermittent</u>														
69 watts	235 w/1.5 min														
	+ 95 w/2 min														
	+ 85 w/1.5 min														
	+ 65 w/0.5 min														
	+ 5 w/2.0 min														
5. Inertial reference-occultation measurement system	Continuous for one year period.	Automatic acquisition and tracking of preselected stars must be provided. Extreme precision required in occultation time measurement.	Servo performance expected to deteriorate with time but not considered a major problem except from reliability standpoint.												
6. Propulsion system															
a. Orbit injection	Entry into parking orbit and final orbit only.	$\Delta V$ requirements up to 1000 fps.	Engine is cast off after injection into the final orbit.												
b. Attitude control and stabilization	Limit cycle continuous	Maintain attitude control to $1/2\%$ .	Total of 12 low level thrust nozzles to provide attitude control and stabilization.												
c. Orbit keeping system	Operation only for a small fraction of each day.	Null position errors to within $1.0$ naut mi with respect to a programmed orbit.	Six engines and three rate gyros, not considered a reliability problem due to infrequent use.												

### III. RECOMMENDED SYSTEM

The recommended guidance and control system is based on the concept of using a combination of radial distance measurements and preselected star occultation times to define the elements of the orbit. These data are measured aboard the vehicle so that the system is completely self contained. The usual problems of a ground-based guidance concept are thus completely eliminated and it should be possible to reduce the costs and location problems of a ground-based tracking system. Some tracking from the earth will be required early in the period immediately following launch, but once in the final orbit no tracking is required by the airborne system for guidance and control purposes.

#### A. SELF-CONTAINED GUIDANCE AND CONTROL

In terms of hardware, the self-contained guidance and control system consists of the following:

##### 1. Sensors

###### a. Pulse radar altimeter

A pulse radar altimeter, for measuring the distance from the satellite to the surface of the earth. The radar is programmed to operate only over sea level water surfaces.

###### b. Tracking telescopes

A system of five tracking telescopes which provide a yaw error orientation signal and the times of occultation of certain preselected stars.

###### c. IR system

An IR (infrared) system of four separate detectors which tracks the local earth vertical and provides pitch and roll error signals used in the attitude control and stabilization system.

###### d. Rat. gyros

A system of three rate gyros, used in the orbit keeping system.

## 2. Support Instrumentation

The support instrumentation includes a general purpose digital computer, a basic electrical power system, an accurate time reference and programmer and servo systems associated with the propulsion system and star trackers.

## B. SYSTEM OPERATION

The star tracking system is aligned prior to launch so that the preselected celestial references will lay approximately within the field of view of the tracking telescopes at the termination of the boost period. The payload is nearly in a horizontal position relative to the earth at boost termination. Also, the guidance system accuracies are not expected to be so large that the tracking telescopes will not be able to acquire the preselected stars. The attitude reference system in the boost vehicle can be used as a source of information to update the tracking telescope platform, and if necessary, a search mode can be built into the tracking telescopes for initial acquisition of the preselected stars. Since the basic electrical power comes from a silicon solar cell system, the launch is timed so that the vehicle is in sunlight at the termination of upper stage boost.

### 1. Upper Stage Guidance Termination

Just prior to separation from the boost vehicle, the power system, the computer, the IR system and attitude control system in the payload vehicle are turned on (with attitude correction signals being generated but not used until separation occurs). At the same time, protective coverings over the IR system, the radar altimeter antenna, the star tracking system and the solar cell area of the power system are cast off. A timing signal in the boost vehicle then generates a "time-to-go" signal which is used in the payload vehicle to fire the main engine (which will place the vehicle in the parking orbit). Separation of the boost and payload vehicles is executed and the attitude control system error signals, which have not been used to this point in time, now begin to operate the thrust nozzles. This action will prevent loss of orientation which might occur as a result of the separation process. The IR system is fixed in the vehicle, as is the radar antenna, so that the pitch and roll error signals now command the attitude (pitch and roll) control system to erect the vehicle to the local vertical. The yaw error signals from the star trackers are used to maintain the boost guidance azimuth direction so that the vehicle arrives at apogee of the transfer ellipse with the vehicle erected to the local vertical (the pitch and roll axes are perpendicular to the local vertical) as defined by the IR system. The azimuthal direction of the vehicle at apogee is determined by the boost vehicle guidance and should coincide with the

precomputed direction set into the star tracking system. The main propulsion system is ignited placing the vehicle on a parking orbit (it is the intent that this orbit be near circular at an altitude of perhaps 400 naut mi). In general, a circular orbit will not be realized. This problem is considered in Section V.

## 2. Parking and Final Orbits

While in the parking orbit, the attitude control system continues to operate, maintaining the vehicle attitude so that the IR system and the radar antenna are always looking along the local vertical. The vehicle is tracked by earth-based stations to determine the orbit and a time for transfer to the final orbit is predicted. This requirement arises from the need to fit the vehicle into the overall pattern of satellites. On receipt of a signal from the tracking station, the main engine is ignited, placing the vehicle on a transfer orbit with apogee at the final orbit altitude (approximately 5600 naut mi). The geometry of launch, transfer orbit and final orbit is shown in Fig. III-1. During the coast-to-apogee period, the vehicle attitude is maintained with the pitch and roll axes perpendicular to the local vertical and with the vehicle azimuth attitude indicated by the star tracking system. In addition, the optical field of view of the IR system is automatically reduced to compensate for the smaller angle subtended by the earth at the higher altitude. A signal is required to ignite the main propulsion system at the time of apogee of the transfer orbit. This is probably most easily accomplished by estimating an early time of apogee in advance, turning on the radar, and firing the main propulsion system when the vehicle passes through the prescribed altitude. In the event the vehicle fails to reach the desired altitude, the firing of the main propulsion system would occur when the radar measurements indicate a maximum radar range has been reached. The radar is turned off at the time the main propulsion system fires, and the main propulsion system is cast off at the end of burning.

## 3. Operational Sequence

In the final orbit, the sequence of operation for the total system is controlled by a predetermined program of switching the radar on and off. The ratio of sea level water surface to land surface is large enough so that the firing can be preset into the computer, thus ensuring that the radar only measures altitude over sea level water surfaces. Turning on of the radar automatically initiates a sequence of recording and averaging radar readings over preselected time intervals, recording occultation times of preselected stars and orbit computations. The recording of data will continue through four star occultations with the radar operating only a small fraction of this time. The orbit computation is signaled by the recording of the fourth occultation. Also, the termination of the orbit computation initiates

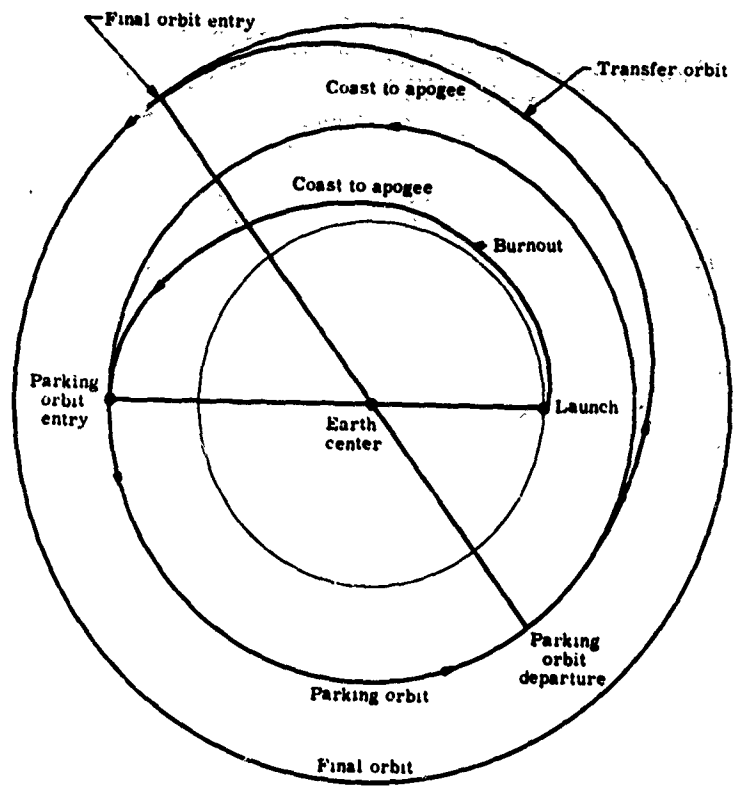


Fig. III-1. Launch, Parking and Final Orbit Geometry

orbit correction. If the series of measurements, computations and corrections require a longer interval of time (than is available from the programmed turn-on of the radar), then the program for turning on the radar is over ridden to the next nearest point in time. The sequence of recording, computation and correcting is repeated when the radar is again turned on.

#### 4. Orbit Computation

The computation of the elements of the orbit is based on the use of a combination of radar altitude and star occultation time data. The planar elements (i.e., the semimajor axis, the eccentricity and the time of perigee passage) are to be determined from radar data and time. The out-of-plane elements (i.e., the inclination, the longitude of the ascending node and the argument of perigee) are to be determined from the star occultation time recordings.

Computation of the in-plane parameters is considered first. Previous work (ER 11439-3) completed under this contract has considered the problem of obtaining a least squares orbit from an excess of radar altitude--time data (which applies here). If the eccentricity of the orbit is small ( $e^4 \ll 1$ ), the radius time relation can be written.

$$r = a (1 - e^2) \left[ 1 + e (\cos M + e (\cos 2M - 1) + e^2 \cdot \frac{9}{8} (\cos 3M - \cos M) + e^3 \cdot \frac{4}{3} (\cos 4M - \cos 2M)) \right]^{-1} \quad (1)$$

where

$$M = \sqrt{\mu a^3}^{-3/2} (t - t_p)$$

In order to expand Eq (1) in a Taylor's series, several partial derivatives are required.

$$\frac{\partial r}{\partial a} = \frac{1}{D} (1 - e^2) \left[ 1 - \frac{3eM}{2D} \left\{ \sin M + 2e \sin 2M + \frac{9}{8} e^2 (3 \sin 3M - \sin M) \right\} \right] \quad (2)$$

$$\frac{\partial r}{\partial e} = -\frac{2ae}{D} - \frac{a}{D^2} (1 - e^2) [\cos M + 2e (\cos 2M - 1)] \quad (3)$$

$$+ \frac{27}{8} e^2 (\cos 3M - \cos M) + \frac{16}{3} e^3 (\cos 4M - \cos 2M)]$$

$$\frac{\partial r}{\partial p} = -\frac{e(1 - e^2)}{D^2} \sqrt{\frac{\mu}{a}} [\sin M + 2e \sin 2M$$

$$+ \frac{9}{8} e^2 (3 \sin 3M - \sin M) \quad (4)$$

$$+ \frac{4}{3} e^3 (4 \sin 4M - 2 \sin 2M)]$$

Then the planar elements satisfying a least squares fit of the  $(r_k, t_k)$  data can be obtained in the following form:

$$a_{n+1} = a_n + \frac{1}{\delta'} \begin{vmatrix} \sum_k l_k r_k & - \sum_k l_k r'_k & \sum_k l_k m_k & \sum_k l_k n_k \\ \sum_k m_k r_k & - \sum_k m_k r'_k & \sum_k m_k^2 & \sum_k m_k n_k \\ \sum_k n_k r_k & - \sum_k n_k r'_k & \sum_k m_k n_k & \sum_k n_k^2 \end{vmatrix} \quad (5)$$

$$e_{n+1} = e_n + \frac{1}{\delta'} \begin{vmatrix} \sum_k l_k^2 & \sum_k l_k r_k & - \sum_k l_k r'_k & \sum_k l_k n_k \\ \sum_k l_k m_k & \sum_k m_k r_k & - \sum_k m_k r'_k & \sum_k m_k n_k \\ \sum_k l_k n_k & \sum_k n_k r_k & - \sum_k n_k r'_k & \sum_k n_k^2 \\ \sum_k l_k^2 & \sum_k l_k m_k & \sum_k l_k r_k & - \sum_k l_k r'_k \end{vmatrix} \quad (6)$$

$$t_{p_{n+1}} = t_{p_n} + \frac{1}{\delta'} \left| \begin{array}{c} \sum_k t_k m_k \\ \sum_k t_k n_k \\ \sum_k m_k^2 \\ \sum_k m_k n_k \\ \sum_k n_k r_k \\ \sum_k n_k r_k' \end{array} \right| \left| \begin{array}{c} \sum_k m_k^2 \\ \sum_k m_k n_k \\ \sum_k n_k r_k \\ \sum_k n_k r_k' \end{array} \right| \quad (7)$$

where  $e^4 \ll 1$ .

$$\delta' = \begin{vmatrix} \sum_k t_k^2 & \sum_k t_k m_k & \sum_k t_k n_k \\ \sum_k t_k m_k & \sum_k m_k^2 & \sum_k m_k n_k \\ \sum_k t_k n_k & \sum_k m_k n_k & \sum_k n_k^2 \end{vmatrix}$$

$$l_k = \frac{1 - e_n^2}{D} \left[ 1 - \frac{3 e_n M}{2D} \left\{ \sin M + 2 e_n \sin 2M \right. \right. \\ \left. \left. + \frac{9}{8} e_n^2 (3 \sin 3M - \sin M) \right\} \right]$$

$$m_k = -\frac{2 a_n e_n}{D} - \frac{a_n (1 - e_n^2)}{D^2} \left[ \cos M + 2 e_n (\cos 2M - 1) \right. \\ \left. + \frac{27}{8} e_n^2 (\cos 3M - \cos M) + \frac{16}{3} e_n^3 (\cos 4M - \cos 2M) \right]$$

$$n_k = -\frac{e_n (1 - e_n^2)}{D^2} \sqrt{\frac{\mu}{a_n}} \left[ \sin M + 2 e_n \sin 2M \right. \\ \left. + \frac{9}{8} e_n^2 (3 \sin 3M - \sin M) + \frac{4}{3} e_n^3 (4 \sin 4M - 2 \sin 2M) \right]$$

$$D = 1 + e_n \cos M + e_n^2 (\cos 2M - 1) + e_n^3 \frac{9}{8} (\cos 3M - \cos M)$$

$$M = \sqrt{\mu a_n^3} (t_k - t_{p_n})$$

$$r_k = \frac{a_n (1 - e_n^2)}{D}$$

It is expected that the computation time for the least squares estimates of the "in-plane" orbit parameters would take only a few minutes. Stored values of the desired orbit elements would be used in the computations outlined above.

The orbital plane orientation elements (i. e., the inclination, the argument of perigee and the longitude of the ascending node) are calculated from noting the time at which certain preselected stars are occulted by the earth and surrounding atmosphere. The upper limit of the occulting surface is known\* to an accuracy of approximately 1 mi, so that the occulting surface takes the form of a cylinder with known radius for all practical purposes.

The time of occultation is defined to be that time when light from the star being tracked is refracted by a predetermined small amount. At the time of occultation the vehicle is simultaneously located on the occulting surface in a trajectory defined by the relation

$$r = \frac{a(1 - e^2)}{1 + e \cos \psi}$$

$r$  = radial distance of the satellite from the center of the earth

$a$  = semimajor axis of the orbit

$e$  = eccentricity of the orbit

$\psi$  = angular distance of the vehicle from the line of apsides.

It has been shown\* that at the time of occultation the following equation holds:

---

\* (WADD Technical Report 61-78 December, 1960)

$$\begin{aligned}
1 = \frac{R^2}{r_k^2} = & \cos^2 \delta_k \left[ \cos^2 (\theta + \omega) \cos^2 (\alpha_k - \Omega) \right. \\
& + \sin^2 (\theta + \omega) \cos^2 i \sin^2 (\alpha_k - \Omega) \\
& + \sin^2 \delta_k \sin^2 i \sin^2 (\theta + \omega) \\
& + \left[ 2 \cos^2 \delta_k \cos i \cos (\theta + \omega) \sin (\theta + \omega) \right] \times \\
& \quad \cos (\alpha_k - \Omega) \sin (\alpha_k - \Omega) \\
& + \left[ 2 \cos \delta_k \sin \delta_k \sin i \cos (\theta + \omega) \right] \times \\
& \quad \sin (\theta + \omega) \cos (\alpha_k - \Omega) \\
& + 2 \cos \delta_k \sin \delta_k \cos i \sin i \sin^2 (\theta + \omega) \sin (\alpha_k - \Omega)
\end{aligned}$$

where

$$r_k = \frac{a(1 - e^2)}{1 + e \cos \theta}$$

- a = semi major axis of the orbit, known from the radar measurements
- e = orbit eccentricity, known from the radar measurements
- r = radius of the occulting surface (known)
- $\delta_k$  = declination of the occulted star, known from computer storage
- $\alpha_k$  = right ascension of occulted star, known from computer storage
- $\theta$  = true anomaly, known from radar data processing
- $i, \omega, \Omega$  = the inclination, argument of perigee and longitude of the ascending node, respectively. These are the unknown quantities.

It is evident that a measurement of the time of egress and the time of ingress of a single star, plus a measurement of either the time of ingress or time of egress of our additional star, will supply three equations in the required three unknowns (provided the orbit is noncircular). The measurement of the time of ingress and time of egress of three different stars would, of course, supply six equations which could be used to determine the orbital elements.

#### 5. Maneuvers for Orbit Correction

The orbital correction system employs a set of six rocket motors fixed to the satellite structure in such a manner that two motors are aligned along each of the body axes (one forward and one aft). The alignment of the thrust vector for the various maneuvers is accomplished by vectorially adding three components (monitored by an integrating accelerometer on each axis) which are known with respect to a local vertical coordinate system.

This type of system has several advantages over one in which the vehicle remains stationary while the engines are gimballed or one in which the vehicle attitude is changed to position the thrust of a single motor. Most of these advantages arise from the fact that this approach requires no complex mechanical arrangements, does not produce large disturbing moments during thrust periods, and is capable of reversing the direction of any thrust component in a simple manner in the shortest time possible. These advantages make the system ideally suited for this mission as defined in the previous discussions.

##### a. Orbital corrections

Two means of making orbital corrections have been investigated. These are:

- (1) Independent adjustment of each orbital element.
- (2) Linear differential corrections.

The first of these schemes has been devised for the general case of orbital corrections in which the corrections are relatively large and the orbit of arbitrary nature (arbitrary in the sense that the elements can be varied from one problem to another). This routine has also been successfully employed for the small correction; however, there are more simple routines which can be utilized under these conditions. A sequencing routine has also been devised to minimize the amount of energy required if more than one adjustment is required. This technique for corrections will be investigated further for the range of orbital altitudes involved in the study, and numerical results showing the effects of finite burning time will be generated.

If the maneuvers are small, the remaining scheme is adequate from the standpoint of agreement with the desired motion. This technique uses a reference trajectory defined prior to launch, or determined at some time before transferring from the parking orbit, and determines the partial derivatives of the various orbital elements with respect to the controlled parameters. A matrix of these error coefficients and the measured deviations at some time are used to define the corrections required. This procedure has been checked out and has proved to reduce the magnitude of the uncorrected error to near negligible proportions for the cases in which the deviations from the reference orbit are small (on the order of 40 mi or less the x, y and z coordinates). The computations required in this routine are simple, and only sine and cosine functions need be made available in addition to the stored constants. Thus, it is possible to utilize a reasonably simple computer. This routine was investigated in additional detail for a variety of ascent trajectories to provide midcourse guidance data for the range of trajectories considered. The results of these corrections were compared to both the reference trajectory and the uncorrected trajectory to show the accuracy of the scheme.

Another approach to station keeping where extreme precision in position determination is desired has been formulated based on the equations of motion written in a rotating coordinate system centered in a circular orbit which is regressing at a uniform rate about the equator. All large accelerations have thus been eliminated from the equations, making it possible to study motions which are generally neglected provided that the displacements do not get larger than those assumed in the formulation of the equations (approximately 50,000 ft). The terms of these equations which have been considered pertain to the motion about an oblate spheroid in the absence of other accelerations (gravitational, atmospheric, meteoric, etc.). Thrust terms have, of course, been added in order that control schemes can be investigated. These equations have an additional desirable feature in that since the displacements are small, the reference system is essentially equivalent to a vehicle-centered local vertical system. The thrust components required to produce the desired motion are thus those as seen by the vehicle. These equations are:

#### Equations of Motion

##### Accelerations

$$\begin{aligned} \ddot{\mathbf{x}} = & c_1 \sin \omega_0 t \cdot \left[ a_{11} + b_{11} \cos 2 \omega_0 t \right] \mathbf{x} - a_{12} \sin \omega_0 t (\dot{y}) \\ & - b_{12} \cos \omega_0 t (y) - a_{13} \cos \omega_0 t (z) - b_{13} \sin \omega_0 t (z) \\ & - T \mathbf{x} \left[ \frac{1}{m_0} - \frac{1}{m} \right] \end{aligned}$$

$$\begin{aligned} \ddot{y} = & c_2 \sin 2 \omega_0 t - a_{21} \sin \omega_0 t (\dot{x}) - b_{21} \cos \omega_0 t (x) \\ & - \left[ a_{22} + b_{22} \cos 2 \omega_0 t \right] y - a_{23} (\dot{z}) - b_{23} \sin 2 \omega_0 t (z) \\ & - T_y \left[ \frac{1}{m_0 - \dot{m} t_b} \right] \end{aligned}$$

$$\begin{aligned} \ddot{z} = & c_3 + d_3 \cos 2 \omega_0 t - a_{31} \cos \omega_0 t (\dot{x}) - b_{31} \sin \omega_0 t (x) \\ & - a_{32} (\dot{y}) - b_{32} \sin 2 \omega_0 t (y) - \left[ a_{33} + b_{33} \cos 2 \omega_0 t \right] z \\ & - T_z \left[ \frac{1}{m_0 - \dot{m} t_b} \right] \end{aligned}$$

Velocities

$$\dot{x} = \dot{x}_0 + \int_0^t \ddot{x} dt$$

$$\dot{y} = \dot{y}_0 + \int_0^t \ddot{y} dt$$

$$\dot{z} = \dot{z}_0 + \int_0^t \ddot{z} dt$$

$$V = \sqrt{\dot{x}^2 + \dot{y}^2 + \dot{z}^2}$$

$$\dot{R} = \frac{d}{dt} (R) = \frac{x\dot{x} + y\dot{y} + z\dot{z}}{R}$$

Displacements

$$x = x_0 + \int_0^t \dot{x} dt$$

$$y = y_0 + \int_0^t \dot{y} dt$$

$$z = z_0 + \int_0^t \dot{z} dt$$

$$R = \sqrt{x^2 + y^2 + z^2}$$

Coefficients

$$a_{11} = \omega_0^2 \left( 1 - \frac{15}{4} \alpha \sin^2 i \right)$$

$$a_{12} = 2 \omega_0 \beta \sin i$$

$$c_{13} = a_{12}$$

$$b_{11} = \omega_0^2 - a_{11}$$

$$b_{12} = 2 \omega_0^2 \sin i \left( \beta - \frac{3}{2} \alpha - \cos i \right)$$

$$b_{13} = -15 \omega_0^2 \alpha \sin i \cos i - b_{12}$$

$$c_1 = R_c b_{12}$$

$$c_2 = \frac{2}{3} R_c b_{11}$$

$$c_3 = \frac{3}{2} R_c \omega_0^2 \left[ \alpha \left( 1 - \frac{3}{2} \sin^2 i \right) + \frac{4}{2} \beta \cos i - \frac{4}{3} \gamma \right]$$

$$a_{21} = -a_{12}$$

$$a_{22} = \frac{c_3}{R_c}$$

$$a_{23} = -2 \omega_0 (1 - \beta \cos i + \gamma)$$

$$b_{21} = \frac{b_{12} + b_{13}}{5}$$

$$b_{22} = \frac{9}{15} b_{11}$$

$$b_{23} = \frac{8}{5} b_{11}$$

$$a_{31} = a_{12}$$

$$a_{32} = -a_{23}$$

$$a_{33} = -3 \omega_0^2 \left[ 1 + 2 \alpha \left( 1 - \frac{3}{2} \sin^2 i \right) - \frac{2}{3} \beta \cos i + \frac{2}{3} \gamma \right]$$

$$b_{31} = \frac{4}{5} (b_{12} + b_{13}) = 4 b_{21}$$

$$b_{32} = b_{23}$$

$$b_{33} = -\frac{12}{5} b_{11}$$

$$d_3 = -\frac{3}{5} R_c b_{11}$$

#### Definitions

$x, y, z$	position coordinates relative to a rotating reference system in a circular orbit which is regressing at a constant rate about the equator (ft) (x normal to orbital plane; z along the radius; y along the velocity vector)
$\omega_0$	the rotational rate of the coordinate system about the earth = $\sqrt{\frac{1.4077 \times 10^{16}}{R_c^3}}$ (rad/sec)
$R_c$	the radius relative to the center of the earth of the desired circular orbit (ft)
$R$	distance from the origin (ft)
$\dot{R}$	range rate relative to origin (fps)
$T_x, T_y, T_z$	thrust components in the specified coordinate system (lb)
$m_0$	the initial mass of the vehicle (slugs)
$\dot{m}$	the mass rate due to burning propellant

$t_b$	the total burning time of rocket motors (sec)
$\alpha$	$1.574 \times 10^{-4}$
$\beta$	$1.365 \times 10^{-4}$
$\gamma$	$4.722 (1 - \frac{5}{4} \sin^2 i) \times 10^{-4}$

### C. THE DEVELOPMENT OF A COMPUTER PROGRAM

To define the requirements for the control system and evaluate several simple control laws, the preceding set of equations has been programmed for the analog computer. This approach is possible due to the fact that the positions and velocities defined by the equations are small and changing slowly. However, because analog equipment is limited in accuracy to approximately three significant figures, several simplifications to the equations can be made based upon the evaluation of the coefficients for this particular orbit and a knowledge of the maximum value of R and V. These coefficients are:

$$a_{11} = 0.8516 \times 10^{-7}$$

$$a_{12} = 0.6505 \times 10^{-7}$$

$$a_{13} = 0.6505 \times 10^{-7}$$

$$b_{11} = 3.351 \times 10^{-11}$$

$$b_{12} = 2.781 \times 10^{-14}$$

$$b_{13} = -9.478 \times 10^{-11}$$

$$c_1 = 0.1526 \times 10^{-5}$$

$$c_2 = 7.357 \times 10^{-4}$$

$$c_3 = -0.0119 \times 10^{-4}$$

$$a_{21} = -0.6505 \times 10^{-7}$$

$$a_{22} = 0.0022 \times 10^{-11}$$

$$a_{23} = -0.5886 \times 10^{-3}$$

$$b_{21} = -1.896 \times 10^{-11}$$

$$b_{22} = 2.011 \times 10^{-11}$$

$$b_{23} = 5.362 \times 10^{-11}$$

$$a_{31} = -0.6505 \times 10^{-7}$$

$$a_{32} = 0.5836 \times 10^{-3}$$

$$a_{33} = 2.555 \times 10^{-7}$$

$$b_{31} = -7.582 \times 10^{-11}$$

$$b_{32} = 5.362 \times 10^{-11}$$

$$b_{33} = -8.043 \times 10^{-11}$$

$$d_3 = -11.066 \times 10^{-4}$$

where

$$R_0 = 5.488164 \times 10^7$$

$$\omega_0 = 0.291824 \times 10^{-3}$$

$$i = 54.736^\circ$$

$$\gamma = 0.7866 \times 10^{-4}$$

From these data it is immediately apparent that, to the first order, all coefficients in the equations of motion except  $a_{11}$ ,  $a_{23}$ ,  $a_{32}$ ,  $a_{33}$ ,  $c_1$ ,  $c_2$ ,  $c_3$  and  $d_3$  are negligible.

The equipment utilized for this problem is listed below:

13 integrators

22 summers

23 inverters

53 attenuators

2 GEDA multipliers (1 used for division and square root)

1 diode multiplier

5 servo multipliers (2 used for division and square root)

9 relays

The results of this computer program are contained in work previously completed\* under this contract, and they indicate that the present approach to the orbital correction problem is feasible.

#### D. CONTROL LAWS

Many techniques can be envisioned for varying the magnitude and direction of the thrust vector to produce the desired motion. However, for the purpose of this study, use will be made of the fact that if the displacements are small, the distance from the origin will vary in an approximate linear manner. Thus, there are two types of corrections: one to cancel the velocity components and one to produce motion toward the desired point. The thrust components\* for these maneuvers are:

$$T_s = T_o \frac{\dot{S}}{V}$$

$$T_R = T_o \frac{S}{R}$$

---

\* ER 11439-3 "Orbital Guidance Systems Study," November 1960.

where

$$S = x, y \text{ or } z.$$

These thrust components may be combined if appropriate restrictions are added to define when each will be employed. The restriction utilized in these studies was that, should the vehicle be moving (or start moving) toward the origin in any component of position (i. e., the sign of  $S$  and  $\dot{S}$  are different), velocity canceling component of thrust is neglected to save energy. Thus,

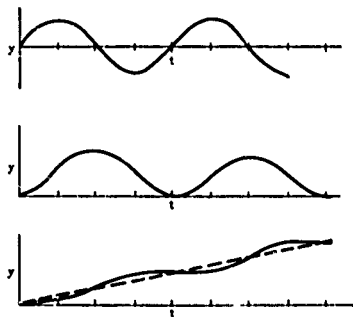
$$T_s = T_o \left[ \frac{S}{R} + \frac{\dot{S}}{V} \right] \quad \text{to produce motion if the signs of } S \text{ and } \dot{S} \text{ are the same}$$

or

$$T_s = T_o \left[ \frac{S}{R} \right] \quad \text{to produce motion when the sign of } S \neq \text{the sign of } \dot{S}$$

$$T_s = T_o \left[ \frac{\dot{S}}{V} \right] \quad \text{to cancel velocity in the different directions}$$

One special note is required in discussion of these figures since investigation of them discloses that the function  $y$  (i. e., the displacement in the orbital plane along the normal to the radius) is diverging at the rate of approximately 0.1 fps on the average. This is the result of two conditions. First, the earth's oblateness produces the term  $c_2 \sin 2t$  in the equation for  $\ddot{y}$ . The contribution of this term is illustrated in the following sketches.



This motion can be envisioned to be the result of a period error due to the earth's oblateness. Since the origin continues to rotate at the prescribed rate, the result is drift. However, the major portion of this drift was included in the motion of the origin; thus it appears that this drift was in part, if not completely, the result of something else.

The second contribution to the drift is the result of loss of numerical significance. Since the motion is only approximately 2000 ft per revolution, the error in the orbital period is only 1 part in  $0.6 \times 10^5$ . This error could result from two factors, dropping terms for simplification or in the computational routines themselves from noise. However, since the degree to which the runs could be repeated was good, it is more probable that simplification resulted in slight errors.

One extension to these laws is necessary to make their evaluation more meaningful: the inclusion of the effects of errors in the position of the vehicle or the origin, and the effects of errors in the attitude of the vehicle during thrusting periods. Since each of these errors will be reflected in the same manner, the following laws for directing the thrust have been studied.

$$T_s = T_o \left[ \frac{S + \epsilon_1}{R} + \frac{\dot{S} + \delta_1}{V} \right]$$

or

$$T_s = T_o \left[ \frac{S + \epsilon_1}{R} \right]$$

$$T_s = T_o \left[ \frac{\dot{S} + \delta_1}{V} \right]$$

where the same restrictions previously noted are valid. These errors can be constants or may be generated (when needed) as functions of time, position etc., if desire.

## IV. SUBSYSTEM DESCRIPTION

### A. RADAR ALTIMETER

#### 1. Introduction

The radar system proposed for performance of satellite altimeter functions must be capable of operating one full year without maintenance or adjustment. This requires that maximum reliability and stability be incorporated in the design of the system along with the added consideration of minimum power consumption. As a result of these requirements, maximum use will be made of solid-state components, such as, transistors, diodes and ferrites.

The weight objective of this radar altimeter is 60 lb which includes the parabolic antenna. The estimated power consumption is not expected to exceed 150 watts. This low power consumption is achieved by maximum use of solid-state components. A block diagram of the radar altimeter is shown in Fig. IV-1.

#### 2. System Design

The purpose of the radar altimeter is to provide an orbiting satellite with accurate altitude data to the earth. The altimeter design, based on radar principles, will meet a range-accuracy requirement of 0.1 mi and provide the reliability and stability characteristics required to ensure one year of maintenance free operation. The range-accuracy requirement is normally met by selecting a transmitted-pulse width which corresponds to the permissible range error. For this radar, the selected pulse width is  $1.0 \mu\text{sec}$ . Another design factor that must be considered is the altitude of operations. When an antenna beam is originated at great distances and projected on the surface of the earth, the projected area becomes quite large. Normally the earth is considered a flat plate for radar altimeter applications; however, when the beam is projected from great distances, its area is so large that the earth's curvature must be considered when determining altitude accuracy.

Since the projected area is a function of antenna beamwidth, the ranging accuracy is not only a function of pulse duration but also dependent on the antenna beamwidth. Figure IV-2 shows the earth's curvature error as a function of antenna beamwidth, and if this error is kept within the pulse duration period, a beamwidth of approximately  $0.54^\circ$  is required to meet this condition.

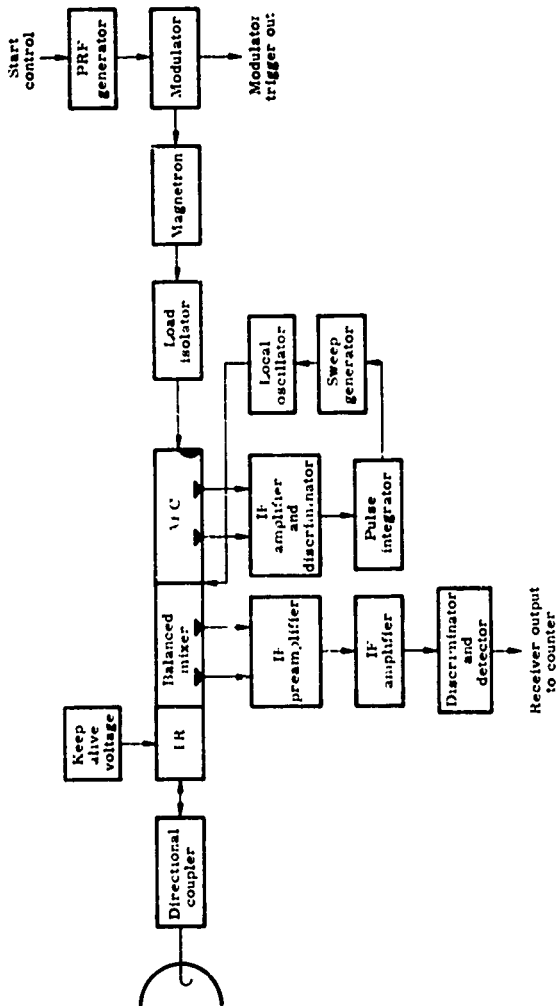


Fig. IV-1. Block Diagram of Radar Altimeter

#### a. Antenna beamwidth

The requirement to obtain a narrow beamwidth now becomes a prime consideration in the design of this radar altimeter. Two methods whereby a narrow beamwidth may be obtained are: (1) using a large antenna and low frequency (X band) and (2) using a small antenna and high frequency ( $K_u$  band). For satellite applications, it is necessary to keep the antenna a reasonable size because it will be carried within the satellite during launch. The antenna sizes investigated were 30 to 60 in. in diameter. From the resulting beamwidths shown in Fig. IV-3 it can be seen that the  $K_u$ -frequency band gives the smallest beamwidths. By referring to Fig. IV-2, it can be determined that the maximum permissible beam is  $0.54^\circ$ . Also, Fig. IV-3 shows that in order to obtain a beamwidth of  $0.54^\circ$  or less, one must operate at  $K_u$  band with an antenna diameter of at least 43 in.

#### b. Antenna gain

Simultaneously with the investigation of antenna beamwidths, antenna gain was calculated for X,  $K_u$  and  $K_a$  band frequencies (Fig. IV-4). An examination of Fig. IV-4 will reveal that  $K_a$  band gives at least 6 db gain over  $K_u$  band and 11 db over X band. This can be stated on a power basis with  $K_a$  band requiring 1/4 the power of  $K_u$  and 1/128 the power of X band.

Considering the fact that a  $0.54^\circ$  beamwidth is required to meet the 0.1-mi accuracy requirements and to maintain a reasonable antenna size, the  $K_a$  band is selected as the operating frequency for the radar altimeter. The antenna diameter is 48 in. to obtain the maximum gain (50.3 db) for a reasonable size antenna. The resultant beamwidth is  $0.5^\circ$  and the earth's curvature error is within the pulse width.

#### c. The $K_a$ band environment performance

A detailed study was made to determine the environmental effects (such as weather, atmosphere and target characteristics) upon the propagation characteristics at  $K_a$  band. A survey of available literature in this field was conducted with the result that several recent findings have made the use of  $K_a$  band very attractive. Reference 1 contains an article on atmospheric absorption along with a summary and bibliography of the major effort conducted in this area to 1961. Figure IV-5

$$D^2 + R^2 = (h + R)^2$$

$$D^2 = h^2 + 2Rh$$

Where  
 $D = \frac{\text{Beamwidth Distance}}{2}$

$R = \text{Earth's radius}$   
 $h = \text{height of earth's curvature}$

Since  $h \ll R$ ,  
 then  $D^2$   
 $h = \frac{D^2}{2R}$

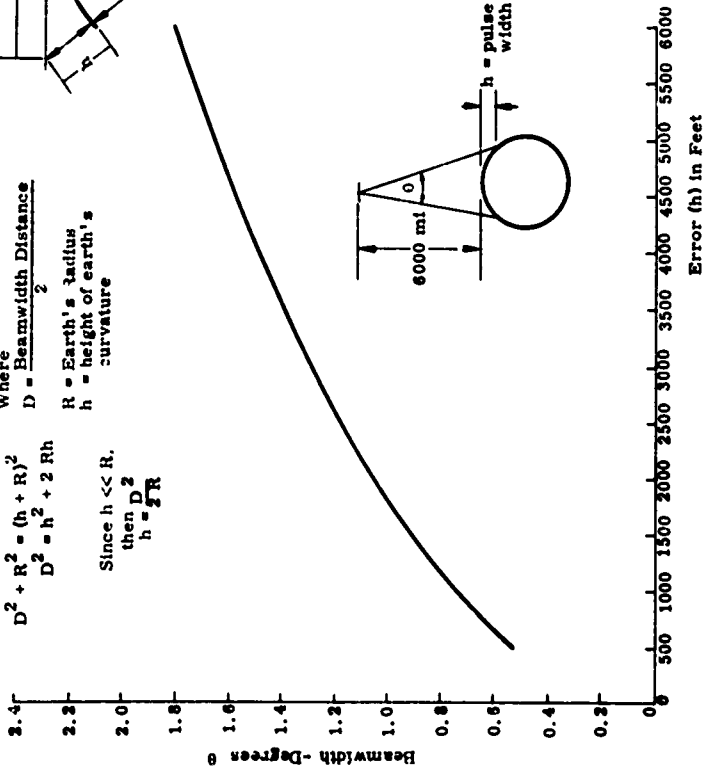
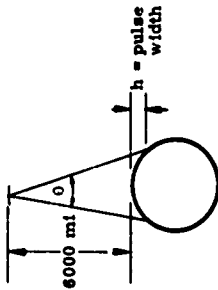
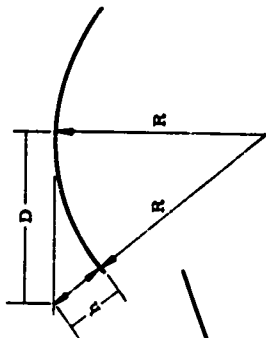


Fig. IV-2. Beamwidth Versus Earth's Curvature Error

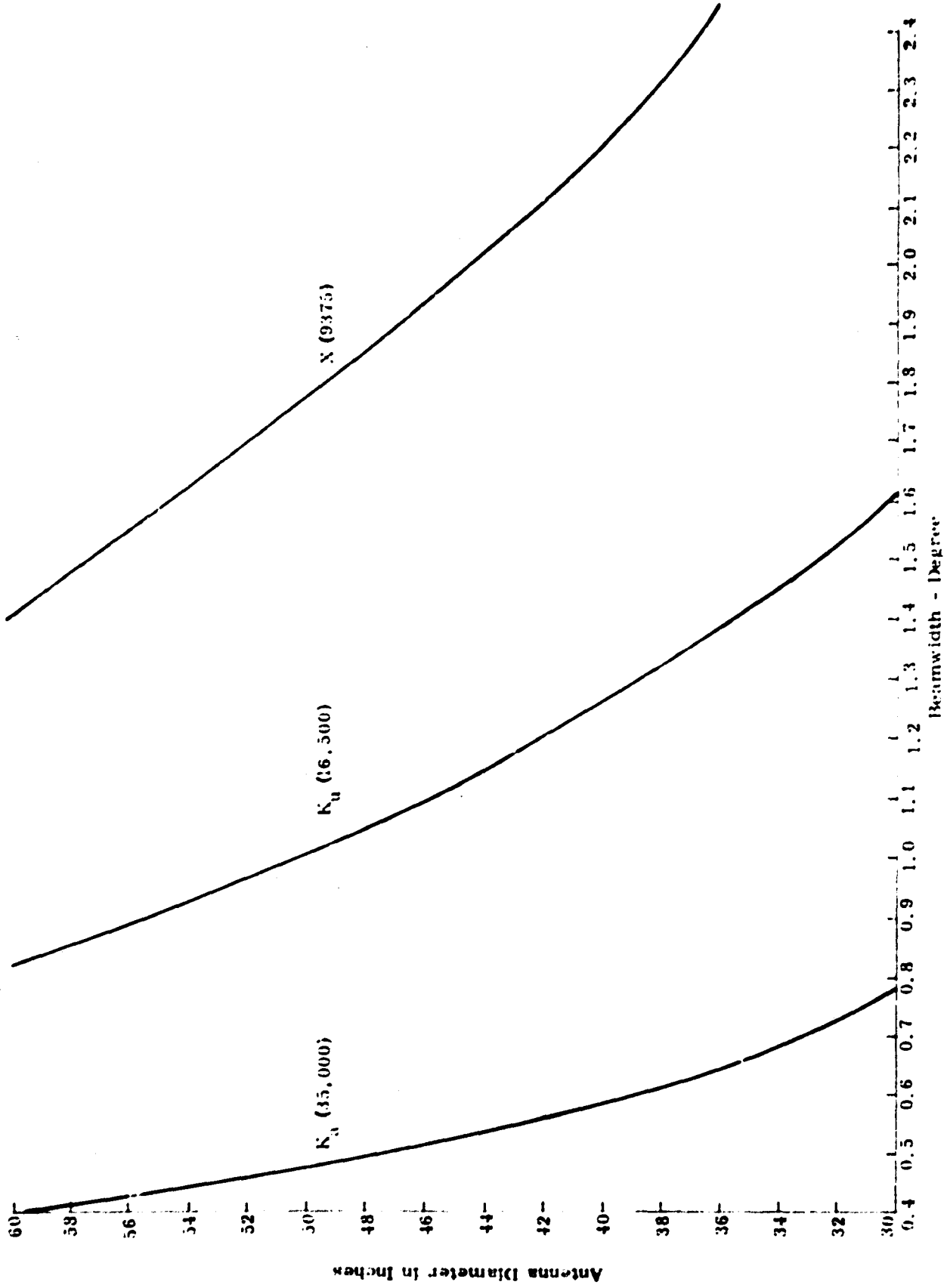


Fig. IV-3. Antenna Diameter Versus Beamwidth

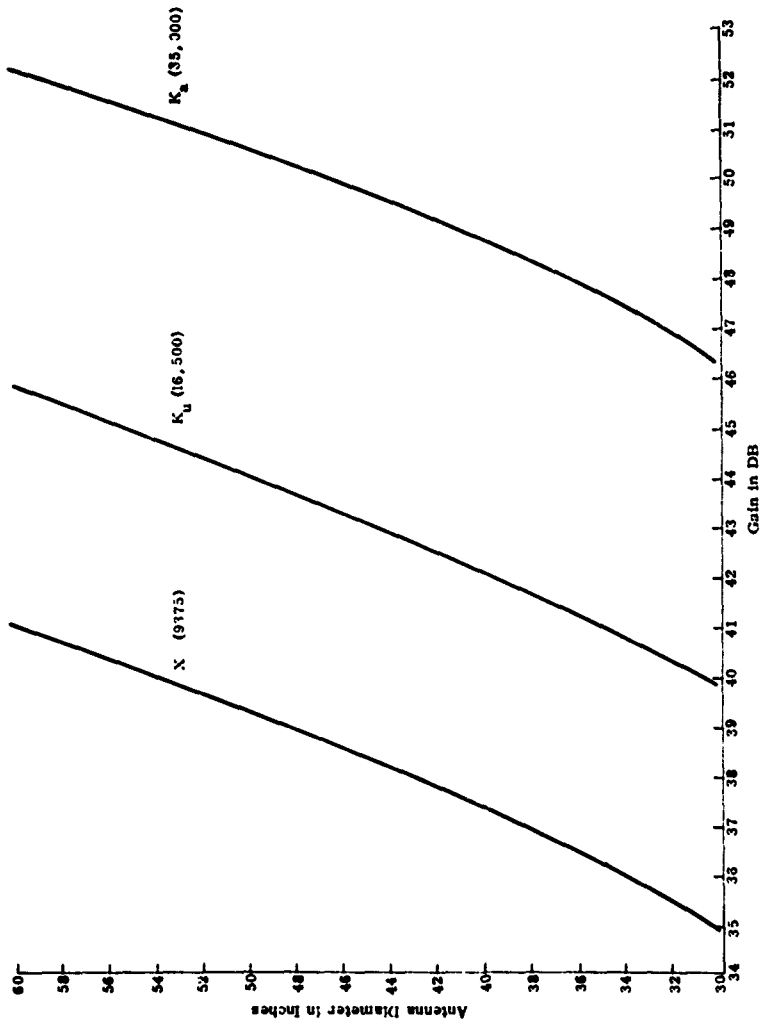


Fig. IV-4. Antenna Diameter Versus Gain.

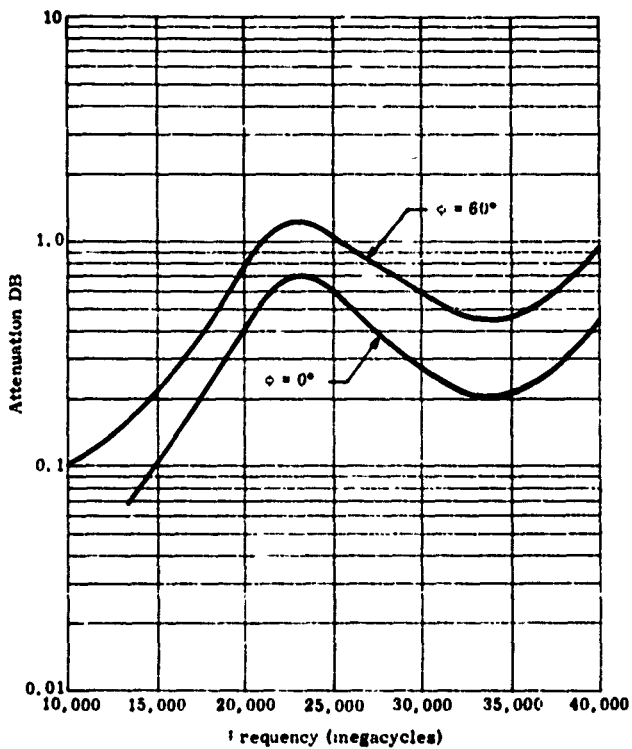


Fig. IV-5. Attenuation for One-Way Transmission Through Atmosphere

shows the total attenuation for one-way transmission through the atmosphere (produced from data in Ref. 1), also, a summary of the available experimental data and theoretical predictions. From this illustration it can be seen that the total two-way transmission loss through the atmosphere is about 0.5 db for  $K_a$  band, as compared to negligible losses at X band. This case is for the vertical transmission path ( $\phi = 0$ ) where the energy propagation distance is the shortest propagation distance through the atmosphere. Figure IV-5 also shows that attenuation is not especially critical to the angle of entry up to angles of  $60^\circ$ . The radar altimeter will operate with a nominal  $0^\circ$  angle of entry with very small divergences.

Another area studied was the target reflection characteristics. In this application the radar altimeter will only be operated over water. Radar ranging over land is not practical due to the unknown land elevations which would result in altitude errors. The back scattering from water and several land terrains have been measured at X,  $K_u$  and  $K_a$  bands using vertical polarizations by the Naval Research Laboratory and are reported in Refs. 2 and 3. The average radar cross section of water echo per unit area of the surface,  $\sigma^0$ , is plotted as a function of frequency for angles of incidence of  $0^\circ$  and  $5^\circ$  (Fig. IV-6). It can be seen that the effective  $K_a$  band reflectivity is 10 db greater than the effective X band reflectivity. This effective gain at  $K_a$  band is not adversely affected by winds that cause the speed and magnitudes of the waves to change.

#### d. Summation of gains

In the preceding paragraphs the various factors affecting gain (such as frequency, antenna size, atmospheric attenuation and back scatter) were discussed. A tabulation of these gains are presented below with dimensional gains referenced to operation utilizing a 48-in. diameter antenna.

	Frequency		
	X	$K_u$	$K_a$
Antenna gain db	+38.9	+43.8	+50.3
Back scatter db	+ 4.0	+ 7.3	+14.0

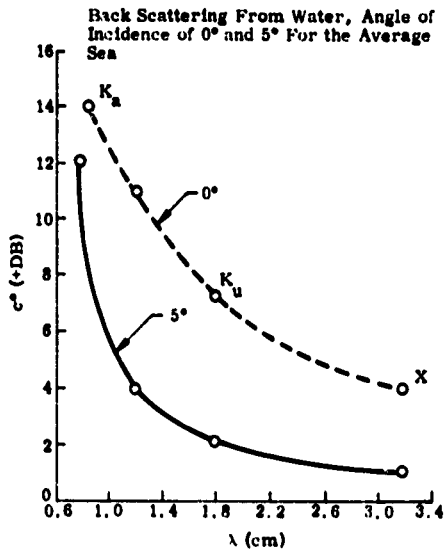


Fig. IV-6. Back Scattering of Water As a Function of Frequency

Atmospheric attenuation db	0	- 0.3	- 0.5
Total db	+42.9	+50.8	+63.8

From the above summary it can be seen that operation at  $K_a$  band provides 21-db more gain than X band. Since  $K_a$  band is the only frequency band producing a beamwidth sufficient to maintain a 0.1-mi range accuracy and since a 21-db gain is provided above X band, it is concluded that the radar altimeter operate at  $K_a$  band. Other factors affecting radar performance (such as receiver noise figure, signal-to-noise requirements, plumbing losses, radome losses and degradation due to operation) will be covered in subsequent paragraphs.

### 3. Radar Range Performance

The expression for radar range used for preliminary design includes the relationship of transmitter pulse power, antenna gain, wave length, pulse length, pulse repetition rate, receiver noise figure and target size. The expression used is

$$R_{\max} = 5.44 \sqrt{\frac{P_T G_0^2 \lambda^2 \tau (\text{PRF})^{1/3}}{\text{NF}}} A_E \quad \text{naut mi}$$

where

- $P_T$  = peak power, watts
- $G_0$  = ratio, gain over isotropic
- $\lambda$  = wave length, meters
- PRF = pulse repetition frequency, cps
- NF = noise factor ratio
- $A_E$  = effective area, square meters
- $\tau$  = pulse width, microseconds

This expression has been developed for an antenna beam that is fixed relative to the target (i.e., searchlighting), as is the case of the radar altimeter.

Since the orbiting altitude of the radar altimeter will be at least 6000 mi (5210 naut mi), the system must be capable of providing this range. The following design factors have been selected for this radar.

$$G_0 = 50.3 \text{ db} = 1.07 \times 10^5$$

$$\lambda = 0.86 \text{ cm} = 8.6 \times 10^{-3} \text{ meters}$$

$$\tau = 1 \times 10^{-6} \text{ sec}$$

$$\text{PRF} = 15 \text{ pulses/sec}$$

$$\overline{\text{NF}} = 10.5$$

$$A_E = 61.5 \times 10^8 \text{ sq m}$$

Rearranging the range equation to solve for  $P_T$ :

$$P_T = \frac{R_{\text{max}}^4 \overline{\text{NF}}}{(5.44)^4 G^2 \lambda^2 \tau (\text{PRF})^{1/3} A_E}$$

$$P_T = \frac{(5210)^4 11.2}{(5.44)^4 (1.07 \times 10^5)^2 (8.6 \times 10^{-3})^2 (1 \times 10^{-6}) (15)^{1/3} (61.5 \times 10^8)}$$

$$P_T = 740 \text{ watts}$$

To the above transmitted power the following losses and gains must be added.

**Losses:**

Propagation                      0.5 db

Plumbing                            3.2

S/N ratio	17.0
one-year degradation	10.0
	30.7 db

**Gain:**

Back scatter	14.0 db
--------------	---------

Net gain = losses (-30.7) + gain (+14.0) = -16.7 db = 46

Required transmitted peak power becomes

$$P_T = 740 \text{ watts} \times 46$$

$$P_T = 36 \text{ kw (peak power)}$$

Thus it is shown that a  $K_a$ -band radar, transmitting 36 kw of peak power, is capable of performing the satellite radar altimeter mission. The nominal transmitted power that the radar will use is based on available magnetrons. The magnetron selected for this altimeter, Sylvania 5789, transmitting 40 kw, has an acceptable reliability and performance history.

#### 4. Modulator Design

The modulator determines the waveform and the power of the output pulse released through the magnetron. Basically, the modulator consists of the high-voltage power supply, the charging network, the pulse-forming network, the discharge circuit and the pulse transformer (Fig. IV-7). Reference 4 was used to help determine these modulator components.

One of the unusual characteristics of the modulator (Fig. IV-7) is that it uses resistance charging for storing energy in the pulse-forming network. This charging method was selected because of the low-pulse repetition frequency required by the long range between the satellite and earth. Traditionally, airborne modulators have used inductance resonance charging to obtain high charging efficiencies (over 90%). However, to obtain resonance charging at low pulse repetition frequencies, an inductance that is prohibitive in size is required and consequently resistance charging must be used. The efficiency of resistance charging can be a maximum of only 50%.



a. Voltage on the pulse-forming network and the switch

The discharging efficiency,  $n_d$ , is assumed to be 75%, the peak forward pulse-forming network voltage is

$$V_N = \sqrt{\frac{4 Z_N P_1}{n_d}}$$

$Z_N$  = impedance of pulse-forming network

$P_1$  = pulse power in the load

$n_d$  = discharging efficiency

$$V_N = 2 \sqrt{\frac{50 \times 13}{0.75}} \times 10^2 \approx 6 \text{ kv}$$

This voltage is well within the specifications of the BOMAC 5959 hydrogen thyratron tube which has been selected as the switch. Another switching method investigated was the rotary spark gap. The attractive feature of this switch was the low power consumption and no requirement for warmup. However, the rotary spark gap was not selected at this time because of the difficulty of adapting it in applications requiring airtight enclosures.

b. Capacitance of pulse-forming network

The approximate pulse-forming network capacitance is given by

$$C_N = \frac{\tau}{2 Z_N}$$

$\tau$  = pulse width

$Z_N$  = impedance of pulse forming network

$$C_N = \frac{10^{-6}}{2 \times 50} = 10,000 \text{ } \mu\text{f}$$

### c. Charging resistor

The requirement on the series-resistance isolating element in this charging circuit is simply that it must be large enough to allow only negligible current to be taken from the power supply during the pulse and the deionizing time for the switch, but not so large that the  $\tau C$ -time constant becomes comparable to the interpulse interval. To get the highest network voltage from a given power supply voltage with this arrangement, the length of the interpulse interval should be several times greater than the RC-time constant in the charging circuit. The interpulse interval is 62 ms and a time constant of 6.2 ms is selected to obtain a high network voltage. The maximum efficiency of the resistance charging is 50%.

$$T_C = R_C C_N$$

$$T_C = \text{time constant}$$

$$R_C = \text{charging resistance}$$

$$C_N = \text{pulse-forming network capacitance}$$

$$R_C = \frac{T_C}{C_N} = \frac{6.2 \times 10^{-3}}{10^{-8}} = 620,000 \text{ ohms}$$

### d. Shunt-diode circuit

In order to maintain a constant peak forward voltage on the network after an accidental short circuit in the load, it is necessary to dissipate, as rapidly as possible, the inverse voltage left on the network by means of a shunt-diode circuit across the network. For maximum effectiveness, the time constant of the network capacitance and resistance of the shunt circuit should be as small as possible when compared with the charging period. Since  $T_C = 6.2 \times 10^{-3}$  sec, the time constant of the shunt-diode circuit ( $T_S$ ) is selected as  $6.2 \times 10^{-5}$  sec because the circuit is generally effective when its time constant is 1% of the charging time.

$$R_S = \frac{T_S}{C_N}$$

$T_S$  = time constant of the shunt-diode.

$R_S$  = resistance of shunt-diode circuit.

$C_N$  = capacitance of pulse-forming network.

$$R_S = \frac{T_S}{C_N} = \frac{6.2 \times 10^{-5}}{10^{-8}} = 6200 \text{ ohms.}$$

This protective circuit would consist of the shunt resistor with a stack of diode rectifiers. The maximum rating in the diode rectifiers would not be exceeded because, for a peak inverse voltage of 6.2 kv, the peak current after a complete short circuit is  $6200/1300 = 4.8$  amps. The full current will persist for several  $\mu\text{sec}$  and then quickly be reduced. For longer short-circuit current periods, the protective relay circuit will be energized and will remove the excess dissipation.

#### e. Power supply

The power supply is designed as a standard full-wave rectifier with a choke input filter to minimize the effect of the input voltage waveform on the pulser output. The d-c voltage required for normal operation can be arrived at by the use of an estimated charging ratio of 1.0 for resistance charging.

$$E_{bb} = \frac{V_N}{R_{ch}} = \frac{6 \text{ kv}}{1} = 6 \text{ kv}$$

$E_{bb}$  = high voltage supply

$V_N$  = voltage on pulse-forming network

$R_{ch}$  = charging ratio

The average current from the power supply is approximately

$$I_{c \text{ avg}} = \frac{P_l}{E_{bb} \text{ nd } nc}$$

$P_1$  = pulse power in the load

$E_{bb}$  = high voltage supply

$n_d$  = discharging efficiency

$n_c$  = charging circuit efficiency

$$I_{c\text{ avg}} = \frac{2.2}{6 \times 10^3 (0.75)(0.5)} = 1 \text{ ma}$$

#### f. Hold-off diode

The maximum expected peak current through the charging circuit

$$I_{c\text{ pk}} = \frac{\sqrt{2} I_{c\text{ avg}}}{T_C \text{ PRF}} = \frac{1.4 \times 10^{-3}}{6.2 \times 10^{-3} \times 15}$$

$$I_{c\text{ pk}} = 15 \text{ ma}$$

#### g. Protection

Protection against short circuits in the load is normally achieved by the shunt-diode circuit, which prevents dangerous overvoltage on any pulser component and keeps the average current very nearly constant. For prolonged short circuits, it is desirable either to turn off the pulser, or to change its output from high to low power. Since the largest current change resulting from a fault occurs in the shunt-diode circuit, a protective relay is used in this circuit. Also, a thermal relay was selected for this function because of its long operating delay. A restarting cycle will be introduced to increase the power-out in progressive steps until full power is achieved.

#### h. Pulse transformer

The pulse transformer is used to reduce the maximum working voltage that is necessary and makes the switching problem easier which results in weight saving, simplifies design and increases reliability. The pulse transformer in this modulator will increase the working voltage from 6 to 12 kv.

#### i. Pulse-forming network

The pulse-forming network serves the dual purpose of storing exactly the amount of energy required in a single pulse and discharging this energy into the magnetron in the form of a pulse whose shape is controlled by the magnetron's characteristics. The energy is stored in a combination of three inductances and capacitors to produce a pulse width of 1.0  $\mu$ sec. The rise time, overshoot, ripple and decay time will be controlled to generate the pulse shape that will contribute to maximum magnetron life, stability and spectrum output.

#### j. Pulse repetition frequency generator

The pulse repetition frequency (prf) is based on the range at which the radar is to be used. For this application, the range is 6000 mi with a 15 prf. These pulses will be generated by a free-running multivibrator (Fig. IV-7), the output of which will trigger the controlled rectifier into a conducting stage. This will permit the thyatron to conduct and discharge the energy stored in the pulse-forming network.

### 5. Solid-State Modulator

Recent developments in modulator techniques have resulted in solid-state modulators which operate without thyatron switching and are reported in Ref. 5. The thyatron is replaced by a combination of a controlled rectifier and transformers.

A basic pulse-modulator circuit is shown in Fig. IV-8. This modulator uses resistance charging and the capacitor  $C_1$  charges up to the line voltage. The hold-off diode prevents further discharge until the control device is triggered. During the charging cycle, the saturable transformer  $T_1$  is driven into saturation and only a negligible charge is transferred to the capacitor  $C_2$ . When the controlled rectifier is triggered, the energy stored in  $C_1$  is transferred to  $C_2$  through transformer  $T_1$  which now makes flux change. Like any magnetic "pulsator",  $T_1$  saturates again when  $C_1$  is discharged and  $C_2$  has reached its peak. Similarly, the energy stored in  $C_2$  discharges through a pulse transformer into the magnetron. One advantage of this modulator is its capability of operating from low voltage sources (20 to 100 volts) to produce a 12-kv pulse. Additional advantages are obtained by a reduction in weight and power consumption and an improvement in reliability.



All solid-state modulators have been developed and tested for radar sets using resonant charging and high pulse repetition frequencies (400 to 1000); however, no developmental information has been reported for low pulse repetition frequencies. This solid-state modulator concept is being investigated to determine its operational capability. Since it provides considerable savings in power consumption, weight and improved reliability its use is recommended if the operational requirements can be met.

## 6. Receiver

### a. General

The specifications of the receiver signal channel are:

Mixer (double-balanced)-- $K_a$  band, noise figure,  $F_N = 9.5$  db

IF amplifier-gain = 110 db

Bandwidth = 2.0 mc

Center frequency = 30 mc

Noise figure = 4.0 db

Local oscillator =  $K_a$  band, reflex klystron.

The specifications of the receiver AFC channel are:

Mixer (double-balanced)-- $K_a$  band

IF amplifier gain = 20 db

Bandwidth = 3.6 mc

Discriminator--these specifications will be determined by the frequency stability of the magnetron.

The preliminary design of the receiver has been chosen on the basis of immediately available components. It is realized that new components which will possibly become available in the near future would enhance the present design characteristics. However, it is felt that an adequate receiver system can be developed in three to four months (with consideration given to low power consumption, low noise figure, and light weight) using components currently available. Due to the desired lifetime of

the satellite system, it will be advantageous to use the components well below their maximum ratings. The required altimeter lifetime of one year would indicate that if transistors, for example, were operated at or near their maximum ratings, a degradation in reliability will occur.

b. Mixer

The signal channel mixer and the AFC channel mixer are to be incorporated in one double-balanced mixer. The two channels will consist of two 1N-53B microwave diodes each in a MA-531 double balanced mixer operated at  $K_n$  band. The isolation between the transmitter and the mixer will result in a power level of 1.0 mw delivered to the mixer. This power level is at a test frequency of 34,860 mc and the maximum overall noise figure of the diodes is 10.5 db. However, Fig. IV-10 shows that at this nominal operating frequency the noise figure can be reduced to 9.5 db. The system performance has been calculated using a noise figure of 10.5 db.

The two mixers, one for the signal channel and one for the AFC channel, receive their signal inputs through the duplexer and attenuator, respectively. Both of these mixers must get their local oscillator r-f power from the same source. It is desirable that the mixer should absorb as much of the signal power incident upon it as possible, otherwise reflected power is lost. However, with non-ideal components there must be some power lost in the form of VSWR. The VSWR ratio for this mixer (approximately 1.3) indicates a low absorption efficiency for this component.

The mixer crystal can withstand an input power of 1 mw. The r-f attenuator which is placed between the transmitter and the mixer must have a very large attenuation. This attenuation is computed to be 76 db, based on the peak output power of the magnetron of 40 kw. The attenuator essentially behaves like a high-pass filter, which passes the energy above its critical frequency. The critical or cutoff frequency will be slightly higher than the nominal transmitted frequency of 35,000 mc. At this frequency the attenuator will be small in size. This is due to the fact that attenuation in decibels is proportional to length of the element (in wave length) and this length is adjusted to give the required fraction of transmitted power to the mixer.

It may result that the second harmonics of the 30-mc IF frequency are large enough to work the AFC circuits, since the attenuator is a high-pass element. If this happens, then the local oscillator may be locked-on at a 15-mc interval instead of the 30-mc interval (for which the signal channel is designed). These harmonics are generated by the transmitter, local oscillator and crystal mixer. Transmitter

harmonics may be suppressed, before the AFC signal reaches the crystal, by the insertion of resistance strips, mode-dampening fins, or ferrets slugs into the attenuator. In the proper orientation and position in the guide, these act like low-pass filters in that the harmonics are attenuated more than the fundamental component in the transmitter pulse. However, using the double-balanced or "four-crystal" mixer, all harmonics of even order generated in the crystals are balanced out. Similarly, any troublesome TR leakage power and resultant transients are likewise balanced out. As the second harmonic is the only one with a large enough amplitude to affect the AFC lock-on, we shall not be concerned with the third harmonic and other higher order harmonics of the odd integer type (which are not taken care of in the balanced mixer). Even if the odd harmonics present a problem, these will be blocked out by the low-pass filter described above.

### c. Signal channel

The heart of the signal channel is the IF preamplifier and IF amplifier circuits. The overall signal receiver bandwidth has been selected as 2.0 mc on the basis of making a compromise between maximum signal-to-noise ratio and an allowance for frequency drift. The maximum practical signal-to-noise ratio is usually obtained at  $B = \frac{1.2}{\tau}$ . Thus, for maximum signal-to-noise ratio and  $\tau = 1 \mu$  sec, the bandwidth would be 1.2 mc. However, the long term operation of the system necessitates a consideration of circuit drift due to component aging. This is accomplished by deviating from maximum signal-to-noise bandwidth and increasing the bandwidth to 2 mc. It may be necessary that the bandwidth be reduced somewhat in conjunction with maintaining the gain and bandwidth requirements of the AFC IF-amplifier. It may also be noted, in defense of the wider bandwidth system (2 mc), that it costs very little in minimum detectable signal and affords the advantages of greater pulse fidelity and reduced criticalness in LO tuning and automatic frequency control.

In keeping with an overall system simplicity, it is advantageous to use synchronous single-tuned stages in the main IF amplifier as part of the preliminary design criteria. In addition to being a simple device, the single-tuned amplifier is the least critical of the general type amplifiers.

As identical single-tuned stages are cascaded, the overall bandwidth (measured between the 3-db points) goes down quite rapidly. The overall bandwidth is related to the number of stages of amplification by the following formula, (1)

$$\text{Overall bandwidth} = (\text{Bandwidth of 1 stage}) \times \sqrt{2^{1/n} - 1}$$

The values of the conversion factor  $\sqrt{2^{1/n} - 1}$  are given below, where n represents the number of cascaded stages.

n	1	2	3	4	5	6	7	8	9
$\sqrt{2^{1/n} - 1}$	1	0.64	0.51	0.44	0.39	0.35	0.32	0.30	0.28

The IF stages are essentially identical through the preamplification and postamplification circuits. Since the received signal is essentially of the same amplitude at all times, there seems to be no immediate need for automatic gain control circuits at any point in the amplifier. The omission of the AGC is one more step in the direction of simplicity of design. This is possible due to the fact that, for this particular application, the receiver is always at a fixed distance from the reflecting target (earth). This means that the echo signal is always at a fixed magnitude, hence there is no variation in received signal which might necessitate gain control. It is important to point out that using AGC with transistor amplifiers is not easily accomplished, due to the characteristics of transistors. That is, the absence of remote cutoff characteristics results in problems in controlling gain. Among these problems are signal-handling ability, range of control, and the sharpness of the transistor characteristic change as a function of control current (these factors are interrelated). Another factor is the low level of power in the control circuits. Additional problems are encountered due to the temperature sensitivity of transistors. However, in an effort to broaden the application of the altimeter for other space vehicles, it should be noted that some of these problems may be circumvented through the use of electrically controlled attenuators, having low minimum insertion loss and operating the transistors with fixed operating points. Although these problems are critical, it is felt that the development time would not be considerably lengthened if AGC was added.

- (1) The relationship used in the case of the AFC IF amplifier is an approximation to this exact formula and is more accurate as the number of stages is increased. Therefore, the conversion factor

$$\frac{1}{1.2\sqrt{n}}$$

could be used here in place of  $\sqrt{2^{1/n} - 1}$ .

#### d. Automatic frequency control

The automatic frequency control unit consist of three sections: (1) the IF amplifier, (2) the discriminator circuit, and (3) the d-c amplifier and sweep circuit.

##### (1) IF amplifier

The number of stages of amplification will be kept at a minimum in an effort to preserve bandwidth while maintaining an adequate level of amplification. To avoid degrading the overall receiver bandwidth below 2 mc, a 6 mc single-stage IF bandwidth has been selected. This bandwidth is wide enough to permit a sufficient number of stages for required amplification. The overall bandwidth of the amplifier is related to the number of stages and the single-stage bandwidth by the following formula:

$$\text{Overall bandwidth} = \frac{\text{Single-stage bandwidth}}{1.2 (n)^{1/2}}$$

where n represents the number of stages. From the above formula the maximum number of stages to be utilized for the AFC IF amplifier are computed:

$$n = \left[ \frac{\text{Single-stage bandwidth}}{\text{Overall bandwidth}} \right]^2 \times \left[ \frac{1}{1.2} \right]^2$$

$$n = \left[ \frac{6}{2} \right]^2 \times \left[ \frac{1}{1.2} \right]^2$$

$$n = 6.25$$

or the closest integer value less than the computed value which would be 6. Also the maximum number of stages to be utilized here without degradation of bandwidth below 2 mc would be 6. However, it turns out that 6 stages will not be necessary, as adequate gain is obtained from fewer stages of amplification. A trade-off between gain and bandwidth is necessary to facilitate best operation of the AFC circuit. The IF amplifier section will be built around 2N502 transistors (or equivalent) with an overall gain of approximately 20db. The number of stages of IF amplification will not exceed 2.

##### (2) Discriminator

The output of the IF amplifier is fed into a discriminator circuit whose peak-to-peak separation is approximately 2 mc. Since there

is some production variation in the maximum response frequency of the IF amplifiers and in the crossover frequency of the discriminator (due to manufacturing variations in the tuning coils and condensers), provisions are usually made for the ready shifting of the crossover point over a small interval, corresponding to the anticipated maximum departures from design center values. Preservation of the symmetry of the discriminator characteristics is of prime importance in the design and performance of the discriminator network. If the discriminator curve is asymmetrical, zero output is not produced at the crossover point but at some other frequency.

It is essential to the operation of the discriminator that the bandwidth of the preceding IF amplifier be broad enough so that the overall peak-to-peak separation is not decreased from the value determined by the main IF amplifier requirements. In other words, the IF amplifier must not "bottleneck" the discriminator bandwidth. This is why it is necessary to make the AFC IF bandwidth 3.6 mc, which is sufficiently large so that discriminator symmetry is unaffected. With an overall bandwidth of 3.6 mc, it can be seen (overall bandwidth equation) that a maximum of 2 stages of IF amplification are required. It should be noted that this is in sharp contrast to the 6 stages computed to be necessary for an overall bandwidth of 2 mc.

The detection of a change of frequency by the discriminator is accomplished by a transformer, which by special connections, distorts the frequency change into a varying voltage amplitude change. After distortion, the output voltage of the discriminator will be capacitor coupled to a two-stage video amplifier with low gain, which in turn feeds into a diode-phantastron control circuit. Solid-state diodes will be used in the discriminator.

### (3) DC amplifier and klystron sweep circuit

For AFC purposes, it is necessary that the control circuit have a self-triggering generator to start the sweeping cycle; which consists of a linear down-sweep of the plate voltage, followed by a quick recovery and a quiescent period while awaiting the next trigger. With the transmitter turned off, the phantastron plate will execute a series of saw-tooth downward sweeps, separated by moderately long recovery periods. When the transmitter is turned on, pulses appear at the discriminator output and the sweep will be stopped as soon as the discriminator crossover frequency is passed. At the same time positive pulses appear at the output of the discriminator video amplifier. These pulses are coupled to the shunt-diode detector and cause it to develop a negative voltage. As soon as the voltage across the diode becomes equal to the voltage on the phantastron control grid, the current flow in the input resistance ceases and the downward sweep of the plate therefore stops. Thus, the system is locked.

The sweep rate of the phantastron is given by

$$\frac{de_p}{dt} = \frac{E_c - e_g}{(R_c + R_1) C_1}$$

where

$E_c$  = cathode voltage, dc

$e_g$  = grid voltage, RMS (control)

$e_p$  = plate voltage, RMS

$R_c$  = shunt resistance across shunt diode

$R_1$  = input resistance to control grid

$C_1$  = coupling capacitor between control grid and plate.

The amount of voltage that appears on the oscillator repeller is a function of the output resistance divider and the sweep rate,  $\frac{de_p}{dt}$ .

The prime requirement of the control circuit is that the frequency shifts in the transmitter must be "followed" by the local oscillator with a sufficiently small time lag.

#### e. Ranging channel

The postamplification signal is taken from the receiver and fed into a ranging channel for the purpose of computing the range from satellite to earth. The counting circuit is initiated by a trigger pulse from the modulator. The incoming signal from the receiver will stop the counting element. Most of the counting circuitry (which includes a clock) will be incorporated as an integral part of the computer, which is carried in the vehicle. This computer is described in detail in another section of the report.

The entire receiving system has been designed on a preliminary basis with the idea of developing a prototype with state-of-the-art components and present circuit design technology. Simplicity, rather than complexity, is the paramount philosophy in the design of the whole system; therefore, this same idea has been followed implicitly in the receiver design.

## 7. RF Transmission System

The r-f transmission system will consist of standard microwave components which are commercially available and meet military specifications. A block diagram of the r-f transmission system is shown in Fig. IV-9. Representative components that may be purchased are listed below.

Directional coupler--Microwave Associates	Model 662
Duplexer with 35db AFC coupler--Microwave Associates	Model 1032A
AFC attenuator (36db)--Microwave Associates	Model 1023E
Double-balanced mixer--Microwave Associates	Model 531C
TR tube (tunable)--Microwave Associates	Model 5790
Load isolator--Microwave Associates	Model 156
Crystals (4)--JAN	IN53B
Local oscillator--Varian Associates	Model 97

All of the above components are required to produce an operating r-f transmission system with the exception of the directional coupler which is included for measuring transmitter power output during test and final checkout. A load isolator is inserted near the magnetron to isolate the magnetron from any load mismatch by absorbing power reflected back toward the magnetron. The benefits that are derived from the use of an isolator include improved magnetron spectrum, improved AFC performance, and reduction or elimination of magnetron pullings, moding, skipping and sparking.

The microwave assembly is capable of operating in the 34,500- to 35,200-mc region. The transmitting VSWR will be a nominal 1.20 and the receiving VSWR 2.00. The overall insertion loss will be approximately 3.0 db.

## 8. Antenna Design

The antenna is a paraboloidal reflector 48 in. in diameter. The operating frequency is 35,000 mc. The antenna will be designed to produce a uniform amplitude and phase distribution to obtain a maximum

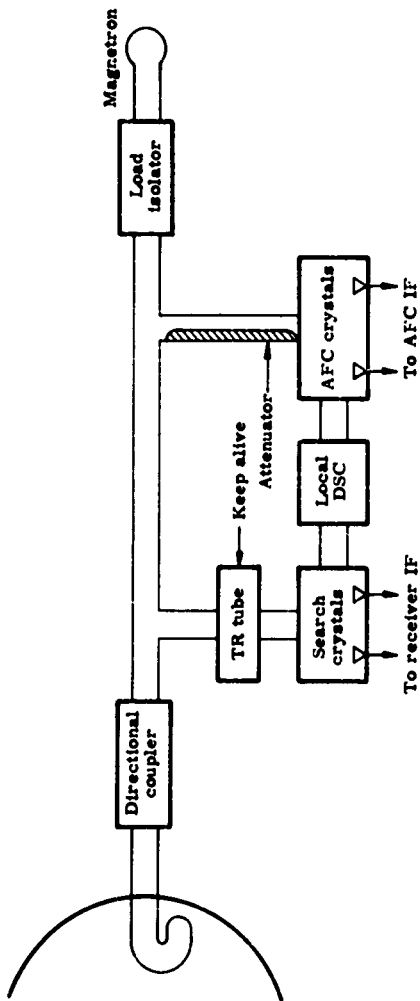


Fig. 9. Block Diagram of RF Transmission System

design gain of 50.3 db. The factors affecting gain will be given primary consideration in the design of the antenna. These factors are:

- (1) Dependence of the optimum angular aperture on the feed pattern.
- (2) Backlobe interference effect.
- (3) Phase-error considerations.

The beamwidth and side-lobe characteristics as well as the gain are related to the aperture field distributions. The antenna will be designed to maintain low side-lobe levels, with care given to the field distribution in regard to the discontinuity at the edge of the aperture. The antenna will have vertical polarization.

### 9. Radome

Radomes are usually installed for aerodynamic streamlining and protection from weather. These two factors do not exist for the radar altimeter when operated in space vehicles. The operation of a radar is considerably improved whenever it is not required to transmit through a radome. A radome adversely affects radar operation by absorbing some of the transmitted r-f energy incident upon it. Reduction in range results from attenuation of the transmitted and received signals. In extreme cases (if sufficient reflected energy finds its way back to the transmitter), total blanking of the receiver or severe range reduction can result. In addition, changes in the transmitted frequency due to pulling must be followed by the automatic frequency control (AFC) in such a way as to maintain a constant difference between them (the IF frequency).

Normally, the AFC is strong enough in the case of a relatively stable magnetron to follow larger frequency changes than those ordinarily produced by radomes. However, the AFC circuit involves a time constant that may be considerably longer than the interval required for the change caused by the radome reflection. Therefore, elimination of the satellite radome will permit full utilization of the radar range by elimination of radome attenuation losses (0.5 to 0.7 db). Also, elimination of radome reflections will contribute to more stable AFC and magnetron operation.

## 10. Conclusion

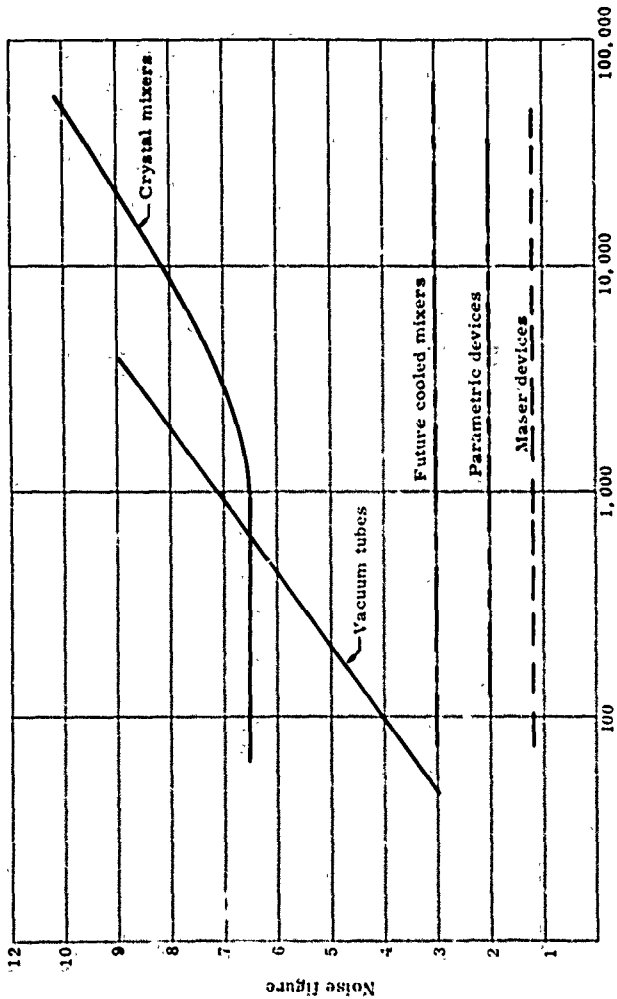
The  $K_a$  band radar described in this section was compared with the performance characteristics of  $K_u$  and X band systems. The  $K_a$  band radar was selected for this altimeter function because it produced the narrow beam width required to minimize the error caused by the antenna beam projected on the earth's curvature. The  $K_u$  and X bands would have required antennas with considerably larger diameters than the  $K_a$  band system. The  $K_a$  band provides the larger amount of gain for a given antenna diameter. The gain for a 48-inch antenna at  $K_a$  band is 50.3 versus 39 for X band. Also, backscatter gain from water is considerably greater at  $K_a$  band than at the other two bands. When compared to X band, this backscatter gain advantage is 10 db. However, receiver sensitivity at X band is usually 3 db greater than  $K_a$  band due to more sensitive crystals. (Fig. IV-10).

The selection and reliability of components at X band is admittedly greater than at  $K_a$  band because X band has been a popular frequency for airborne and ground-based applications. These components include the magnetron and r-f plumbing system. However, components and subassemblies affected by the choice of operating frequency such as the receiver, AFC (except the klystron) and modulator are not frequency sensitive nor do they favor either X or  $K_a$  band. Thus, the choice of frequency band is not restrictive as far as these components are concerned.

There is no apparent weight or power consumption advantage by using either frequency band because the component consuming almost all of the power and contributing the most weight is the modulator which is not frequency sensitive.

The length of time the magnetron will be operated in the transmitting mode is well below its rated lifetime. This short operating time should enable the magnetron to operate for the life of the satellite. The reliability of the entire radar system is analyzed in Section VI, Reliability Analysis.

The overall radar system error is a combination of the location of the target within the transmitted pulse duration and the delays inherent in the receiver system. The error contributed by the pulse width is 1.0  $\mu$  sec. The receiver delay is normally about 0.1  $\mu$  sec for IF amplifiers using tubes. For the IF amplifier, which will be using transistors, the IF delay may be as large as 1.0 to 2.0  $\mu$  sec. As a result of these combined errors, it is expected that the total



Frequency - MCS

Fig. 10. Crystal Noise Figures

radar system range measuring error can be as large as 0.3 mi. However, the overall range error cannot be accurately determined until the radar described in this report is built and the error measured. Once the receiver delay error and its characteristics are determined, it will be possible to compensate for portions of the error and thus obtain an error that is less than 0.3 mi.

The schedules for design, development, construction and testing of prototype models of this radar are discussed and shown in Section VII, Development Plan.

## B. IR HORIZON SENSOR

One method of determining the vertical direction from a vehicle orbiting the earth is to determine three or more points on the earth's circumference as seen from the orbiting vehicle. This can be done by locating the earth-space interface with one or more telescopes. If this determination is to be made both day and night, the visible portion of the spectrum cannot be used, and IR (infrared) sensors must be used. These are passive devices which detect the discontinuity between the cold space background (approximately 4° K) and the much warmer earth and its atmosphere (approximately 215° to 300° K). The total radiation from a perfect radiator (which the earth and its atmosphere closely approach) at 220° K is  $1.33 \times 10^{-2}$  watts per steradian field of view per  $\text{cm}^2$  of collecting surface, while that from a perfect radiator at 4° K is only  $1 \times 10^{-7}$  times this, or  $1.45 \times 10^{-9}$  watts/steradian/ $\text{cm}^2$ . Thus there is an enormous difference in radiation received as the earth's horizon is scanned. This enables the earth-space discontinuity to be located fairly accurately, so that the local vertical can be determined to an accuracy of about 10.1 degree.

An IR horizon scanner operating in the vehicle considered here, will be required to operate over a considerable range of environmental conditions. The unit must be flexible in its look angle capabilities since it is required to operate at altitudes of 300 to 6000 naut mi. The power requirements and reliability must be compatible with the one year operating life requirement. These requirements place somewhat contradictory demands upon the unit in that the variable altitude requirement indicates a need for a variable look angle or scanning detection system, while the operational life of one year in a space environment indicates that a system with a fixed field of view and no moving parts is desirable. The latter type of system, having no moving parts, might be expected to have both reduced power requirements and increased reliability as compared with scanning systems.

An IR horizon scanner observing the earth from a position outside the atmosphere is required to detect the earth as it appears against a 4° K space background and to discriminate the earth from the sun, moon and stars. In the case of these celestial bodies the following lists some of the major infrared sources as well as their approximate irradiances on the earth and their apparent temperatures.

<u>Celestial Body</u>	<u>Irradiance (w/cm<sup>2</sup>) 3 to 13.5 <math>\mu</math></u>	<u>Temperature (° K)</u>
Sun	$9.3 \times 10^{-2}$	5,300
Moon (full)	$1.6 \times 10^{-8}$	5,800
Saturn	$5 \times 10^{-12}$	5,800
Jupiter	$1.7 \times 10^{-11}$	5,800
Mars	$1.7 \times 10^{-11}$	5,800
Venus (at brightest)	$1.1 \times 10^{-10}$	5,800
Mercury	$1.1 \times 10^{-10}$	5,800
Sirius	$9.5 \times 10^{-12}$	10,600
Betelgeuse	$3.2 \times 10^{-11}$	2,810
Canopus	$4.5 \times 10^{-12}$	7,100
Antares	$3.4 \times 10^{-12}$	2,900
Arcturus	$3.3 \times 10^{-12}$	4,900
Aldebaran	$2.7 \times 10^{-12}$	4,300
$\beta$ Centauri	$1.2 \times 10^{-12}$	21,000

Except for the sun and moon it is obvious that very few of these bodies will be observed by a system having a sensitivity lower than  $1 \times 10^{-10}$  watts/cm<sup>2</sup>. If spectral filtering is included in the equipment, a further reduction in threshold sensitivity can be utilized. For the 5800° K sources, 92% of the energy is of wave length shorter than 1.8  $\mu$  and over 98% of the energy is of wave length shorter than 3.2  $\mu$ . For the coolest source listed above (2810° K), 64% of the energy radiated is of wave length shorter than 1.8  $\mu$  and 87% is of wave length shorter than 3.2  $\mu$ . On the other hand, of the radiation from the 300° K earth, only 0.02% is of wave length shorter than 3.2  $\mu$ . Thus a filter having a short wave length cutoff somewhere between 1.8  $\mu$  and 3.2  $\mu$  would have a negligible effect on the earth radiation received, but it would virtually eliminate the stars and planets as sources of radiation. Thus a sensitivity of  $1 \times 10^{-10}$  to  $1 \times 10^{-11}$  watts/cm<sup>2</sup> in the 2- to 13- $\mu$  region

appears adequate to ensure that only the sun and moon would be observed in the space background. However, the sun can be discriminated against by means of its brightness, and both the sun and moon can be discriminated against as a result of their angular size as seen from the orbiting vehicle. Calculations, to determine the sensitivity required to detect the earth with a reasonable field of view, show that  $1 \times 10^{-11}$  watts/cm<sup>2</sup> is in an order of magnitude more sensitive than is required.

The IR radiation received from the earth will consist of: (1) reflected and scattered sunlight, (2) emission from the earth as modified by atmospheric absorption and (3) emission from the atmosphere. The earth itself can be considered to be approximately a sphere with a polar radius of 3420.15 naut mi and an equatorial radius of 3441.73 naut mi; radiating as a gray body of high emissivity and a temperature near 300° K. The causing discontinuities, as the earth is scanned by an infrared telescope, will be hot sources and adjacent extended areas (which are either at different temperatures or which have a different emissivity at the spectral wave lengths received by the observing equipment). Examples of hot sources are forest fires, steel furnaces, missile launches and, to a lesser degree, extended structures heated either internally or externally to a temperature above the background. In the case of forest fires, the sources will be extended, and in the case of the lower orbit, this could fill the field of view. Such a source would have a characteristic temperature of 1000° F black body and could exceed the threshold level of the equipment by as much as three orders of magnitude. Steel furnaces and missile launches, although more intense (2000° to 5000° K), are physically much smaller and will not fill the field of view. In the case of a missile launch, the duration is short and any effect would be transient in nature. In either of the latter cases the change in energy would not be sufficient to be detected by the equipment, particularly if a filter having a short wave length cutoff (3 μ) is used.

Representative of the adjacent areas which are at different temperatures and/or which have different emissivities, are the water-land interfaces. Here, both can be extended sources and fill the field of view of the equipment. Under these conditions the minimum discontinuity which can be detected, the noise equivalent temperature (NET) of the system, is expressed

$$NET = \frac{1.11 T^2 T_A \sqrt{A_D}}{T_0 D^2 D^2 \rho^2 \sqrt{t_d}} \left[ \int_{\lambda_1}^{\lambda_2} \frac{H}{\lambda} d\lambda \right]^{-1}$$

where

T = Temperature of the source

- $T_A$  = Average atmospheric transmission  
 $A_D$  = Detector area, in  $\text{cm}^2$   
 $\epsilon$  = Emissivity of the source  
 $T_O$  = Average optical system transmission  
 $D^*$  = Specific detectivity of the detector, in  $\text{cm}(\text{cps})^{1/2}/\text{watt}$   
 $D$  = Collector diameter, in cm  
 $\rho$  = Angular resolution, in radians  
 $t_d$  = Dwell time of the detector on one resolution element  
 $H_\lambda$  = Spectral radiance of the source, in  $\text{watts}/\text{cm}^2/\text{cm}$   
 $\lambda$  = Wave length variable.

The actual NET of a particular system will not be computed until later when the system parameters have been determined. However, it can be seen from the equation that observed temperature discontinuity can be an actual temperature difference, a difference in emissivity, or a combination of both. Furthermore, the actual value of temperature difference, on the ground which would be observed, will vary with atmospheric transmission and the relative contribution of earth radiation and atmospheric radiation (as modified by the selective absorption of the atmosphere). It is evident that discontinuities, of sufficient magnitude to be detected, can exist at earth-water interfaces and can provide observable signal fluctuations. Therefore, it is necessary to make the system sufficiently insensitive so as not to detect these discontinuities.

The black body radiation from the earth will be modified by the atmosphere through which this radiation passes. The atmospheric absorption bands are dependent upon the constituents of the atmosphere. At the lower altitudes these include:  $\text{N}_2$ ,  $\text{O}_2$ ,  $\text{CO}_2$ , Ne, He,  $\text{H}_2$ , Xe, Ra,  $\text{CH}_4$ ,  $\text{N}_2\text{O}$ ,  $\text{O}_3$ ,  $\text{SO}_2$ ,  $\text{CH}_2\text{O}$ ,  $\text{I}_2$ ,  $\text{NH}_4$ , CO, HDO,  $\text{H}_2\text{O}$ , NO, OH and  $\text{NH}_3$ . Of these,  $\text{CO}_2$ ,  $\text{H}_2\text{O}$ ,  $\text{N}_2\text{O}$  and  $\text{O}_3$  are of major importance in the absorption and reradiation of infrared energy at wave lengths to  $20 \mu$ .

The black body IR energy radiated from the earth is absorbed at selected wave lengths by these constituents of the atmosphere and reradiated at wave lengths and intensities representative of the temperature and pressure of the absorbing gas. This results in some spectral

bands of energy (radiated by the earth) being passed with minimum attenuation (so-called atmospheric "windows") while other bands of energy are totally absorbed. In the latter spectral bands, the energy received by the equipment outside of the atmosphere will have the form of black body radiation of the altitude temperature where the atmosphere is viewed as opaque. For the principal water absorption bands, this will be at an altitude near the tropopause (for a standard atmosphere this corresponds to an altitude of approximately 36,000 ft, with an apparent temperature of 215° K). For other absorption bands this apparent temperature will vary depending on the viewing angle, which determines the apparent altitude at which the atmosphere becomes opaque. If the altitude is 36,000 to 82,000 ft, the temperature will be near 215° K. For lower level clouds, the radiation from the earth will be absorbed or reflected and the radiation observed from above will have the characteristic of the clouds temperature (which may be assumed to be that of the adjacent air). Thus the thermal radiation observed from above will have an apparent temperature which can be expected to vary from ground temperature to 215° K.

At the shorter wave lengths, reflected sunlight is a most important source of observed energy. This energy may be reflected from the surface of the earth or from clouds and particles in the atmosphere. In all cases it will have the radiation characteristics of a 6000° K black body, as modified by the intervening atmosphere. At wave lengths longer than  $3\ \mu$ , the sunlight reflected from clouds will be reduced by an order of magnitude from the peak value.

Thus, in summary, an IR altitude control unit must detect and locate accurately the discontinuity between a 4° K background and a 215° to 300° K black body at three or more points about the periphery of the body. The precise position of the discontinuity detected can lie at the edge of the earth or in the atmosphere, depending on the weather and threshold sensitivity and spectral band of the equipment. The maximum altitude of the observed discontinuity for the spectral band of interest will be near the tropopause, except for high altitude clouds. In the standard atmosphere the tropopause is at 36,089 ft, but in extreme conditions the actual altitude can be as high as 10 mi (comparable in height with the maximum altitude of cumulus clouds). Thus the maximum error in the local vertical, resulting from the uncertainty as to the location of the discontinuity, is less than 0.2 deg for the 300-mi orbit and approximately 0.05 deg for the 6000-mi orbit.

#### 1. Current Systems

The IR horizon sensors currently developed are as follows:

- (1) Scanners which sweep a 360 deg path and determine the position of the center of the pulse, resulting from scanning the

earth. By using two such scanners (sweeping the earth in perpendicular directions) the local vertical can be established. An example of this type of scanner is the Barnes Model 13-200, which was used on the Tiros satellite. Somewhat the same general principles are used in the Barnes Models 13-100, 13-132 and 13-142 horizon sensors, and the ITT scanner. (1) (2)

- (2) Scanners which sweep a cone, the instantaneous field of view being displaced from the vertical by an angle corresponding to the angle subtended by the radius of the earth for the altitude of operation. The vertical is determined when the sweep is tangential to the earth and does not cut across the horizon discontinuity (i.e., the Advanced Technology Labs scanner for the Discoverer satellite). (3)
- (3) Horizon sensors which scan a limited sector about the horizon, detect the discontinuity, and then center the scan so the line of sight is directed to a point on the horizon. When the information from a minimum of three such units is processed, the local vertical can be determined (i.e., the Barnes Model 13-160 sensor). (4)
- (4) Fixed optical systems which use multiple detectors to center the position of the earth.

The advantage of class I systems above is that the initial relative position of the earth need not be accurately known. In one axis, the earth can have any relative position, while in the other two axes, it is only necessary that the earth be viewed sometime during the sweep. Errors or variation in altitude change only the pulse length of the signal to be processed, with no mechanical repositioning of the optics required. The disadvantages of such a system include: (1) the necessity of using two such equipment and (2) the inclusion of any necessary sun protection should a detector be used which would be damaged by viewing the sun, or which has a long recovery time and which requires a large field of view and/or very broad spectral coverage to provide necessary

- 
- (1) Horizon Sensors for Vertical Stabilization of Satellites and Space Vehicles, M. H. Arc and M. M. Merlen, Proc Nat Specialists Mtg on Guidance of Aerospace Vehicles, 25 to 27 May 1960.
  - (2) Attitude Reference Devices for Space Vehicles, P. E. Kendall and R. E. Stalcup, Proc IRE 48 (4) 765.
  - (3) Horizon Scanner for Discoverer, M. D. Ewy, Proc IRIS 5 (1) 233.
  - (4) All Altitude Horizon Sensor System, Barnes Engineering Company Report BEC-4241-SRI, 2 September 1960.

sensitivity. Since calculations show that a narrow spectral band is inadequate, the equipment will accept wave lengths which could be generated by earth discontinuities, and data processing must be such as to minimize the resulting errors. Such equipment has been built and flown.

Of extreme importance in equipment of this design is the requirement that a spinning motion be maintained for the period of operation. Not only does this require continuous input power but the mechanical problems of providing seals and lubrication in a space environment indicate questionable reliability in a satellite with a one year operational life. Moreover, some of the advantages of this type of system is lost by vehicle restrictions with regard to the directions in which the sensors can look.

The class II systems require either high accuracy in initial positioning of the satellite or a variable look angle. One such scan technique is to increase the look angle from a fixed angle until a signal is obtained or a maximum angle is reached. If no signal is received then the angle is decreased until a signal is received from sweeping across the edge of the earth. The local vertical is then determined by orienting the axis of scan and the offset angle so the sweep is tangential to the earth. If the orbit is elliptical this variation in scan angle must be continued or the errors will increase. For the low altitude orbit a change in altitude of 40 mi would reduce the obtainable accuracy by approximately 0.50 deg unless the scan angle is adjusted. For a perfect circular orbit this would be unimportant but the mechanical problems of continuous operation discussed above are applicable.

The class III systems have the advantage of combining a reasonable search capability, permitting error in initial positioning of the vehicle, with high accuracy of vertical determination ( $\pm 0.1$  deg) while maintaining a minimum limitation on the variation in usable altitude. After acquisition, thermal discontinuities across the earth will be outside the field of view and will not introduce inaccuracies. Since a small angle oscillating scan can be mechanized using a tuning fork vibrator technique the difficulty of continuously spinning a mirror is eliminated. The major disadvantage of this type system is the requirement for at least three sensor heads and the necessity of providing appropriate mounting and field of view for each.

The class IV systems use a fixed array to maintain the image of the earth centered and thereby provide a reference for the local vertical. These systems are limited as to flexibility in altitude and accuracy. Unless sophisticated optical techniques are utilized, considerable "blurring" of the edge of the image can occur. One approach to overcome this source of error has been the use of a reflecting cone optical

system, the so-called "inside out scanner" <sup>(5)</sup> which increases the usable look angle of the equipment. Since no mechanical scanning is used some provision such as electronic switching must be used to provide an easily amplified signal thus maintaining the most important advantage of such a system, its lack of moving mechanical parts.

In summary, a scanning system, class I, would be adequate for a short life satellite where initial positioning accuracy is not possible. As the operational life requirement is extended the question of power and reliability becomes increasingly doubtful. For a long life fixed altitude orbit a fixed array or multiple fixed field-of-view sensors appear more desirable. If high accuracy and a variable altitude orbit are involved a system of sensors capable of being continuously pointed at the horizon and capable of tracking the horizon is required. For the trajectory of interest it appears that a horizon scanner of multiple sensors similar to those discussed under class III above would offer the most promise.

## 2. Recommended Detector

The type of detector to be used in an IR sensor depends to a large extent upon the magnitude and spectral distribution of target and background radiation. Radiation from the earth, assumed to be at a temperature of about 300° K, peaks at a wave length of about 10 $\mu$ , with 1/4 of the energy at shorter wave lengths. For high altitude clouds, assumed to be at a temperature of 220° K, the radiation peaks at about 13 $\mu$ . Less than 0.01% of the radiation from a 300° K body and less than 0.0001% of the radiation from a 220° K body occurs at wave lengths below 3 $\mu$ . It therefore seems desirable to use long wave length detectors even though they may be several orders of magnitude less sensitive than shorter wave length detectors.

The detectors to be used for this application must be operated uncooled because of space, weight, power and reliability requirements. Uncooled detectors which could conceivably be used include lead sulfide, PEM indium antimonide and thermistors. Lead sulfide cuts off at about 3 $\mu$  but has the highest detectivity of any IR detector; PEM indium antimonide cuts off at about 6 $\mu$  but has a far lower detectivity; and thermistors are generally made to be sensitive to about 15 $\mu$  but have a still lower detectivity. In weather when the ground can be seen or in overcast weather in daytime, both lead sulfide detectors and thermistors should be suitable. Because of their long wave length capability, however, thermistors should be suitable under some weather conditions when lead sulfide is not, and therefore only thermistor detectors have been considered in the calculations below. No attempt has been made to optimize the spectral band used. Preliminary calculations show,

---

<sup>(5)</sup> Inside-Out Horizon Scanner, J. Kilpatrick, Proc IRIS 6 (1), 195.

however, that no narrow spectral band device is suitable, and the broad region from 3 to 15 $\mu$  has been used. No consideration has been given here to the problem of an irradom except to allow for its transmission losses; to the scanning mechanism; or to the data processing.

Assuming that the limiting noise of the system is detector noise, which seems quite reasonable for space backgrounds, the signal-to-noise ratio is given by the expression

$$S_N = \frac{\left(\frac{\pi D^2}{4}\right) \left(\frac{\lambda_T}{\pi R^2}\right) \int_{\lambda_1}^{\lambda_2} T_{A\lambda} T_{O\lambda} R_{\lambda} H_{\lambda} d\lambda}{\left(\frac{\sqrt{A_D}}{L^{**}}\right) R \sqrt{\Delta f}}$$

where

- D = Diameter of collecting optics (cm)  
 $\lambda_T$  = Instantaneous field of view of detector (cm<sup>2</sup>)  
 R = Distance from detector to radiation source (cm)  
 $T_{A\lambda}$  = Spectral atmospheric transmission  
 $T_{O\lambda}$  = Spectral optical system efficiency  
 $R_{\lambda}$  = Spectral responsivity of detector (volts/watts)  
 $H_{\lambda}$  = Spectral radiant energy at source (watts/cm<sup>2</sup>/μ)  
 $A_D$  = Detector area (cm<sup>2</sup>)  
 $\Delta f$  = Bandwidth of electronics (cps)  
 $D^{**}$  = Hemispherical D\* of the detector (cm-(cps)<sup>1/2</sup>/watt).

Neglecting atmospheric transmission since in this case radiation from the atmosphere is considered in the absorption bands, assuming  $T_{O\lambda}$  and  $R_{\lambda}$  to be independent of wave length over the spectral region considered, and making the substitution  $\lambda_T = \rho^2 R^2$ , where  $\rho$  is the angular resolution of the system in radians, we get the expression

$$S_N = \frac{D^2 D^{**} \rho^2 \Gamma_0 \int_{\lambda_1}^{\lambda_2} H_{\lambda} d\lambda}{4 \sqrt{A_D} \sqrt{\Delta f}}$$

Assume a type c scanner having a mirror that oscillates through  $\pm \alpha$  deg at a rate of N cps, so that the line of sight moves  $\pm 2\alpha$  deg or  $8\alpha N$  deg/sec. If the field of view is  $\rho$  radians, the average dwell time of the detector on each resolution element is

$$t_d = \frac{\rho}{8\alpha N \times 0.01745} \text{ sec.}$$

If the frequency bandwidth is made the reciprocal of this we get

$$S_N = \frac{D^2 D^{**} \rho^{5/2} T_o \int_{\lambda_1}^{\lambda_2} H_{\lambda} d\lambda}{4 \sqrt{\lambda_D} \sqrt{8\alpha N \times 0.01745}} = \frac{D^2 D^{**} \rho^{5/2} T_o \int_{\lambda_1}^{\lambda_2} H_{\lambda} d\lambda}{1.5 \sqrt{\lambda_D} \alpha N}$$

The collector diameter D is limited by the weight and space limitations of the system. A diameter of 3 in. or 7.62 cm, has been assumed. The resolution  $\rho$  should be as large as possible in order to get as high a signal-to-noise ratio and as long a dwell time as possible. A large  $\rho$  means that the ratio of detector size to focal length must be large, and for a detector of reasonable size and a fixed collector size, the value of  $\rho$  is limited by the minimum f/number that can be used. For this application, a detector size of 0.2 x 0.2 cm and a resolution of  $1 \times 10^{-2}$  radian is considered. This gives an f/number of 2.62, which is reasonable, a focal length of 20 cm, and for an N of 30 rps, a dwell time of about 2.4 ms which is about equal to the average thermistor time constant.

For simplicity, the sky and ground radiation has been divided into four spectral bands, the 3- to 5.5- and the 7.5- to 13- $\mu$  bands in which the radiation is assumed to originate at the ground or lower atmosphere and is approximated by a 280° K black body; and the 5.5- to 7.5- $\mu$  and 13- to 15- $\mu$  bands in which atmospheric absorption and emission are high and therefore the radiation is assumed to come from the high altitude atmosphere, approximated by a 220° K black body.

$$\begin{aligned} \int_{3.0}^{5.5} H_{\lambda} d\lambda &= 5.46 \times 10^{-4} \text{ (watts/m}^2\text{)} \\ \int_{5.5}^{7.5} H_{\lambda} d\lambda &= 2.85 \times 10^{-4} \\ \int_{7.5}^{13} H_{\lambda} d\lambda &= 116.0 \times 10^{-4} \\ \int_{13}^{15} H_{\lambda} d\lambda &= \frac{13.32 \times 10^{-4}}{= 137.63 \times 10^{-4} = 1.38 \times 10^{-2}} \end{aligned}$$

Using these values,  $D^{**}$  of  $10^7$  and  $T_o$  of 0.6, we get

$$S_N = 29.2$$

This is sufficiently high to show that the system considered, though not optimized, would give very good results as far as signal energy is concerned.

The NET of the system considered, using the formula previously given and the system parameters above, is  $0.332^\circ$  K. This is far less than the mean ground temperature fluctuation of about  $1.5^\circ$  K, indicating that temperature variations on the earth itself could be seen. The system must be made less sensitive in order that only the earth-space interface will be seen. This can be done most easily by decreasing the collector diameter or narrowing the spectral bandwidth.

There is available at the present time an infrared horizon sensor of the type required for this application. It is the Barnes Engineering Company Model 13-160 Horizon Sensor. The sensor head consists essentially of a germanium-immersed thermistor detector having a field of view of  $0.50 \times 3$  deg; an oscillating mirror which moves the instantaneous field of view back and forth through  $\pm 2$  deg at a nominal rate of 30 cps; and a tracking mirror which moves through 70 deg at a rate of 12 deg/sec to locate the earth-space discontinuity. Three or four of these sensor heads are used with an electronics unit to form the complete attitude sensor. The tracking mirror of each head is driven by a motor so as to center the oscillating field of view at the earth-space discontinuity. A voltage is picked off a potentiometer driven with the tracking mirror, and for the three-sensor system the voltages from these three potentiometers are combined to give two error signals from which pitch and roll errors can be derived. If four sensor heads are used they can be connected in such a way as to give a three-sensor system with a redundant head for improved reliability or as a four-sensor system which gives roll and pitch errors directly.

This unit has not yet been flown or thoroughly tested. However, one unit has been bench tested continuously for more than six months to date without failure. The company has built hundreds of IR horizon sensors of other types, some of which have flown in satellites, so they are well aware of many of the problems to be encountered. Nevertheless, reliability estimates based on parts lists and known component failure rates indicate for the three-head device a failure rate in excess of three per year. The four-head device without redundancy would be even less reliable, so that a four-head unit used as a three-sensor unit with redundancy is suggested at this time as the type of attitude control system to be used. The four sensor heads of the Barnes unit weigh four lb each and the electronics package 7 lb. Assuming a modified electronics package to take care of the redundant sensor would weigh an additional

2 lb, the total weight of the unit would be about 25 lb. The average power required is approximately 6 watts at 24-v dc and the maximum power 10 watts. The accuracy of determination of the local vertical is  $\pm 0.1$  deg.

A block diagram of the system is shown in Fig. IV-11, while Figs. IV-12 through IV-15 illustrate detailed portions of the design as well as critical elements of system logic. Figure IV-16 illustrates the mechanical layout of the system.

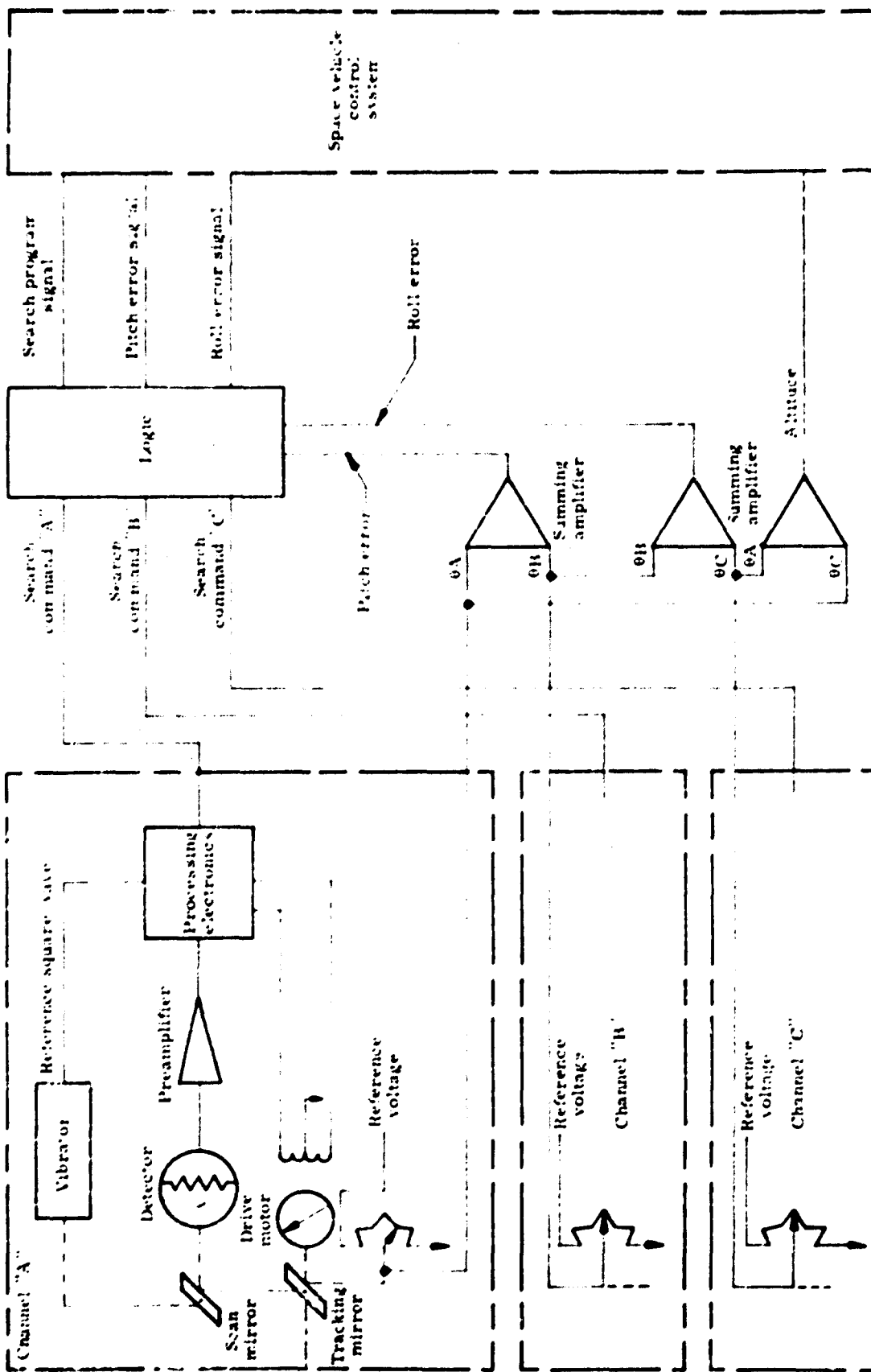


Fig. IV-11. System Functional Block Diagram

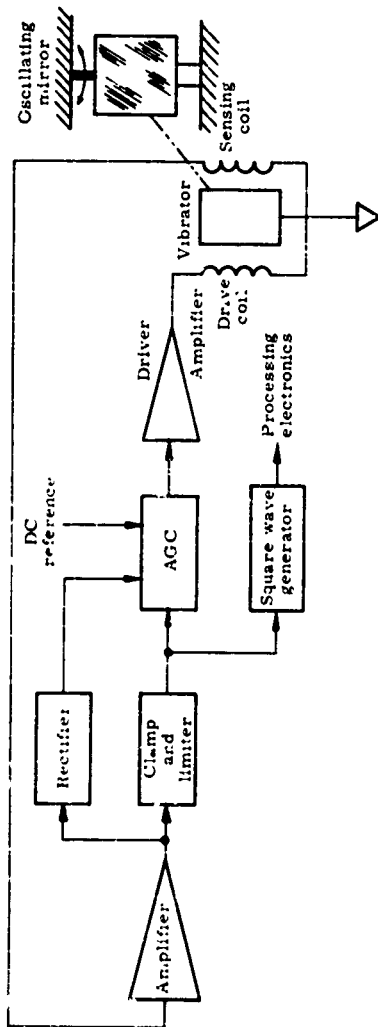


Fig. IV-12. Vibrator Electronic Control System--Block Diagram

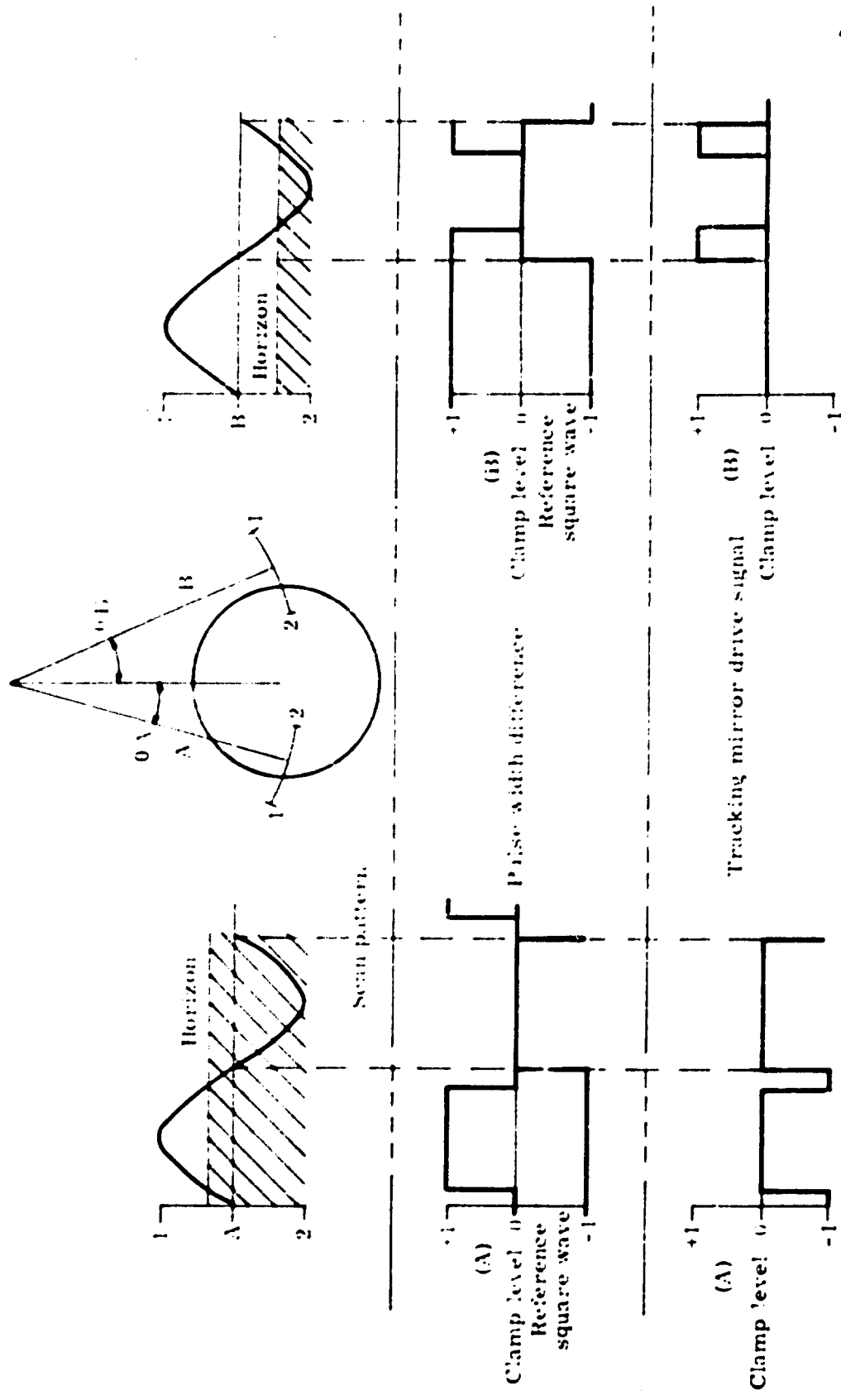


Fig. IV-13. Tracking Mirror Position Sensor Waveforms

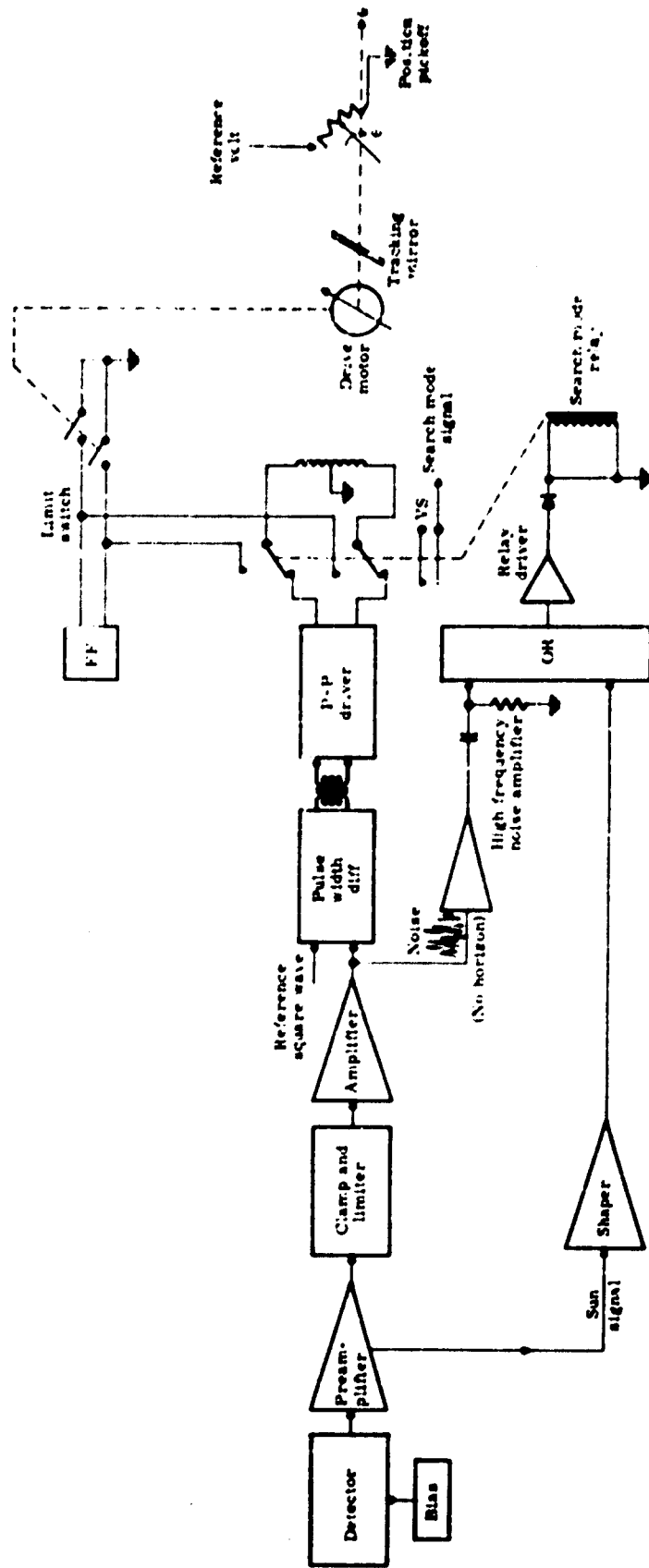


Fig. IV-14. Sensor Processing Electronics--Block Diagram

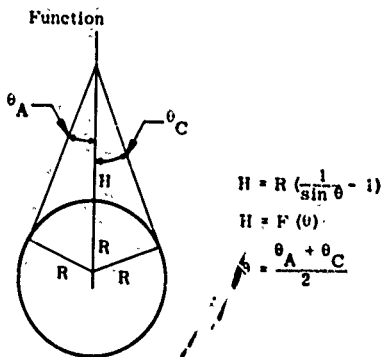
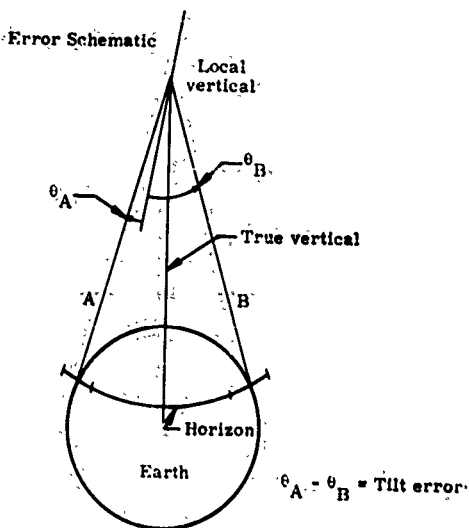


Fig. IV-15. Altitude Error and Function

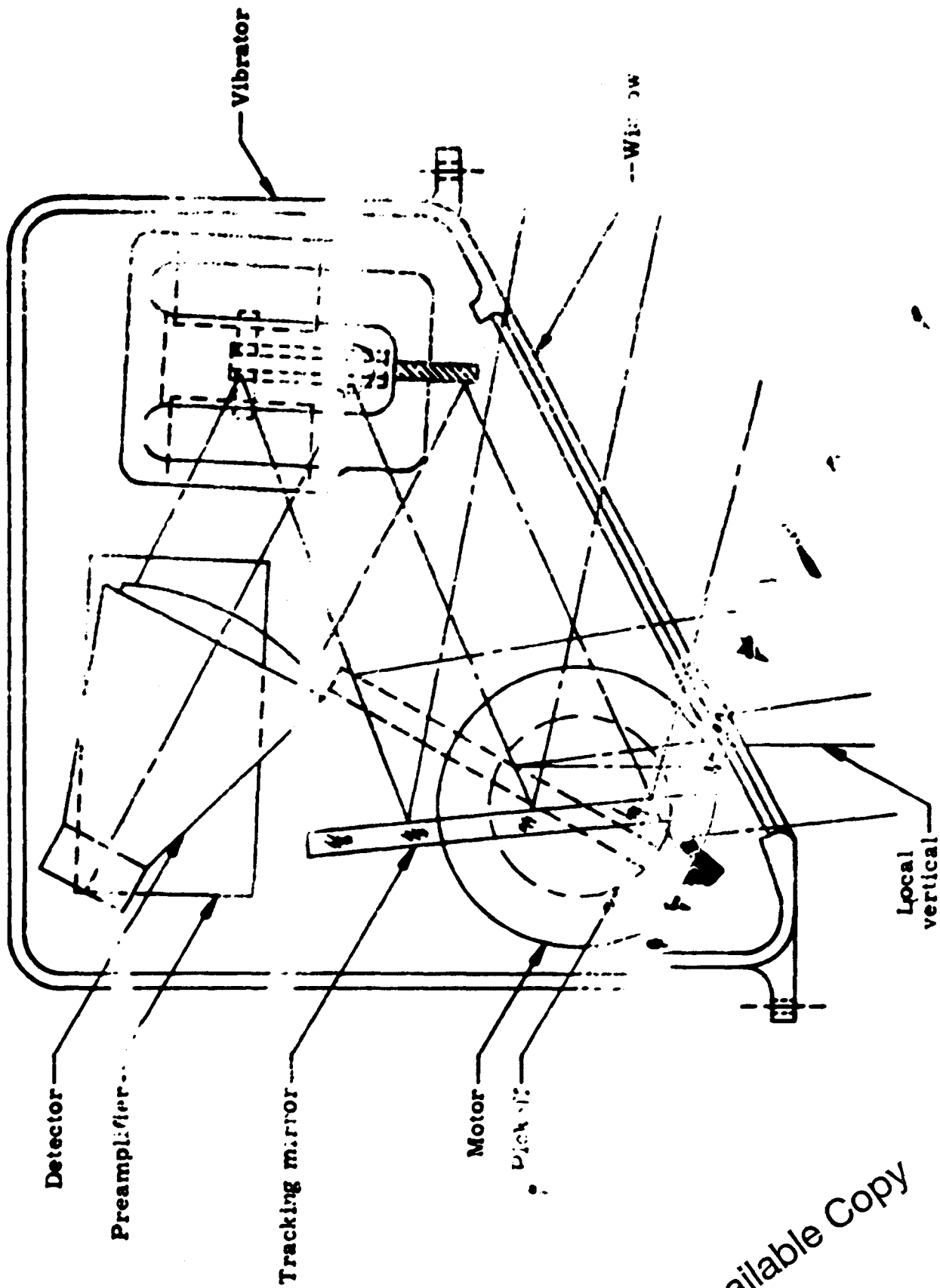


Fig. IV-16. Horizon Sensor

Best Available Copy

### C. OCCULTOSCOPE--STAR TRACKER

An orbit program which is preset on the ground prior to launch is stored in the self-contained guidance system. The stored "ideal" orbit pattern is compared by on-board equipment to determine vehicle orientation and, should corrective action be required, the thrust impulses are activated (see Fig. IV-17).

Two major sensing instruments supply data for orbit computation.

- (1) The radar altimeter measures orbit-distance from earth and supplies the following computation data:

$e$  = eccentricity  
 $a$  = semimajor axis  
 $t_p$  = time of perigee.

- (2) The star tracker provides:

(a) Celestial orientation coordinates.

(b) Occultation time data, which permits the computation of orbit orientation elements in inertial space:

$i$  = inclination of orbit  
 $\omega$  = angle in orbital plane between ascending node and perigee  
 $\Omega$  = angle in equatorial plane between reference direction and node.

#### 1. Initial Alignment

While the vehicle is on the launching pad, the occultoscope-star tracker platform is aligned and locked on to a preselected reference star pattern (i.e., the platform is caged in the orientation, which it will require during launch to lock on to the reference stars).

During countdown the platform servos are "slaved" to the inertial platform in the booster stage and an opaque protective dome is closed over the occultoscope-star tracker platform.

During the boost period, this platform remains aligned to the stars under the dome by receiving alignment signals from the inertial platform.

After separation of the booster and leaving the earth's atmosphere, the dome opens and the platform begins to align itself by tracking the

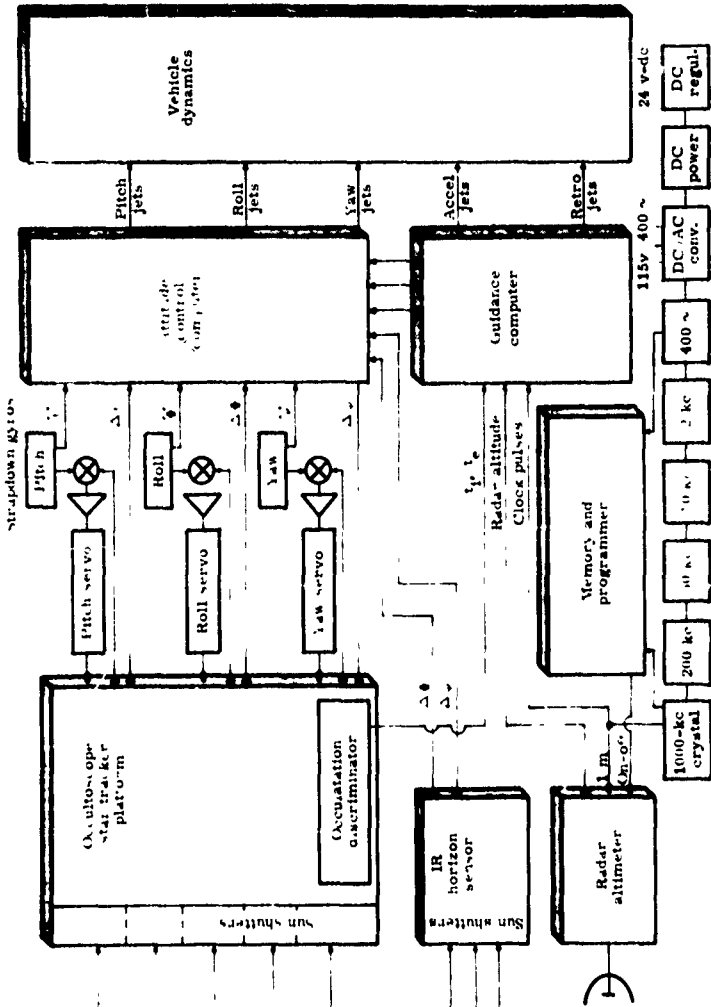


Fig. IV-17 Occultoscope Star Tracker Block Diagram

preselected star pattern. Errors in alignment during launch will remain small enough to keep the telescopes within their acquisition angles.

## 2. Equipment Description

The occultoscope-star tracker consists of an array of five telescopes, each one locked on to one particular star on the celestial sphere. This telescope platform is gimballed in the nose of the vehicle and aligns itself in inertial space (regardless of vehicle position and attitude) with three geared servo drives.

### (a) Orbit axial tracking

Two of the telescopes are oriented toward stars in the vicinity of the axis of the orbit, which will be called the left axial and the right axial (or pivotal) telescopes. Each telescope tracks a given star to an accuracy of 10 seconds of arc in a field of view of two degrees. The photo detectors supply orthogonal error signals (left/right or yaw; clockwise/counterclockwise or roll) to the platform servo, which in turn orients the platform for optimum alignment. This platform error signal is the average of the two error signals from the two axial telescopes.

### b. Orbital plane tracking

Three of the telescopes are locked on to stars approximately in the orbital plane and roughly 120 degrees apart in stellar space. Platform alignment in the pitch axis will be controlled by the average of the error signals from these telescopes. The averaged pitch error signal will command the pitch servo to realign the platform.

### c. Occultation time measurement

This measurement is obtained by recording the instant at which a star dips into the horizon of the earth. This horizon includes the earth's atmosphere, where the dip would be very gradual due to the diminishing air density in the upper atmosphere (see Fig. IV-18). Considerable refraction in the line of sight between the telescope and the reference star takes place during the transition of the horizon. This will result in an "off center" signal from the occulted star, as compared to the undisturbed orientation of the two other telescopes. As the star dips into the atmosphere, the apparent tracking error increases steadily. A preset angle limit (20 seconds of arc) will be chosen to obtain a sharply defined condition to trigger the occultation time recorder. This time is called the "ingress" of the vehicle entering the "shadow" of the star behind the earth. The "egress" of the vehicle from the shadow (or reappearance of the star on the telescope sensor) will supply another time mark, resulting in three ingress and three egress time signals (see Fig. IV-19).

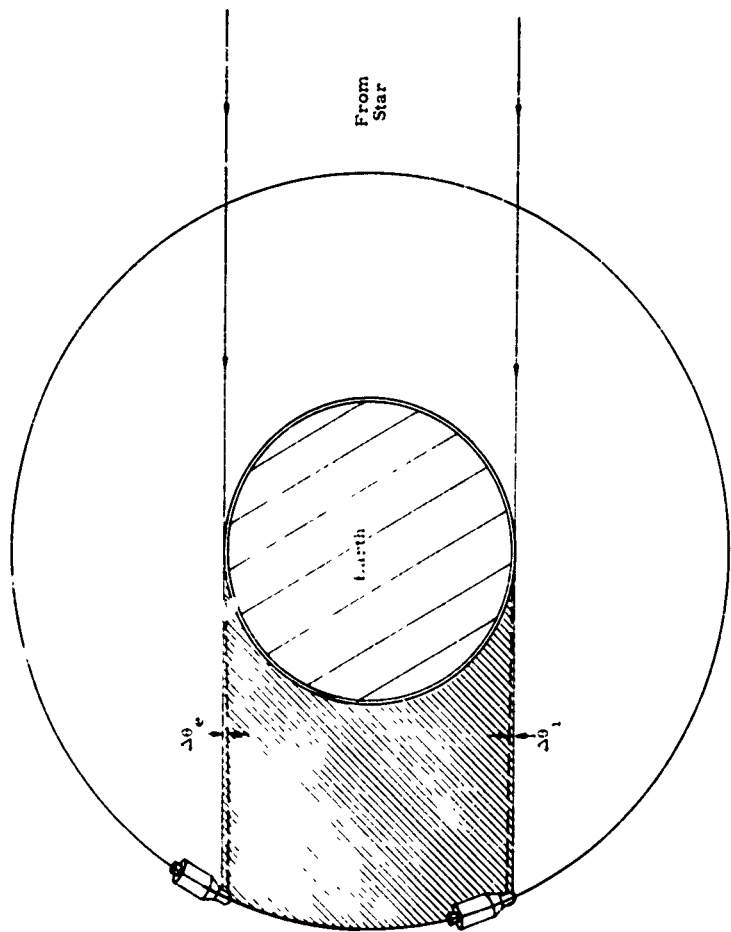


Fig. IV-18. Atmospheric Refraction During Occultation

### 3. Sun-Shutter

If sunlight should fall on a telescope and reach the sensitive detector through a 2-in. lens, the detector would be destroyed. To protect the detector, a 1/4-in. ID tube (blackened inside) is mounted alongside each telescope, containing a cadmium sulfide photoconductor cell (RCA type 7412 or equivalent). If sunlight falls on the target of this photocell, it triggers an Eccles-Jordan flip-flop transistor circuit, and a relay will rotate an opaque vane into the light path of the star detector, shielding the sensitive cathode from excessively intense illumination.

Simultaneously, the flip-flop circuit sends an inhibit command to the occultation sensing circuit to avoid the generation of a false occultation time signal by the sun-shutter.

### 4. Star Detectors

Photomultiplier tubes are the most sensitive detectors in the visible spectrum available today, and are generally used in astronomical work. The occultoscope (as proposed by General Mills) and other star tracking instruments use nine-stage photomultiplier tubes of the 1 P21 type or similar.

The photomultiplier is a delicate glass structure, requiring a closely regulated supply voltage of approximately 1000 vdc. The output varies sharply with changes in supply voltage, ambient temperature affects sensitivity and noise factor.

A sensitive photovoltaic detector with a Gallium-Arsenide junction has become available from Philco Corporation, designated Type GAU-401, and is claimed to equal or exceed the sensitivity of photomultiplier tubes. It is housed in a TO-18 transistor case, measuring less than 0.25 in. diameter and less than 0.25 in. length.

The spectral sensitivity ranges from 0.40 to 0.90 $\mu$  and peaks at 0.85 $\mu$  which offers good coverage of the light emitted from most bright stars.

It was therefore decided to use the new Philco GAU-401 photodetectors, with a corresponding improvement of the star tracker reliability, and less space requirement.

### 5. Redundancy and Reliability

The configuration of star-tracking telescopes is chosen in such a way that redundant reliability is obtained if one or even two of the telescopes should fail.

- (1) Should failure of one of the axial telescopes occur, perfect space reference would still be maintained with the orbital telescopes providing sufficient reference.
- (2) Should failure of one of the orbital-plane telescopes occur, perfect platform alignment would be maintained. During occultation of one of the remaining two stars, the other telescope will supply sufficient tracking data.
- (3) If a position with one telescope aimed at the sun should occur, the sun-shutter on this telescope will insert an opaque shield in the light path well before the illumination level becomes excessive.
- (4) If the moon should occult one of the stars used as reference, no adverse effects will be experienced, except a temporary loss of this star's signal. If the moon should be half or fully sun-illuminated at the time, the star telescope will put out a steady-state signal (rather than the pulse resulting from scanning the point-sized star). This steady-state signal will be ignored by the occultation time discriminator.
- (5) Pitch and roll error signals can augment the horizon sensor to stabilize vehicle attitude and hence provide redundant operation for maximum reliability.

## 6. Mechanical Design

The five telescopes are rigidly mounted on a drum which can rotate 360 degrees in pitch to allow continuous star orientation while the vehicle goes through a 360-degree attitude rotation during each orbit (Fig. IV-20).

The two axial telescopes are mounted in the 2-in. diameter bores of the pitch axis bearings, and can be oriented up to 10 degrees away from the orbital axis. One of these bearings carries a slip-ring assembly to bring electrical connections in and out of the platform, while the other carries the realignment servo drive and pickoff synchro.

A fork-shaped gimbal carries the drum bearings and is supported in a single (but long) bearing at the rear to provide roll-axis rotation; the roll axis alignment servo is mounted here with 45-degree freedom. Electrical connections are brought out through flexible leads.

The gimbal design of a celestial platform differs from that of an inertial platform in that the conventional full-ring gimbals must be cut down if a wide-angle field of view is required. A "dead zone" of less than 60 degrees pitch field-of-view to the rear of the vehicle is desirable for occultation time measurements. Occultation of the telescope (by vehicle structure) occurs once in every orbit (for 60° of orbit). An inhibit command is given during this period to prevent generation of a false occultation signal.

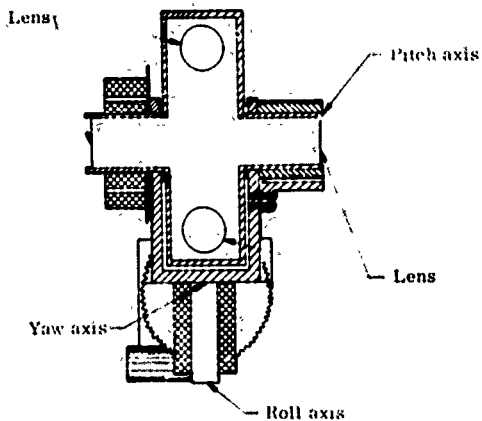
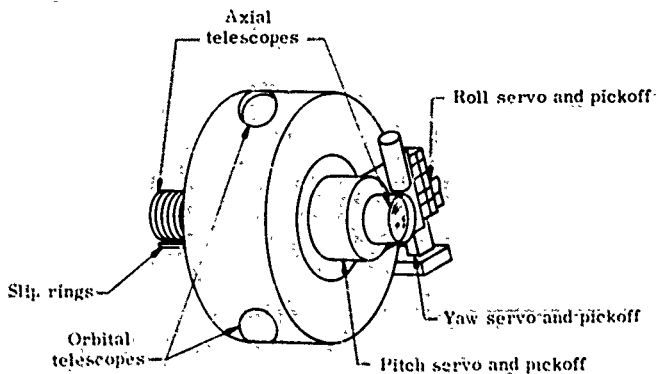


Fig. IV-20, Oculoscope-Star Tracker

**TABLE IV-1**  
**Some Data of Typical Bright Stars**

No.	Name	Visual Magnitude	Temperature (°K)	Effective Flux (watts/cm <sup>2</sup> )	
				$10^5 (0.3 \text{ to } 3.6\mu)$ $\times 10^{-12}$	$10^5 (0.3 \text{ to } 13.5\mu)$ $\times 10^{-12}$
1	Sirius (α Canis Majoris)	-1.60	11,200	1.92	9.46
2	Mica (α Ceti) (variable)	1.70	2,340	1.80	6.16
3	Betelgeuse (α Orionis) (variable)	0.92	2,810	3.15	5.15
4	Canopus (α Carinae)	-0.82	6,206	1.55	4.45
5	Antares (α Scorpii)	1.22	2,900	1.88	3.38
6	Arcturus (α Bootis)	2.24	3,750	1.72	3.28
7	(α Crucis)	1.61	2,810	1.67	2.73
8	Aldebaran (α Tauri)	1.06	3,110	1.64	2.70
9	Rigel Kent (α Centauri) (double)	0.01	4,700	1.16	2.61
10	Capella (α Aurigae)	0.21	4,700	0.95	2.17
11	Vega (α Lyrae)	0.14	11,200	0.39	1.91
12	Rigel (β Orionis)	0.34	13,000	0.71	1.66
13	(β Gruis)	2.24	2,810	0.94	1.33
14	Procyon (α Canis Minoris)	0.48	5,450	0.56	1.45
15	Achernar (α Eridani)	0.60	15,000	0.23	1.37
16	(β Hydras) (variable)	3.6	2,250	0.85	1.36
17	Pollux (β Geminorum)	1.21	3,750	0.70	1.34
18	(β Centauri)	0.86	23,000	0.26	1.18
19	Scheat (β Pegasi)	2.61	2,810	0.66	1.09
20	Mirach (β Andromedae)	2.37	2,980	0.62	1.02

Best Available Copy

The roll-alignment bearing is supported by a vertical shaft which can be servo rotated  $\pm 45$  degrees in a bearing mounted on the vehicle frame to provide yaw axis alignment. An identical servo drive maintains orientation, and a synchro resolver supplies yaw-error signals to the attitude computer.

	<u>Pitch</u>	<u>Roll</u>	<u>Yaw</u>
Degrees rotation range	360 deg	$\pm 45$ deg	$\pm 45$ deg
Electrical connections	Slip rings	Flex leads	Flex leads
Usable field of view	300 deg	90 deg	90 deg
Pickoff angle	Synchro	Synchro-resolver	Synchro-resolver
Occultation pickoff	Yes	None	None
Sun-shutters	Yes	Yes	Yes
Slits, scanning	1, on orbital scopes	1, on axial scopes	1, on axial scopes

#### 7. Occultoscope-Star Tracker Components:

The platform will contain the following components:

<u>Components</u>	<u>Qty.</u>
Lenses, achromatic, radiation-resistant glass 2-in. diameter, 8-in. focal length	5
Vibrating slit assemblies with driving coils	5
Photodetectors Philco Type G.U-401	5
Resistors, deposited film type 1/4 w 1%	10
Capacitors, 0.01 mf/600 volt ceramic	10
Sun-shutter:	
Photocells (cadmium sulfide) RCA No. 7412	5
Transistors, NPN silicon, medium power	10

<u>Components</u>	<u>Qty.</u>
Relays, miniature DPDT with vane attached	5
Miniature servo motors, 24-volt, 400 cycle, 2 phase	3
Worm gear assemblies	3
Synchro transmitter	1
Synchro resolvers	2
Slip-ring assembly (10 ring) 2-in. ID, 1.5-in. long	1
Gimbal assembly, 3 gimbals	1
Preamplifiers, 3 NPN transistors each	5

## 8. Time Standard

### a. Precision quartz-crystal oscillator

A self-contained precision time standard must be carried in the satellite to supply time signals for the:

- (1) Radar altitude echo-time clock.
- (2) Orbit programmer.
- (3) Digital computer clock pulses.
- (4) Radar altimeter sequence timer (to turn radar altimeter on only over water).

Because of the requirement of self-contained operation, resetting of this timer (to correct for drifts) is not possible. This makes it necessary to include a time standard of the highest stability, and solid-state amplifiers only should be used. Precision crystal oscillators have been developed (for example, by Peter G. Sulzer of The National Bureau of Standards), and with the most advanced temperature controls were reported stable to 1 part in  $10^9$  (short term drift), and 1 part in  $10^8$  with aging. The James Knights Company, Sandwich, Ill., manufactures a 1-mc (Model FS 1100T) frequency standard, transistorized, with drifts of less than 1 part in  $5 \cdot 10^{-10}$  per day.

### b. Atomic clock

For precision navigation satellites, still higher stability may be required, and the most stable self-contained time generators known today (atomic clocks) would have to be considered. Stability of 1 part in  $4 \times 10^{11}$  has been obtained in laboratory atomic clocks, and an airborne version of the "Atomichron" (National Radio Co., Malden, Mass.) yields an overall long term stability of 1 part in  $10^9$  within airborne environmental conditions.

The nuclear magnetic resonance of cesium gas at approximately 9192.632 mc, is the frequency-determining element, and is reproducible as a primary standard, if gas purity, temperature and magnetic fields are controlled.

To avoid the need for frequency-synthesizer equipment, a direct fraction of 9192.632 mc would be used, such as 16.415 or 1.03 mc.

The National Radio "Airborne Atomichron" weighs 65 lb and consumes 250 watts of power. It is equipped with vacuum tubes.

A satellite version of the Atomichron will be available in 1962 with a weight of 25 lb and power consumption of 80 watts. Transistors will be used throughout, except for two electronic tubes at the highest frequencies. An all solid-state atomic clock is under development at National Radio Co., which will use no electron tubes and consume less than 30 watts.

Frequency standards using nuclear magnetic resonance are also produced by IIT Federal Laboratories and Varian Associates.

### c. Frequency dividers

The 1-mc frequency standard (1.03 mc, if an atomic clock should be used) will serve as a source of clock pulses, both for the digital computer and the radar altimeter. This corresponds to approximately 0.1-mi altitude increments.

The dc-to-ac converter (400 cps) will be governed by the frequency standard through a chain of frequency dividing multivibrators. They consist of transistors, resistors and capacitors, and are resonated with L-C elements for highest reliability. Stages of 200, 50, 10, 2 kc and 400 cps are chosen to keep the step ratio at 5:1 or smaller.

This 400-cps precision frequency ensures precise programming of the radar altimeter on-cycles and orbit computations. Accuracy of the occultoscope-star tracker and of the horizon sensor will also be improved with a precise 400-cps source.

### 9. Programmer and Memory

In order to establish and maintain a precision orbit for a duration of one year or longer, the following information must be stored in the vehicle prior to launch:

- (1) Precision timing source (described elsewhere).
- (2) Radar altitude demand storage.
- (3) Occultation demand storage.

In addition, for practical reasons, the radar altimeter must be turned on only when over water surfaces in order to avoid errors from high altitude lakes, ore deposits, etc. This will be performed by the:

- (4) Radar altimeter transmit-programmer.

For short term (one or two orbit cycles) data storage, an "electronic scratch pad" is required to store individual radar altitude and occultation time data:

- (5) Electronic scratch pad.

### 10. Radar Altitude Demand Storage

A matrix of miniature ferrite cores (square loop material), connected with straight enameled copper wires, serves as the memory unit for altitude demand. The number of "bits" (clock pulses) required for the planned orbit is "written" into the matrix prior to launch.

The IBM Corporation has recently developed new types of cores, which permit nondestructive readout; this will greatly simplify the construction of the memory system. Therefore, it is proposed to make use of these cores if their thermal and long-term stability proves to satisfy the environmental and life requirements of the mission.

The use of thin-film memories and epitaxially deposited silicon diode logic can be considered for applications in the coming years. This would reduce size, weight and cost, eliminate matching of cores and increase reliability.

### 11. Occultation Demand Storage

A similar ferrite core memory, as described under radar altitude demand storage, will store the occultation time demands. While the radar altitude demand consists of a number of bits (or an arithmetic

quantity), the occultations consist of single pulses with precisely preset hour-long intervals containing the information between them.

This storage system must also allow nondestructive readout for one year or more.

### 12. Radar Altimeter Transmit Programmer

This is a conventional timer, presetting intervals for a given ground track, so that the radar transmits only over sea level water.

The use of a ferrite core memory appears feasible, but a conventional synchronous motor, camshaft and precision switch combination is less complex and can be made very reliable with proper design.

Two 400-cps synchronous timer motors with gear trains (with periods somewhat longer than the orbit period) are coupled to the camshaft through one-way clutches. Redundancy is achieved because, in case of one motor's failure, the remaining unit continues to rotate the shaft. The motors (A. W. Haydon Inc.) contain lightweight aluminum rotors with negligible moment of inertia. Hermetically sealed precision switches (Haydon Switch, Inc., Series 8102 or similar) will operate reliably for the low duty cycle of this application. Cams can be of the fixed-notch type to avoid possible loosening of adjustable parts.

After completion of each orbit, the cam is advanced to the starting position. This action is required if orbits of other than full-hour periods are chosen.

### 13. Electronic Scratch Pad

The Radio Altimeter readings (six or more per orbit) and occultation times (three per orbit) must be stored in a memory until they are compared to the demands stored in the program unit. Again a miniature ferrite core matrix will be used, but in this case, the conventional (destructive-readout) type can be applied in a "scratch pad" write, read and erase mode.

As an alternative, a rotating magnetic disc-type memory might be considered. Laboratory for Electronics, Inc. (L.F.E.) manufactures Bernoulli Disc memories with storage capacities of 25,000 to 500,000 bits per disc. The Type BD-40 was developed especially for space applications and stores 40,000 bits in 40 tracks, with a resolution of 1024 bits per track circumference.

#### D. THE COMPUTER

Examination of the equations in Section III has shown that the airborne computer requirements will not be difficult to satisfy. The computer selected is a small, lightweight, general purpose digital machine. This computer is designated the B-4 Guidance Computer, and is currently being developed by the Librascope Division of General Precision, Inc. A detailed description of the computer (provided by Librascope) is given in Table IV-2 and the following portions of this section.

TABLE IV-2

##### B-4 Guidance Computer Characteristics

Computer type: General purpose, high speed integrator (Sigmatron), digital

Precision: One part in  $2^{23}$

Number base: Binary

Mode of memory operation: Word parallel, random access

Number of different operations: 40

Memory type: Random access, nondestructive, silicon stack

Instruction type: Two address (operation address and next instruction location)

Memory capacity: At least 6000 words

Word length: 23 bits

Clock frequency: 0.64 mc/sec

Size: 0.37 cu ft

Input/output equipment possible: Variety of analog devices

Multiplications: 2000 per sec

Divisions: 500 (minimum) per sec

Additions: 12,800 per sec

Sine and cosine: 160 per sec

TABLE IV-2 (continued)

Flip-flop count: 30 in general purpose unit  
 20 in high speed integrator

Power requirements: 60 watts (10 watts when not computing)

Operating temperature: -25° C to +103° C

Weight: 19 lb

The nature and quantity of registers follows:

Temporary storage	-5	} 256 words
Word address	-1	
Instruction address	-1	
Accumulator	-1	
Pulse accumulator	-1	
Integrand register	-1	
Clock	-1	

## 1. Computer Description

### a. Word length

The computer word length is 23 bits. Error analysis indicates that a double precision product in multiply is indicated for space guidance requirements.

### b. Address structure

The 6000 words of memory are selectable with the 23-bit word structure. Ten bits specify the word address of the present instruction. The next 10 bits provide the next word address location. The remaining 3 bits specify the desired instruction.

### c. Arithmetic and control logic

The computer general purpose section will now be considered. The Functional Block Diagram for the Random Access Computer is shown in Fig. IV-21. The computer handles memory access in parallel via an M (Memory) register. Accumulator (AC), Multiplicand (MC) and Multiplier (MR) registers are provided for storage of numerical data. The instruction, Order and Control Registers served to provide internal (tacit) computer operation. The schematic details of the Logic portion of the B-4 Random Access Computer are shown in Fig. IV-22.

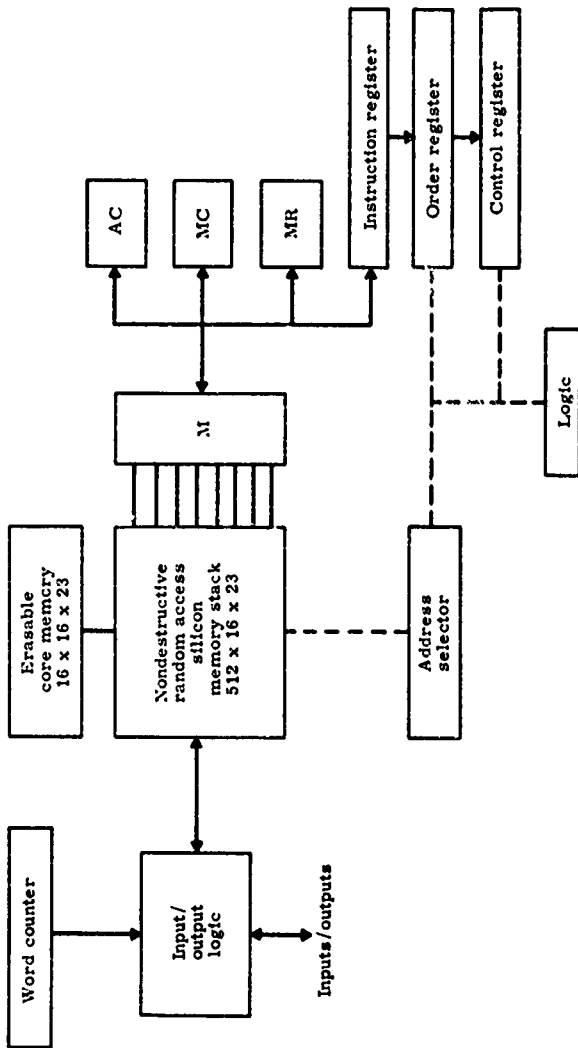


Fig. IV-21. Functional Block Diagram for Random Access Computer

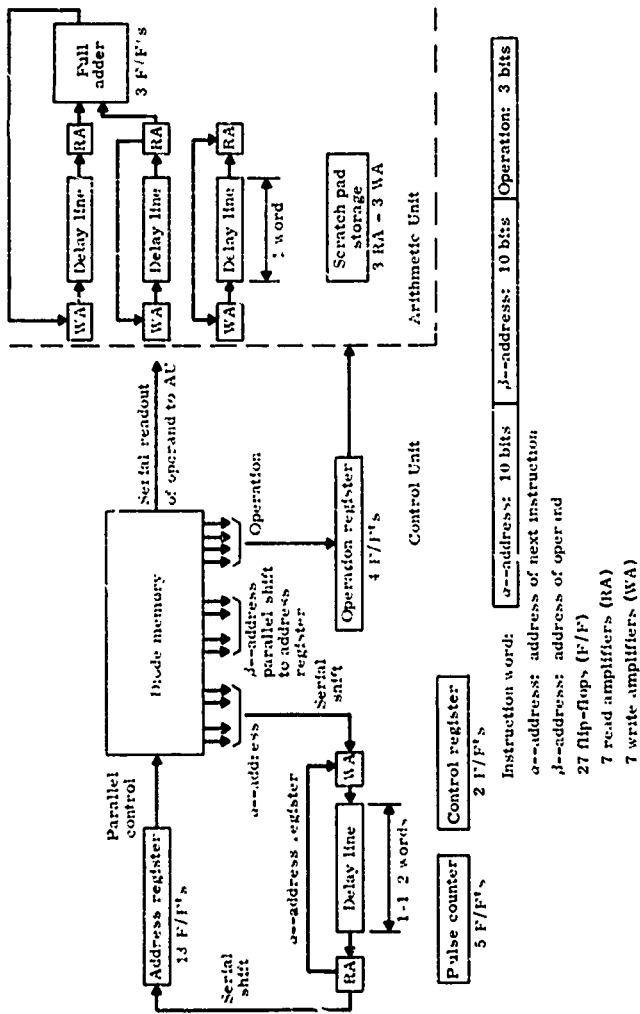


Fig. IV-22. Random Access Computer Logic Schematic

The order structure contains 8 basic orders which are expandable to 40 as discussed in programming. These orders are multiplication, addition and related operations. They are performed at 2000 and 12,800 per sec, respectively, including random access time which is zero.

Multiplication is one of the most frequently encountered operations in the boost stages of a space computation. A fast, accurate multiply is provided. Truncation errors are minimized for sum-of-products and square roots operations. Double-length product accumulation is provided. The operation is mechanized in part by sensing the next higher order of the multiplier while performing either an addition or shift on the present multiplier position.

Operations are performed by permanently wired programs stored in the silicon memory. These also include sine-cosine, division and square root. The program is permanently stored and not destroyed by reading. The internally wired logic and control program reliability govern the computer performance of each instruction.

#### d. Incremental, discrete and input/output functions

A valuable input involves what may be referred to as a high speed integrator, stigmator. High speed summing, storing and processing of incremental inputs are possible from external sources. Real time velocity pulse accumulation for computation, accurate time and/or velocity countdown, control of digital-to-analog converters for information output, and transmission of data link information are typical applications of the high speed integrator.

Operations performed in the input unit are of the incremental type. The design includes four basic units: integration, fast accumulator, velocity accumulator and countdown integrator.

The integrator processes data from the velocity accumulator, from analog-digital inputs, and from the computer. It has complete access to the computer generating time countdown accumulated for thrust termination. Incremental integration can be performed at the rate of 24,000 pps, but is limited by thrust g's and accelerometer resolution.

#### e. Control

##### (1) Switches

Discrete signals are transmitted to the computer by means of externally controlled switches. As a part of the program routine sensing of these, switch positions may be programmed to effect a control or logic change in program flow.

## (2) Outputs

Where an analog shaft position from digital conversion is involved, servo modules are employed. Typical outputs of this type include switching signals to the engines from the computer. The servo modules are sealed and include a servo amplifier, a modulator, a motor generator, a potentiometer, digital-to-analog converter code discs and gear trains for positioning of the potentiometer by the motor.

Outputs from the computer are in the form of positive or negative error voltage representing the sign of the differences between present and desired value of the output. When there is no difference, null is reached and the output voltage is zero. The error voltage is modulated to a 400-cycle signal and fed to the servo amplifier motor combination which provides a shaft position output. The output is thus a shaft position which can be coupled to a synchro transmitter or potentiometer. A digital feedback loop is provided via the computer.

Torquing signals are generated by these digital-to-analog converters. The analog voltage is provided by the slider of a 10,000-ohm center-tapped potentiometer in the converter.

Discrete signals are generated by computed program. These signals may include: (1) main engine cutoff, (2) vernier (booster) cutoff and (3) reorient (sustainer) cutoff. When received by the outer control-loop programmer, these discrete signals control various powered flight phases.

### i. Sine and cosine generation techniques

Incremental sine-cosine generator can be installed as shown in Fig. IV-23.

#### (1) Features:

- (a) Iteration rate: 1600/sec
- (b) Retractable sine and cosine generation no-fix points
- (c) Accuracy assuming maximum roll, pitch or yaw rates of 1 radian per sec is  $6 \times 10^{-4}$  for the generation of 4 sines and 4 cosines.

#### (2) Algorithm:

$$\sum_{i=1}^n Y_{1i} \Delta x_i - \sum_{i=1}^n K_{1i} \Delta Y_{3i} + C_1 = 0$$

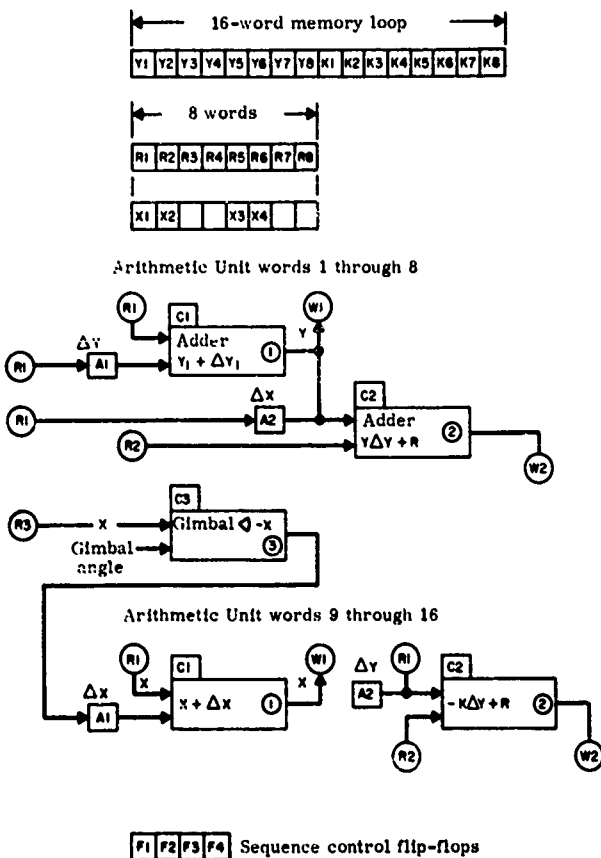


Fig. IV-23. Block Diagram of Incremental Sine-Cosine Generator

$$\Sigma - Y_{31} \Delta X_1 - \Sigma K_1 \Delta Y_{11} + C_2 = 0$$

where  $Y_1$  might be  $\sin \theta$  and  $Y_3$ ,  $\cos \theta$  and  $\Delta x_1$  the increment in  $\theta$ ,  $C_1$  and  $C_2$  are corrections which make the remainders exact during each iteration so that the sine-cosine generation is retraceable.

(3) The sine-cosine generator contains:

- (a) One 16-word memory loop
- (b) Two 8-word memory loops
- (c) Two full adders (1) and (2)
- (d) One subtractor (3)
- (e) Eleven flip-flops as shown in diagram
- (f) Three sense and 3 write windings (S1) (S2) (S3) and (W1) (W2) (W3).

(4) The sine-cosine generation works as follows:

- (a) The sines and cosines are broken down into pairs; i. e.  $Y_1$  and  $Y_3$  become sine and cosine for one argument;  $Y_2$  and  $Y_4$  for the next argument, etc. To each pair of  $Y$ 's is associated a pair of  $K$ -scaling constants  $K_1$ ,  $K_3$ , etc. These are stored on (1) 16-word recirculating memory loop as shown.
- (b) To each  $Y$  and  $K$  there is associated (1)  $R$  which is used to accumulate the partial sums  $Y_1 \Delta X$  and  $-K \Delta Y_2$ , etc.
- (c) The memory for the  $8 \Delta Y$ 's is in the first 8 bits of the  $Y$  integrand word. The remainder of the word is used for the integrand.
- (d) The first 8 bits of the remainders  $R_1$  are used to store the arguments  $\Delta X_1$ .
- (e) During words 1 through 8, the  $Y$ 's are updated in the adder labeled (1) and remainders are updated in the adder (2). Adder (3) compares the gimbal angle with the argument to generate the  $\Delta X$ 's.
- (f) During words 9 through 16, the adder (1), as shown, updates the argument; adder (2) corrects the remainders  $R$  according

to  $-K\Delta Z + R \text{ old} = R \text{ new}$

- (g) All argument changes are stored in the first 8 bits of the R words.

g. Table "lookup"

Table "lookup" was examined for possible use to determine both the sine and cosine of a given angle. Since the B-4 Computer has the capability of transferring information directly from the accumulator to the instruction register, it can be seen that the gimbal angle itself, once read into the accumulator, could act as its own instruction and select both the value of the sine and the cosine from a stored set of numbers. Since the "silicon memory stack" is used to hold the range of values for the trigonometric functions, table "lookup" would be a feasible method of getting sines and cosines. In this case 512 words of 9 bits each would give sine and cosine to angular increment of 0.175 degree at a rate of 1600 per sec.

h. Interpolation formulas

This technique would use a slower basic solution of the sine and cosine value using polynomials and then use a formula such as:

$$\Delta \sin \theta = \cos \theta \Delta \theta$$

to update the value of the sine  $\theta$  between basic solutions. Of course the basic solution rate is dependent upon the maximum rate of change of  $\theta$  and the accuracy required. The following shows how much computer time is saved using this technique:

- (1) Forty basic solutions per sec require 0.12 sec per sec to be used to generate one sine and one cosine to an accuracy of  $10^{-4}$ .
- (2) Five basic solutions per sec and 35 interpolated solutions per sec require only 0.056 sec per sec.

1. Telemetry module

The use of telemetry inputs to the computer provides a valuable means to:

- (1) Communicate with the earth the results of space-borne computations and data reductions, especially in the case of a one-way mission.

- (2) Accept control changes from the earth as a result of earth-derived decisions.

The computer can instrument a mission change if (1) at a given time no telemetry is received and (2) a computer routine for this contingency exists. The typical information rate in such a case is 200 bits/sec for 2.5 ms.

## 2. Random Access Nondestructive Memory

In the interest of providing:

- (1) An advanced technique permitting a more reliable, compact computer.
- (2) Nondestructive, random access memory.

a proven laboratory component is proposed. The large nondestructive, random access memory is to be a "Silicon Memory Stack" supplemented by a feasible, erasable 256-word core memory.

### a. Matrix construction

As shown in Fig. IV-24 (Silicon Diode Sheet), the complete silicon diodes are deposited in 8-mil diameter areas and spaced 8 mils apart. This permits about 64 diodes/linear in. or 3600/in.

By using proven thin-film deposition techniques as developed in Librascope's Applied Research semiconductor group over the past three years, the equivalent to Fig. IV-25 (Silicon Diode Matrix Schematic) can be fabricated employing a combination of proven techniques.

Figure IV-25 also illustrates pictorially the assembly technique. Vertical gold busses, 0 to 3, cross horizontal gold busses, 0 to 2. As shown, the 0-0, 2-0, 1-1, 3-1, 0-2 and 2-2 junctions are silicon-diode connected. The remaining junctions are insulated silicon monoxide.

The matrix is built up of insulating, basic silicon. The basic pure silicon is processed to form a p-n junction. Typical junctions are formed by heating, bombardment and related semiconductor techniques. The required p-type, anode material is formed by adding impurities such as iridium, boron or other Group III elements. In like manner, n-type, cathode material is formed by adding impurities in the Group IV family such as arsenic or phosphor.

Gold buses, p-type silicon, n-type silicon and silicon monoxide are sequentially integrated in a manner well known in thin-film and cryogenic development. The entire matrix is encapsulated in an inert epoxy-glass resin.

The forward-to-back resistance of these silicon diodes has been tested at  $10^6$  ohms. At 30 volts of reverse bias and 150° C, 30  $\mu$ a of

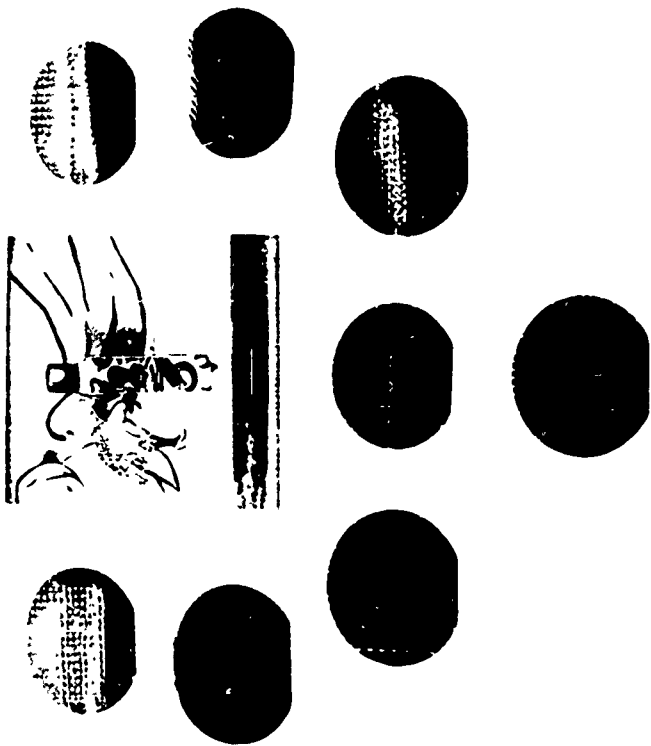
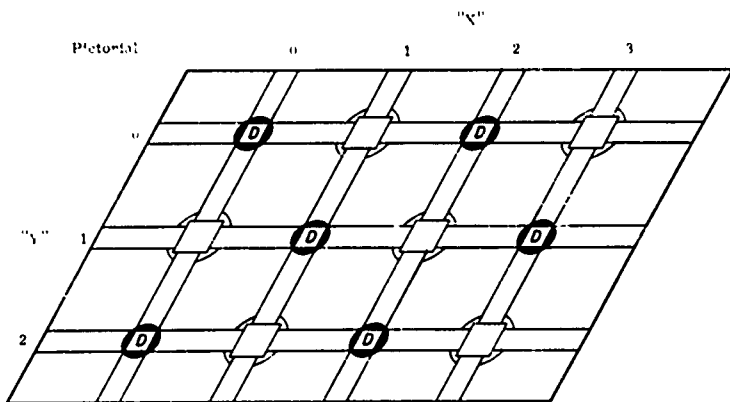
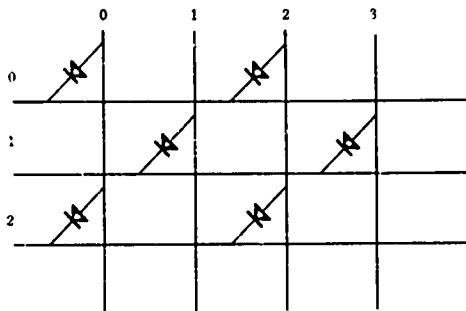


Fig. IV-24. Silicon Diode Sheet

## Schematic



## LEGEND

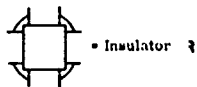


Fig. IV-25. Silicon Diode Matrix

reverse current are typically obtained. Also, 100 ma of forward current at  $-55^{\circ}\text{C}$  and 1 volt is typical. As a result, extremely desirable diode action is now possible in large diode arrays.

#### b. Memory selection system

The details of selecting a given word will now be considered with reference to Fig. IV-26 (Typical Silicon Memory and Selection). From this it may be seen that three main parts involved are:

- (1) Plane and word selection register.
- (2) Sense register.
- (3) Silicon memory stack and diode matrices.

The silicon memory stack and diode matrices are constructed as described in the preceding section. The following matrices connections from a given plane of the silicon memory stack are proposed to be common with the word-selection diode-matrix and 9 to 160 diode matrix. This eliminates an estimated 8158 soldered connections and replaces them in a high reliability, gold-deposited circuit. This is an obvious advantage over 8000-word 23-bit core memories.

Word and plane selector registers identify the desired word and given plane. The diode matrices select the required word in the silicon memory stack. A 23-bit word readout results in setting up the word in the sense register.

Upon selection of a given word the permanently nondestroyed contents of the word would be available. Typical construction involves vertical and horizontal gold-bus deposition by vacuum evaporation. Silicon monoxide insulation is used where no diode is desired at a given junction of vertical and horizontal buses.

Words are selected by the use of binary address inputs from the word selector register. These binary inputs are employed in a diode matrix to generate the decimal (1 to 512) word address. In order to eliminate manual-wired connection, vacuum deposition is employed. Nine sets of control buses select 512-word addresses. With a 23-bit word structure 23 sense lines would exit from the memory. On a per plane basis, 9 sets of address words and 23-bit exit wires control operation of:

- (1) 414 Memory diodes.
- (2) 4608 Matrix-selection diodes.
- (3) 1024 Plane-selection diodes.

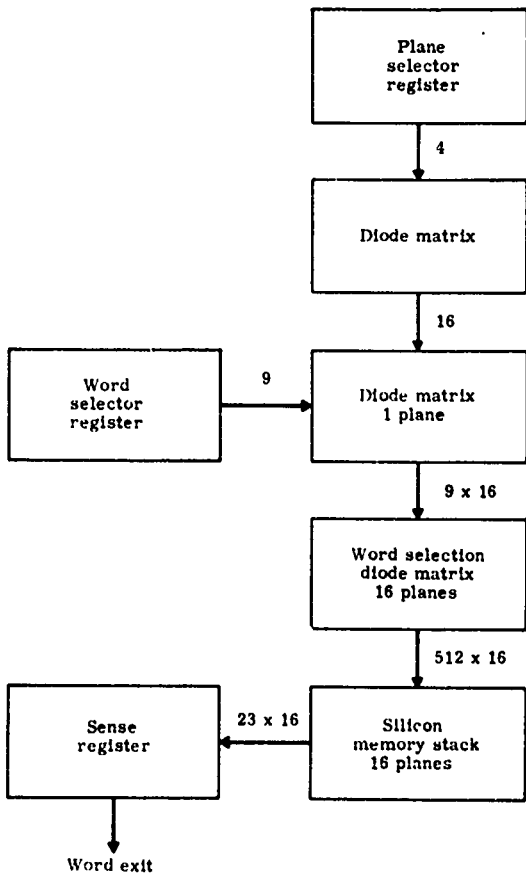


Fig. IV-26. Typical Silicon Memory and Selection

These components are fabricated by semiconductor and vacuum-film techniques without use of hand-wired connections. A demonstrable, schematic of the memory system is shown in Fig. IV-27 (Selection and Storage Schematic). This illustration includes:

- (1) Diode-matrix for word-plane selection.
- (2) Selected memory plane.
- (3) Typical nonselected memory plane.
- (4) Bit exits.

In Fig. IV-27, the binary address corresponding to a decimal address of three is selected, and the upper memory plane of the two memory planes shown is selected. Since diodes are connected to the 3- and 23-bit line for the selected plane at word 3, the bit exit reads 0, 0, 1 . . . . 1. In the nonselected plane the bit exit is all zeros.

Due to the particular memory selection system chosen, the number of hand-wired connections is reduced over present systems. Silicon memory stack diode matrices are packaged in a common plane configuration. This requires only 512 hand-wired connections to the entire 23 x 512 x 16 (190,716) diode memory. Present techniques require 1400 hand-wired connections to a 64 x 64 x 22 (90, 112) bit core memory. This is better than a 60% reduction in the required connections to the memory.

#### c Calculated and experimental switching speeds

As is typical for thin-film systems, the circuit response will not be assumed limited by silicon diffusion or drift mechanisms. The inductive time constant:

$$\tau = \frac{L}{R}$$

will be considered.

Without the use of a shielding conducting ground plane a field of 50 oersteds has been found. This is in partial agreement with a relation for the surface field adjacent to a grid of width  $w$ , current  $I$ :

$$H = \frac{2 \cdot I}{10w} \text{ oersteds.}$$

The calculated inductance value for a grid of 15 $\mu$  in width that is 0.33 cm long is 4 x 10<sup>-9</sup> H.

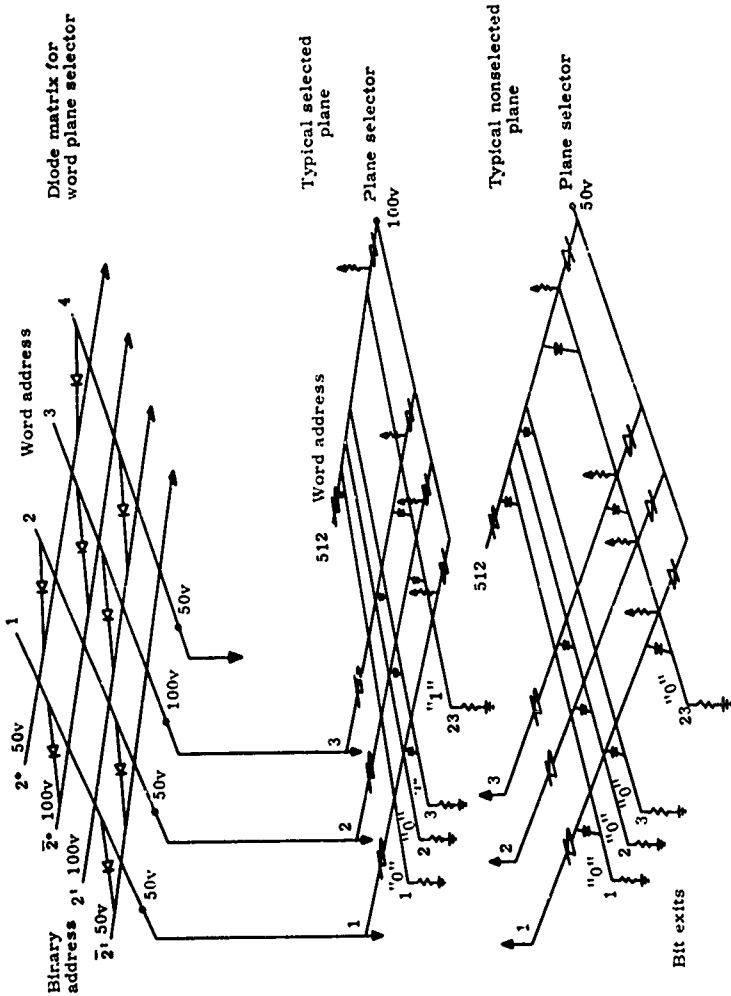


Fig. IV-27. Selector and Storage Schematic

Given 0.01 ohm resistance the time constant is:

$$\begin{aligned}\tau &= \frac{L}{R} = \frac{4 \times 10^{-9} \text{H}}{R} \\ &= \frac{4 \times 10^{-9} \times 50}{0.01} = 20 \mu\text{sec}\end{aligned}$$

This implies that while 23-bit words from the memory are available at a 50-kc rate, the bit rate is better than 3/4 mc/sec.

As an alternate to the above, the use of a conductive ground plane may be considered to improve word selection time. In this case the typical inductance is  $10^{-12}$  h/cm of line length. If a resistance of  $10^{-3}$  ohms is inserted in a 10 cm long loop:

$$\tau = \frac{L}{R} = \frac{10^{-12} \times 10}{10^{-3}} = 0.01$$

Time constants of this magnitude can be achieved without great difficulty. It may be surmised that considerably smaller time constants could be achieved either by making use of thin films, with small cross section (and consequently higher resistance) or by using a material with inherently high resistivity.

It is anticipated that the provision of a shield plane close to the grid reducing the inductance will raise the operation speed by at least an order of magnitude. This has been experimentally confirmed to yield a time constant of less than 3  $\mu$ sec.

### 3. Random Access, Erasable Memory

The use of proven core techniques will be employed to provide an erasable memory. Based on in-the-house Librascope core experience plus recommendations of core fabricators, a demonstrated technique will be employed. While the desirable volume and temperature requirements do not allow a large 6000-word core memory, a 356-word erasable memory is recommended to supplement the "silicon memory stack."

The use of present core techniques in the small erasable memory permits operation over the range  $-25^{\circ}\text{C}$  to  $+100^{\circ}\text{C}$ . This has been proven with transfluxors employing a 300 ma unblock current at  $100^{\circ}\text{C}$  which is varied to be 700 ma at  $-25^{\circ}\text{C}$ . Similarly square-loop cores have been operated over the range of  $-20^{\circ}\text{C}$  to  $+80^{\circ}\text{C}$ . Indications are

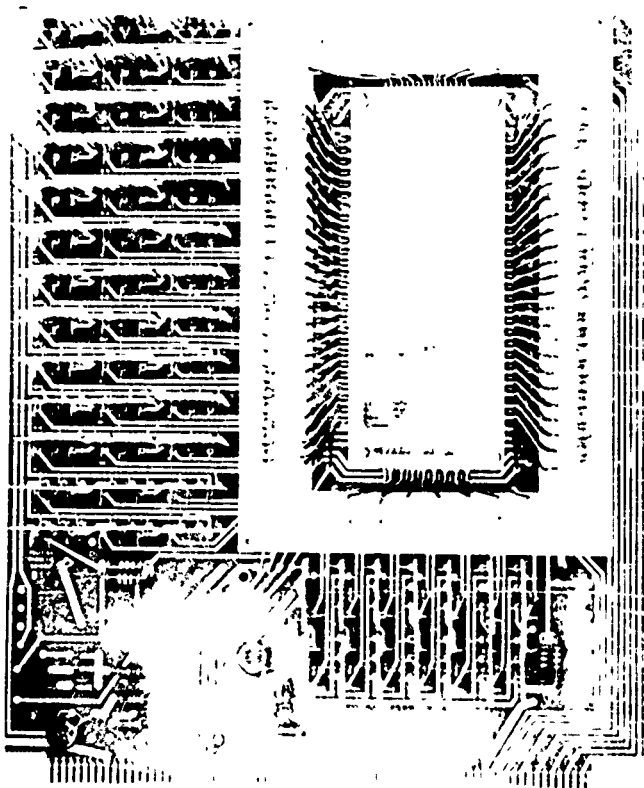


Fig. IV-28. Prototype Core Memory

that the range may be extended to +100° C. Full and half select currents are varied as a function of temperature to permit reliable operations. Such drive current variation is typically performed by use of Thyrite temperature sensitive elements controlling drive current. A prototype core memory system developed by the writer at Librascope is shown in Fig. IV-28. This employs current-steering magnetic switches for word selection. The photograph indicates the approximate size of the erasable memory.

### E. BASIC ELECTRICAL POWER

The one-year mission requirement for the various satellites, as part of the weapon system, automatically limits the choice of power supplies to that of solar or isotope types. The various types of solar power supplies, requiring solar concentrators, can be eliminated due to the close control requirement and the need to eliminate rotating machinery from the satellite. Due to the disturbing torques and the reduced reliability of such systems, the choice of power supply for the system rests with a radioisotope or a nonoriented solar cell system. The radioisotope system was calculated with battery storage for peak loads.

The load analysis for the mission is as follows:

<u>Item</u>	<u>Continuous (watts)</u>	<u>Intermittent</u>
Radar		150 w/1.5 min, every hour
Star tracker	5	10 w/2 min, every hour
Computer	10	60 w/5 min, every hour
Stabilization system		40 w/30 sec, every hour
Horizontal scanner	10	
Rate Gyros	2.5	5 w/60 sec, twice daily
Scan seeker and tracker		
Programmer	5	
Memory programmer	5	
<b>Total</b>	<b>62.5</b>	<b>235 w/1.5 min + 95 w/2 min + 85 w/1.5 min + 65 w/0.5 min + 5 w/2 min</b>

The orbit time will be 6 hr, of which a maximum of 44.75 min will be in darkness, and a minimum of zero (or continuous sunlight) depending on the orbit chosen.

A typical radioisotope generator was developed by The Martin Company to provide 125 watts of power for space applications. The successful demonstration of thermoelectric materials in the program led to selection of a static thermoelectric power conversion system. With an overall system conversion efficiency of 5% with thermoelectric conversion, 2500 watts of thermal energy are required to provide 125 watts electrical output after operating for one year. Cerium-144, a fission product, was chosen as the fuel because of ready availability, economic production and favorable half life characteristics. To provide the necessary thermal energy for conversion to electricity, 880,000 curies of Cerium-144 are required, producing an initial thermal power of 6500 watts. A weight of 200 lb consists of a structurally supported fuel core and an outer shell which houses the thermoelectric system (Fig. IV-29). Its outer configuration (a cylinder with hemispherical ends) has a 34 in. length and a 24 in. diameter.

The generator detail design is shown in Fig. IV-30. The shell of the unit, which contains the thermoelectric elements, is made up of two integral skins. An inner skin of stainless steel serves as the thermoelement hot junction, and an outer skin of aluminum as the cold junction. A thermal insulating material is nested around the elements between the two skins.

The insulation, located at the bottom of the unit, is hinged and is opened by a mechanism to permit a portion of the inner skin to radiate excess heat directly to the surrounding environment. To provide a constant power level, 3280 watts of the initial radioisotope thermal output are radiated to the environment by means of a thermal shutter. During a 1-yr life of the generator, at rated output of 125 electrical watts, the thermal shutter is gradually closed to compensate for radioisotope decay. Heat is generated by a loading of 880,000 curies of Ce-144 contained in an Inconel-X block at the center of the generator. The block is supported from the shell by tubular truss members which, in turn, are suspended by load members passing through the top and sides of the unit. The load members are attached to the flight vehicle structure.

Ground shielding is provided by completely filling the interior of the unit with approximately 4000 lb of mercury. Just prior to launching, this mercury is drained and a water coolant coil (surrounding the isotope fuel block) serves to remove heat from the shield mercury.

The isotope fuel capsule (Fig. IV-31) is a cylindrical Inconel-X block, 11 in. long and 3-3/4 in. in diameter, containing seven equally spaced 1-in. diameter holes drilled through the block parallel to its longitudinal axis. A 0.49-in. thick threaded closure cap is fitted to the top and bottom of each hole. Radio-cerium in the form of ceric oxide fuel pellets is loaded into thin-walled stainless steel tubes prior to installation in the capsule. In this matter, fuel loading operations and

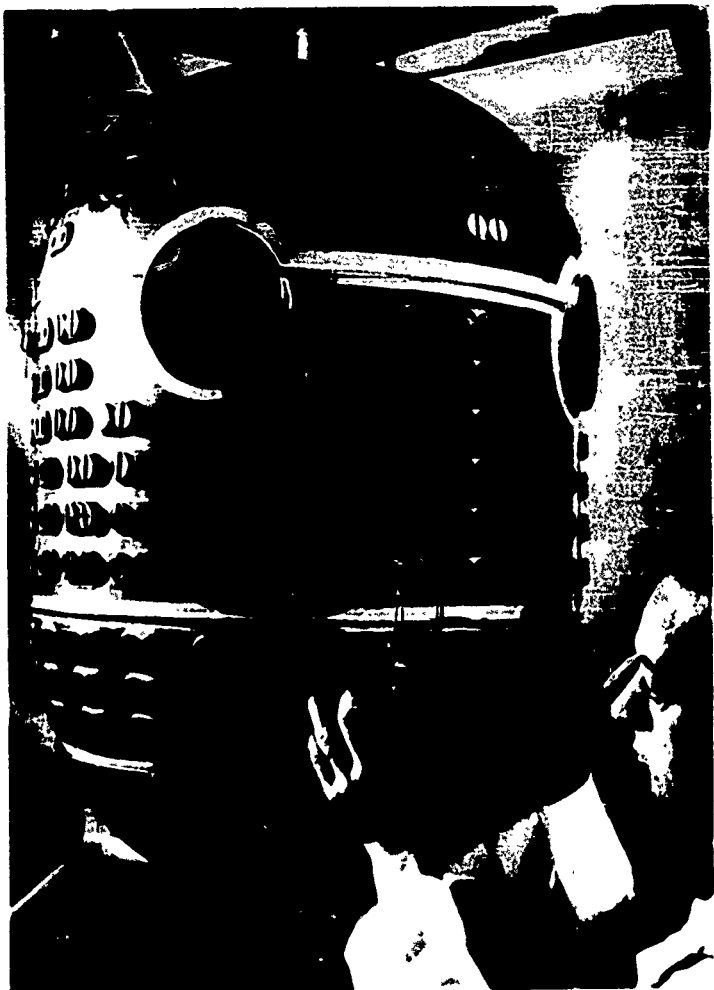


Fig. IV-29. Generator Outer Shell

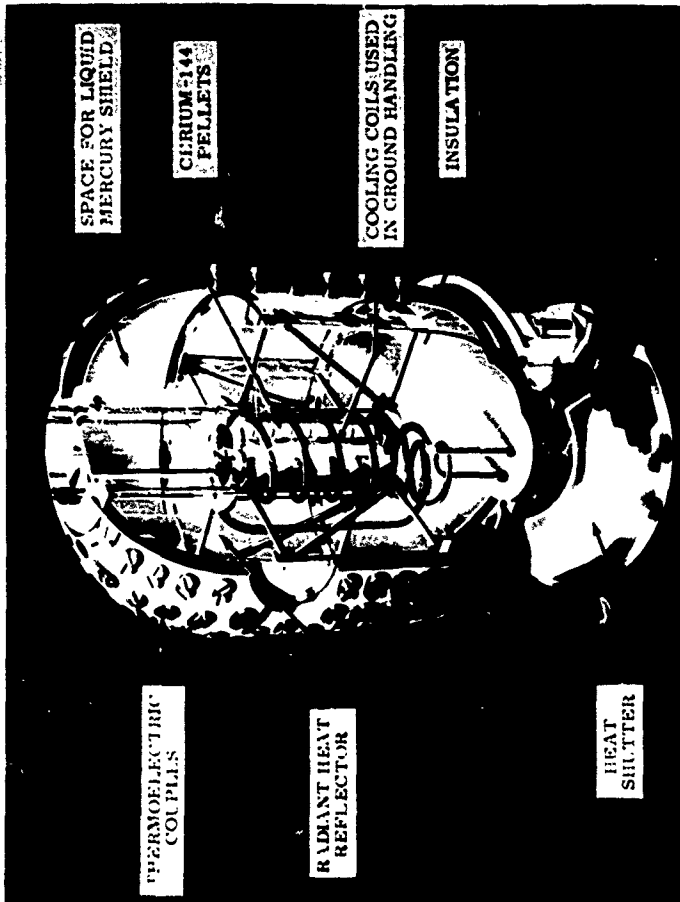


Fig. IV-30. Generator Detail Design

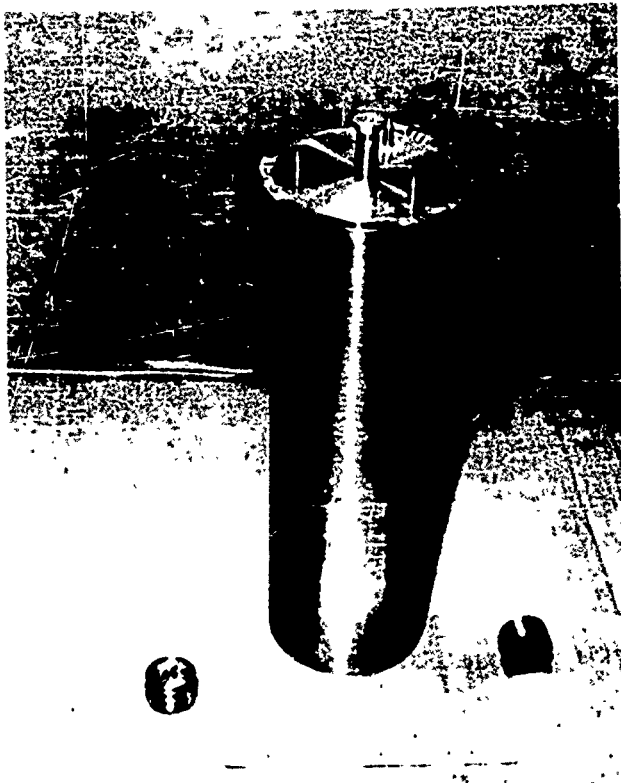


Fig. IV-31 Isotope Fuel Capsule

core surface contamination are minimized. Each fuel tube contains 0.1257 megacurie of Ce-144. A tabulation of design characteristics is given in Table IV-3.

A comparison of radioisotope generators with battery storage is shown in Fig. IV-32. The weight estimates for the thermoelectric generators are those projected for state-of-the-art improvements; by 1965, current weight estimates would be higher. The voltage regulation for the system without battery would be so poor that some sort of voltage regulator would be necessary. Without some energy storage device, a radioisotope generator for the indicated load chart would be entirely impractical because of the large ratio of average-to-peak load (namely 4:1). Therefore, a nickel or silver cadmium battery must be incorporated in the system to carry the peak load.

The voltage regulation is actually performed by the battery; however, a small battery charging regulator must be provided to ensure adequate voltage acceptance level for battery charging. A 2 amp/hr nickel-cadmium battery would supply the peak level requirements every hour. The depth of discharge would be low enough to ensure 15,000 cycles, whereas 8750 cycles per year would be required by the mission profile. A comparison of life and weight between nickel-cadmium and silver-cadmium batteries is shown in Figs. IV-33 and IV-34. The choice of a battery necessary for the high cycle life required is obvious from the curves.

A solar cell generator system with a nickel-cadmium battery for energy storage is the least expensive, from a cost and weight standpoint, and provides an adequate reserve of power. The components are available hardware already proven for the intended purpose. State-of-the-art improvements were not extrapolated for the present design and all weights are based on hardware immediately available and suitable. The system would be composed of three solar cell panels located 120 degrees apart on the surface of the vehicle. Conductive cooling would be incorporated to limit solar cell temperature to 30° C. The satellite will rotate with respect to the sun so that the individual generator outputs will be as shown in Fig. IV-35. The total output will be the algebraic sum of the currents at each voltage. The panels will be composed of 10 shingles of 5 to 12% effective cells in series in a strip, and five 50-strips will be connected in parallel and in series with a protective diode.

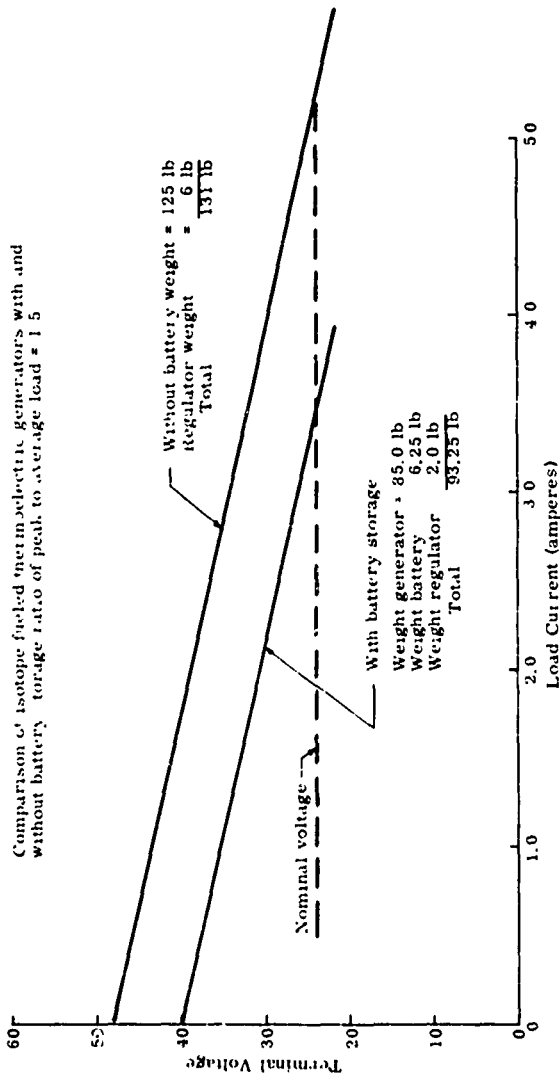


Fig. IV-32. Comparison of Isotope Fueled Thermoelectric Generators

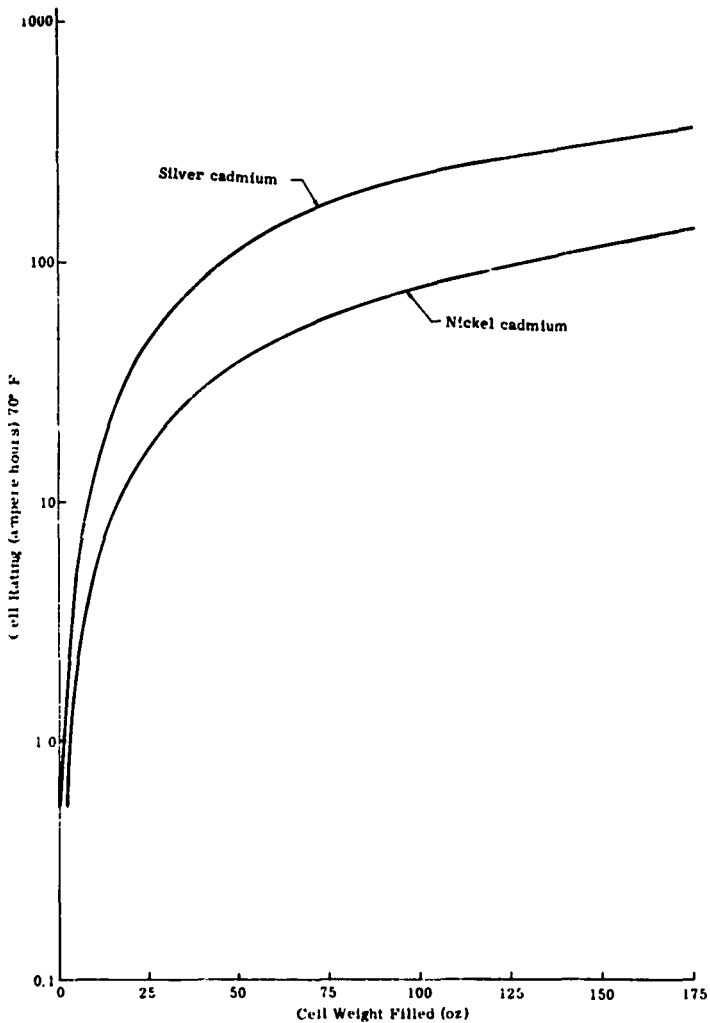


Fig IV-33 Comparison of Silver and Nickel Cadmium Cells

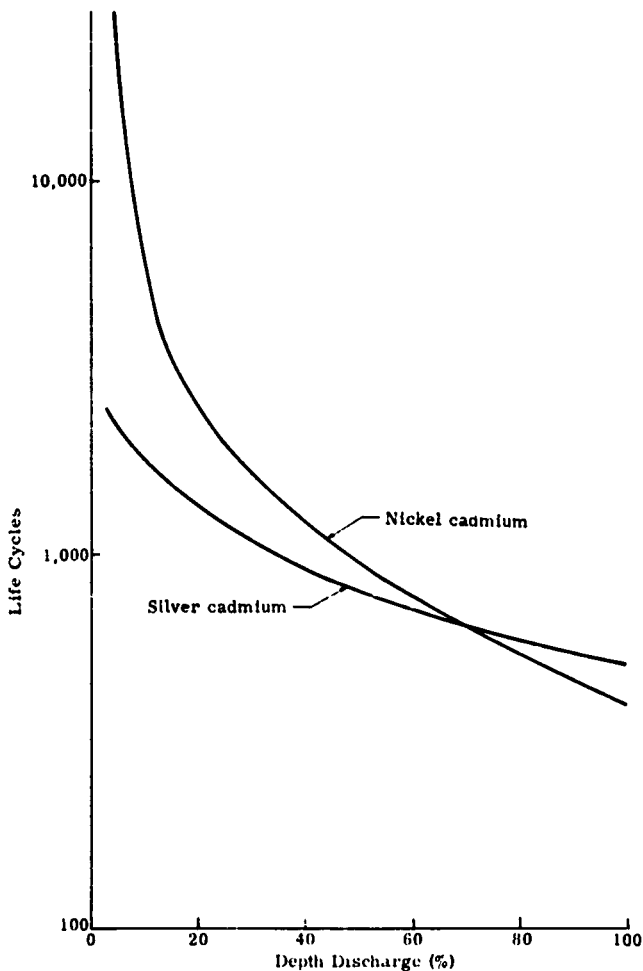


Fig. IV-34. Estimated Life of Nickel and Silver Cadmium Batteries

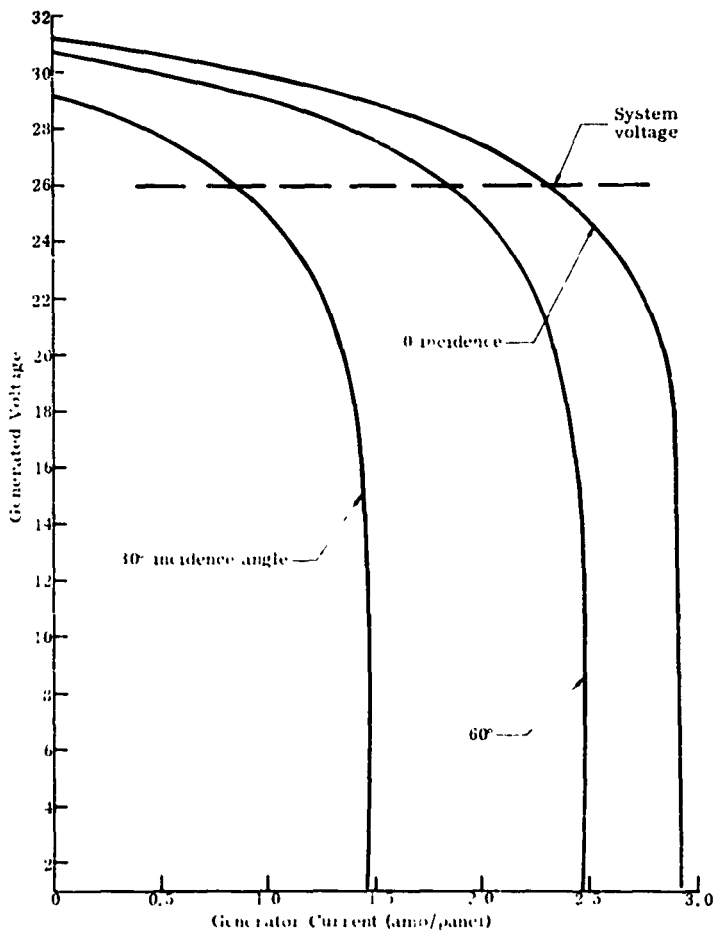


Fig IV-35 Solar Cell Generator Panel Designed for Optimum Battery Charging

TABLE IV-3**Design Characteristics of Radioisotope 125-Watt Generator**

Power output	125 watts for 365 days of constant power
Voltage	28 volts
Current	4.46 amperes
External load	6.28 ohms
Efficiency	6.75% thermoelectric 5.0% actual 50% carnot
Heat loss	530 watts (thermal)
Useful heat	2150 watts (thermal)
Heat dumped (initial)	3280 watts (thermal)
Hot junction temperature	1050° F
Cold junction temperature	55° F
Thermoelectric radiator surface	14.5 ft <sup>2</sup>
Shutter emissivity	0.90
Isotope inventory	880,000 curies Ce-144
Weight	200 lb
Watts	0.625 lb

The battery selected was a 16 amp/hr nickel-cadmium type. The cycle life required for the maximum possible discharge duty is 1460 cycles. From Figs. IV-33 and IV-34, it can be seen that a choice between silver and nickel types exists. The nickel was chosen to be ultra-conservative in regard to life and to remove any loss of capacity connected with cycle life questions. However, it is recommended that a test program be instituted to determine more accurately the type of battery to be used in order to achieve a maximum weight saving. Another factor to be considered in the battery selection is that of voltage regulation. In order to achieve good voltage regulation, the discharge rate

was kept below 25% on the system without the use of any additional voltage regulators.

TABLE IV-4  
Weight Summary of Solar Cell System

	<u>(lb)</u>
Solar cell generators	13.5
16 amp/hr nickel-cadmium battery	29.6
Electrical protection equipment	1.9
Total	45.0

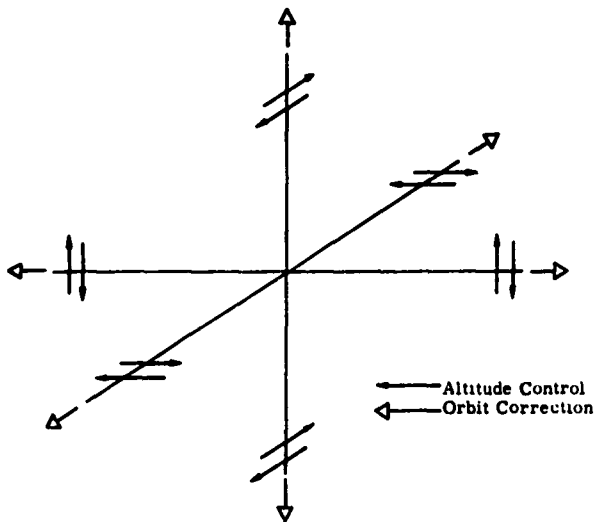
## F. ATTITUDE CONTROL SYSTEM

The characteristics of various attitude control system configurations have been studied in order to define a control system that achieves the desired navigation accuracy and is economical in energy requirements over long mission times in the mission orbit. Reaction jet control systems, flywheel systems, and combinations of these were considered (Refs. IV-10 and 11). For this application, a reaction jet control system is optimum since to use reaction flywheels to maintain alignment with the local vertical demands a constantly increasing flywheel speed which exceeds practical values long before the 1-yr mission time has elapsed. When using reaction jets, two levels of thrust suggest themselves: (1) a large thrust jet for establishing initial orientation and stopping any residual angular rates resulting from injection propulsion cutoff; and (2) a lower thrust jet to maintain control after the limit cycle has been established. This type of operation can be approximated by pulse modulating the thrust from a fixed jet.

It is always difficult to isolate the control system performance from the effects of variations in the vehicle characteristics, since they are so closely interdependent in a closed loop system. Therefore, in this study, a typical satellite was assumed and its characteristics used throughout the analysis of the various control system configurations. The effect of variations in the satellite characteristics was not investigated.

The satellite is assumed to be a cylindrical shape, as shown in Fig. IV-36, with a 6 ft diameter, a 7 ft length, and a weight of 5000 lb. The weight breakdown (Ref. IV-12) is as follows.

<u>Item</u>	<u>Weight (lb)</u>
Rate gyros (3)	1.0
Programmer	17.0
Computer	125.0
Horizon scanner	11.0
Star tracker	30.0
Radar altimeter	60.0
Clock	15.0
Control circuitry	40.0



F g IV-36. Attitude and Orbital Control Jets

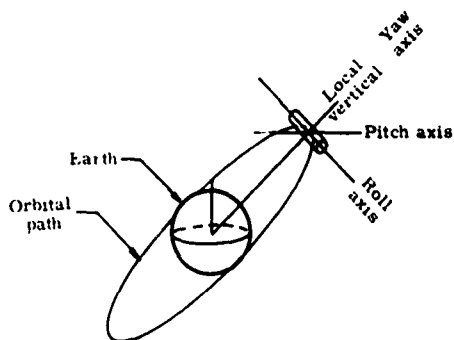


Fig. IV-37 Satellite Axis System

Reaction jets (12)	35.0
Reaction jet fuel	3500.0
Power supply	265.0
Structure	300.0
Payload	<u>616.0</u>
Total	5015.0

The configuration includes 12 fixed reaction jet nozzles (Ref. IV-13) to provide attitude control corrections and 6 fixed jets for the orbital corrections (the jets are positioned as shown in Fig. IV-36). Engineering diagonally opposite jets produces torques to rotate the vehicle. The fuel carried for these jets is sufficient to provide the necessary daily orbital corrections (Ref. IV-14) as well as the thrust necessary to maintain the alignment of the vehicle axis with the earth local vertical as shown in Fig. IV-37.

Since the satellite tends to oscillate continuously about its control axes, it is tentatively apparent that for long mission times many thousands of operations of the nozzles and their control valves will be required. This, of course, suggests a reliability problem. Similarly, the orbital correction thruster will be required to operate approximately 730 times during a 1-yr mission. The system shown in Fig. IV-38 is suggested to enhance reliability. The basic concept is that a hypergolic bipropellant system, which is characterized by an  $I_{sp}$  of approximately 300 sec and high thrust chamber temperatures, is used to provide the thrust for orbital corrections. Choosing the fuel so that it can also be used (with a catalyst) as a monopropellant, provides a source for the large number of chamber pulses required in the attitude control system. However, the attitude control jets operate at a much lower temperature, thus minimizing material problems and increasing reliability.

Another assumption effecting the vehicle configuration is concerned with the propulsion needed to inject from the ascent trajectory into the parking orbit, transfer from the parking orbit to the mission orbit, and inject from the transfer ellipse to the mission orbit. The total velocity changes for these maneuvers are more than 8000 ft/sec. It is assumed that this propulsion system is separated from the satellite after injection in the mission orbit and that its control, therefore, is not part of this guidance system.

As described in Section IV-A, an altimeter is used in the guidance system to determine the in-plane parameters of the satellite orbit. A radar altimeter is proposed and its antenna must be stabilized to look

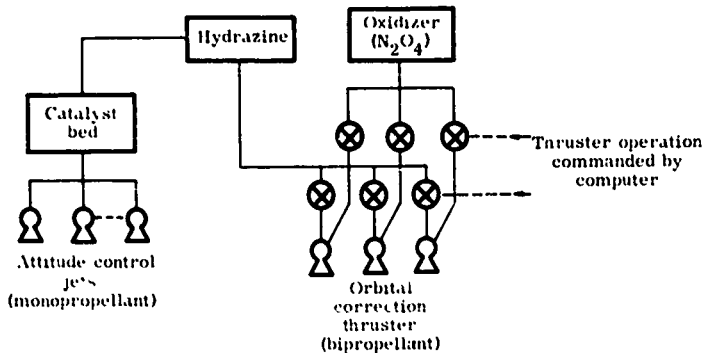


Fig. IV-38 Thrust System Schematic

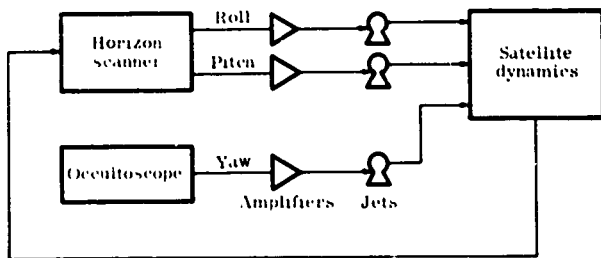


Fig. IV-39. Overall Control System

along the local vertical. The radar must be stabilized to the local vertical to within  $\pm 0.5$  degree in order to obtain the desired accuracy. This can be accomplished either by stabilizing the antenna while the satellite attitude varies or the antenna can be fixed to the satellite and the satellite stabilized to the local vertical. The latter approach has been studied.

An IR horizon scanner is used to determine the local vertical, and is capable of indicating the vertical to an accuracy of  $\pm 0.1$  degree.

The yaw axis attitude reference is the star tracker which is also used to measure the occultation times for determining the out of plane orbital parameters. This device indicates the heading of the satellite relative to its velocity vector to an accuracy of 0.01 degree.

All of the above data and assumptions lead to the control system configuration shown in Fig. IV-39. The reaction jets are inherently on-off devices, and the following sections of this chapter will be devoted to a study of techniques of operating these jets so as to meet the stability requirements and the economical use of fuel. Since the satellite motion is undamped by any natural phenomenon, the overall system operation will be characterized by a continuous bounded oscillation (a limit cycle). The essential design compromise sought is to minimize the amplitude of the limit cycle operation and, at the same time, minimize fuel consumed by the jets. Perturbations can be expected from the torque on the satellite due to small misalignments in the orbital correction thruster. Similarly, slight differences in the initiation and cutoff times of the individual attitude control nozzles will result in perturbing forces. Other disturbing torques arise from secondary effects, such as the dumbbell effect which tends to align the long axis of the satellite with the local vertical. Evaluation of these torques permits the impulse requirements of the jets to be estimated (Ref. IV-15). The maximum perturbation in the pitch and yaw plane is caused by misalignment of thruster used as injection to the mission orbit (1000 ft thrust assumed) by 0.5 degree. For the vehicle dimensions chosen, a 4.3 lb reaction jet is required. Therefore, in the phase plane analysis to be presented, thrust levels of 7.0 lb and 1.0 lb are used to straddle the estimated requirements.

### 1. System Analysis

Initially, a conventional bang-bang approach study to the control system design was conducted at various thrust levels. In addition, the application of pulse modulation of the jets was studied at a single thrust level to provide an insight to the possible performance improvement resulting from more nearly proportional operation. Phase plane trajectories were compared for each case to indicate the characteristics of the limit cycle and the approach to the limit cycle. Total impulse requirements are the sum of the impulse needed to establish the limit cycle plus the impulse required to maintain the limit cycle for the duration of the mission (1-yr).

Figures IV-40, IV-41 and IV-44 are phase plane plots of the control system performance and show a comparison of 3 different control systems for initial conditions of  $50 \times 10^{-4}$  rad/sec from a displacement of  $50 \times 10^{-4}$  rad (0.3 degree).

Lines 1 and 4 are the "thrust on" lines and lines 2 and 3 are the "thrust off" lines. That is, whenever the error ( $\theta$ ) is greater than the error described by lines 1 and 4, a pair of thrusters will be turned on (in the case of the pulse modulated system, the average thrust is proportional to the amount of error greater than the error described by the lines). The spacing between the "thrust on" and "thrust off" lines is determined by the hystereses and time delay of the system. The slope of these lines is determined by the equation  $\frac{d\theta'}{d\theta} = \frac{-1}{m - T_D}$  (where  $m$  is the ratio of rate gain to positional gain and  $T_D$  is the total system time delay). For stability,  $\frac{d\theta'}{d\theta}$  must be negative and less than infinity (that is,  $m - T_D > 0$ ) and the spacing between the "thrust on" and "thrust off" lines must be less than the spacing between the two "thrust on" lines. Since the spacing between the two "thrust on" lines is  $2\theta_P$  ( $\theta_P$  is the angle at zero rate where the thrust will come on) and the spacing between the "thrust on" and "thrust off" lines is (Equation 1)  $\theta = \theta_P(1-r) + (mT_D - T_D^2/2)\alpha$  (where  $r$  is the hysteresis and  $\alpha$  is the acceleration), this says that  $2\theta_P > \theta_P(1-r) + (mT_D - T_D^2/2)\alpha$  or  $m < \frac{P(1+r)}{T_D\alpha} + T_D/2$ .

The equations above describe the limits of  $m$  for stability. Further analysis of the phase plane shows that there is a value of  $m$  between these two limits which minimizes fuel consumption (Ref. IV-16). The formula for  $m$  optimum is as follows:

$$m = - \frac{(T_D^2 + 3b) + \sqrt{(T_D^2 + 3b)^2 + 4[(2a + b)T_D^2 + 2ab]}}{2T_D}$$

where

$$a = \frac{\theta_P(1+r)}{\alpha} + \frac{T_D^2}{2}$$

$$b = \frac{\theta_P(1-r)}{\alpha} - \frac{T_D^2}{2}$$

**Assuming**

$$T_D = 0.02 \text{ sec}$$

$$\gamma = 0.9$$

$$\alpha_r = 49.8 \times 10^{-3} \text{ rad/sec}^2 \text{ (7 lb bang-bang)}$$

$$\alpha_1 = 7.1 \times 10^{-3} \text{ rad/sec}^2 \text{ (1 lb bang-bang)}$$

Solving Eq (2) for these values gives

$$m_7 \text{ lb} = 2.58$$

$$m_1 \text{ lb} = 140$$

Since the maximum usable  $m$  is determined by the signal-to-noise ratio, a maximum of  $m = 10$  was used. For the 1-lb bang-bang system, the rate channel must have a sensitivity of less than 0.01 deg/sec. This sensitivity requirement is just within the range of present day rate gyros and is easily attainable with passive networks (Ref. IV-17).

For the pulse modulated system (Fig. IV-44) no "thrust off" lines were shown, since the hysteresis of the bang-bang system was determined mostly by the hysteresis of the solenoid valve of the thrusting and in addition as  $+$  error approaches the value of the "thrust on" lines, the average thrust approaches zero. When applying this to Equation (1), we get

$$\theta = \theta_p (1 - r) + (m T_D - T_D^2/2) \alpha$$

$$1 - r \rightarrow 0$$

$$\alpha \rightarrow 0$$

$$\therefore \theta \rightarrow 0$$

It is therefore assumed that the "thrust on" and "thrust off" lines are coincident for the pulse modulated system.

**a. High thrust bang-bang system**

Figure IV-40 shows the phase plane for a control system using a 7-lb reaction jet system on a bang-bang type control. Analysis of the limit cycle (dotted lines) shows that average fuel consumption over the

limit cycle is  $170 \times 10^{-6}$  lb/sec. The fuel required to maneuver the satellite from point A into the limit cycle is  $11.7 \times 10^{-3}$  lb. At this thrust level, the period of the limit cycle is 24.8 sec and the maximum angular excursion of the satellite is 0.218 deg.

This is consistent with the accuracy of the IR horizon scanner and the stabilization requirements for the altimeter.

#### b. Low thrust bang-bang system

Figure IV-41 shows a phase plane plot for a 1.0 lb thrust bang-bang type control system. Reducing the thrust level reduces the average fuel consumption over the limit cycle to  $3.78 \times 10^{-6}$  lb/sec. However, the fuel used to maneuver the satellite, from point A into the limit cycle is decreased to  $9.7 \times 10^{-3}$  lb. At this thrust level, the period of the limit cycle is 175 sec and the maximum angular excursion of the satellite is 0.242 deg. In comparing these two thrust levels (the system is the same in all other respects), it is seen that with the larger thrust, the approach trajectory time is shortened at the expense of greater fuel consumption.

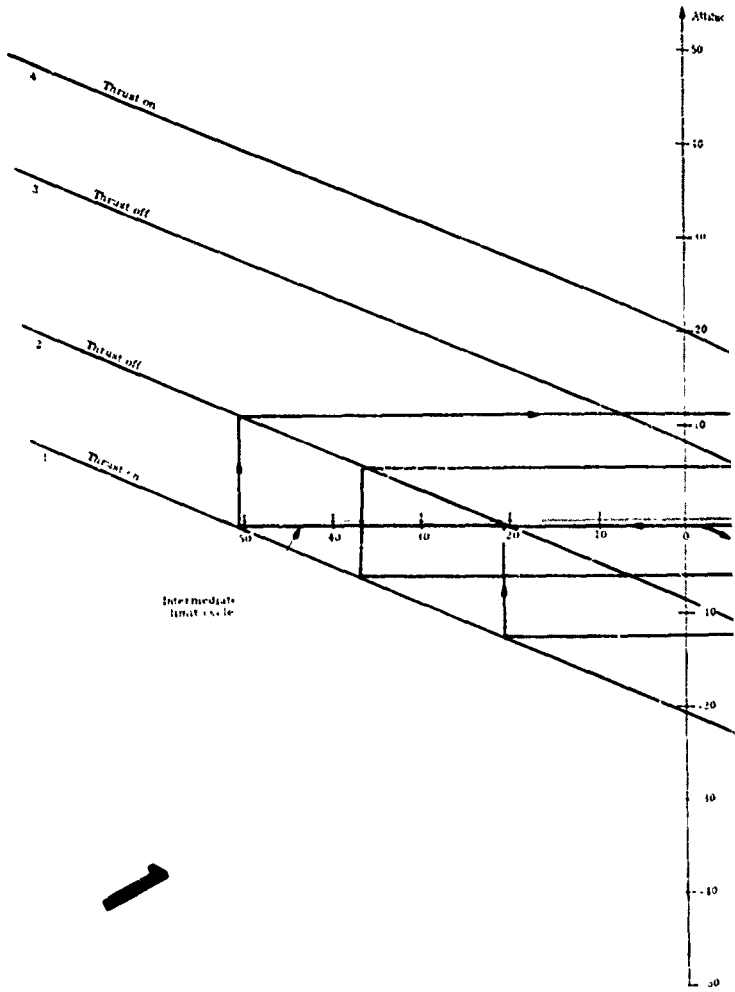
#### c. Pulse modulated proportional control

Reaction jets (full on or off devices) are most easily adapted to bang-bang type control systems. If the jet operation were proportional to error signal, it is possible that greater economy of fuel might be realized. The problem is then to construct some device which will give an average thrust from the reaction jet which is proportional to the error signal.

An obvious way to control the average thrust is by opening the jet in pulses. For instance, "thrust on" for 1 sec, "thrust off" for 9 sec gives an average thrust of  $1/10$  times the maximum thrust. The "thrust on" time divided by the "thrust off" plus "thrust on" time will give the average thrust (or "duty cycle"). Therefore, a pulse generator or modulator, whose duty cycle varies proportionately with input signal, will yield an average thrust which is proportional to the error signal. Figure IV-42 shows a graphical representation of a 0.5 and 0.25 duty cycle.

Examination of the phase plane trajectories shows a dead zone between the two "thrust on" lines. If this dead zone did not exist, the two thrust on lines would be coincident and pass through the origin. This would mean that either positive or negative corrections would be made at all times. Thus, it is apparent that a dead zone (in which no thrusters are operated) is necessary in order to minimize fuel requirements.

In order to control the dead zone in the system, some type of threshold detector must be used. The output versus input characteristics of this detector must be such that when signal inputs are less than the



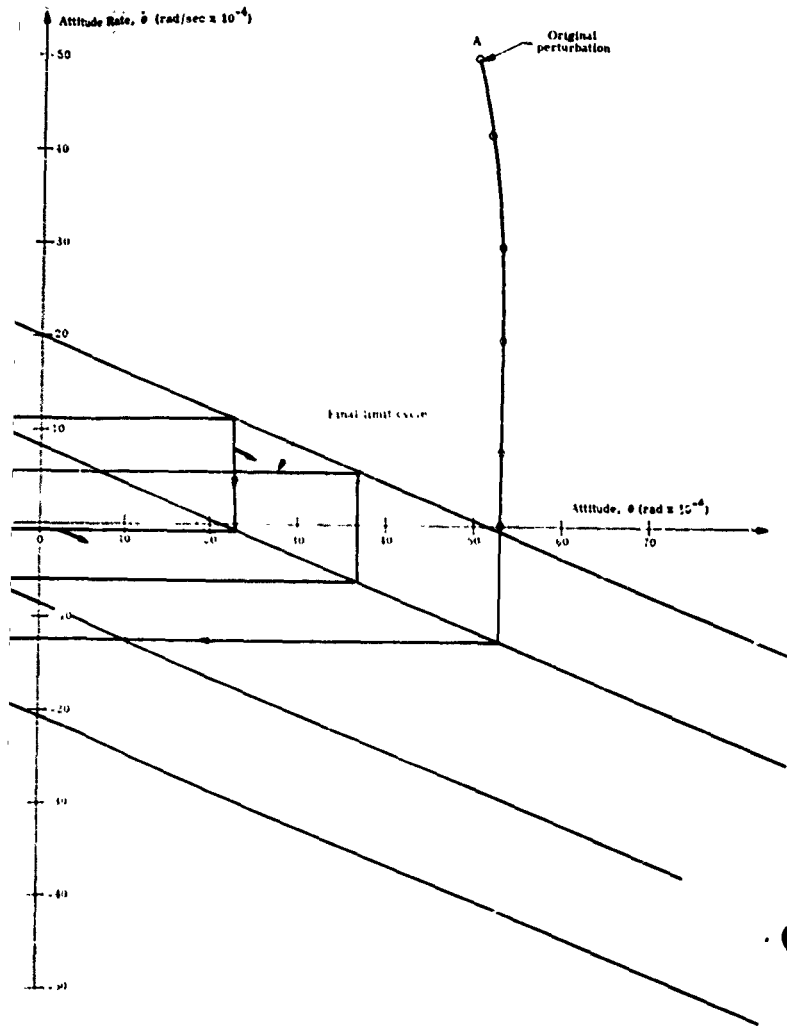
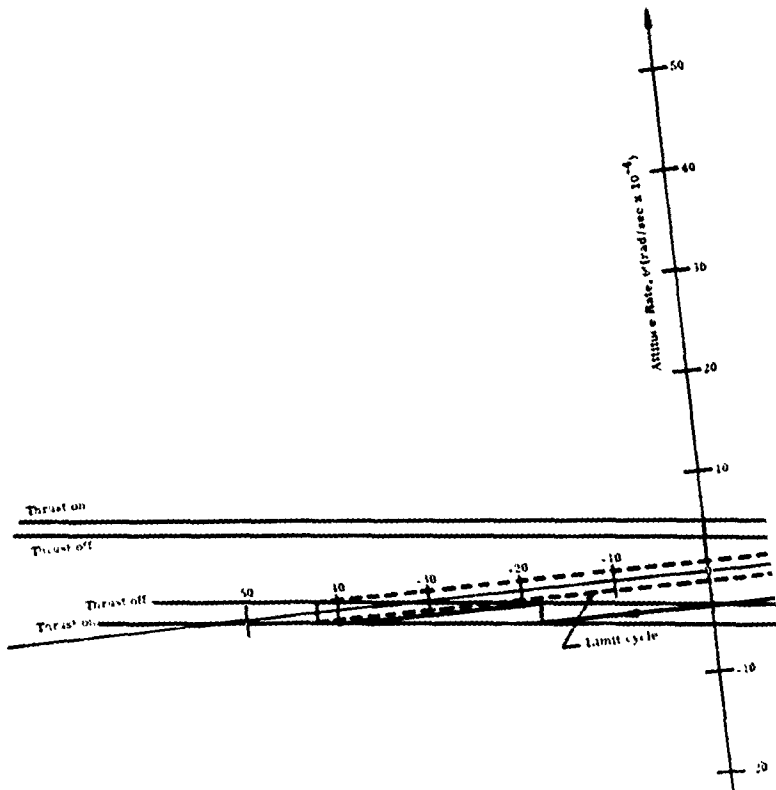


Fig. IV-40. Phase Plane Trajectory for Conventional Bang-Bang Attitude Control System (7-lb thrust)



1 2

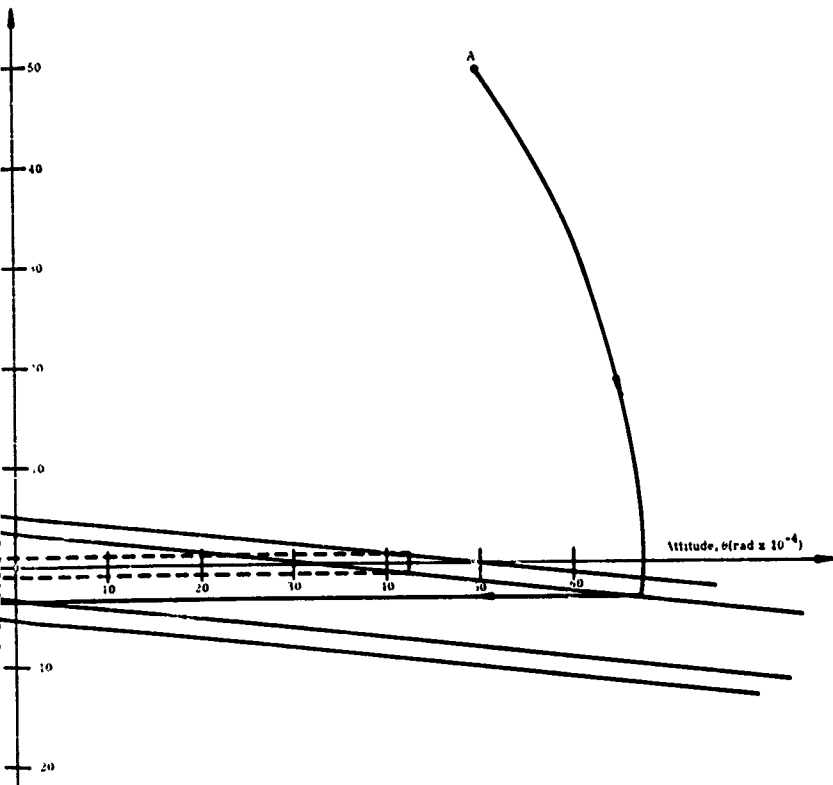


Fig. IV-41. Phase Plane Trajectory for Conventional Bang-Bang Attitude Control System (1-lb thrust)

2

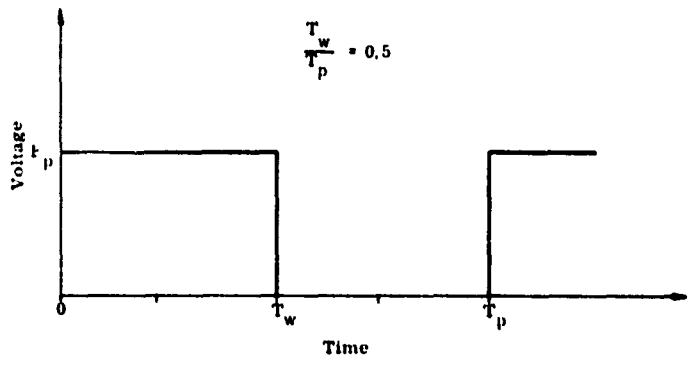
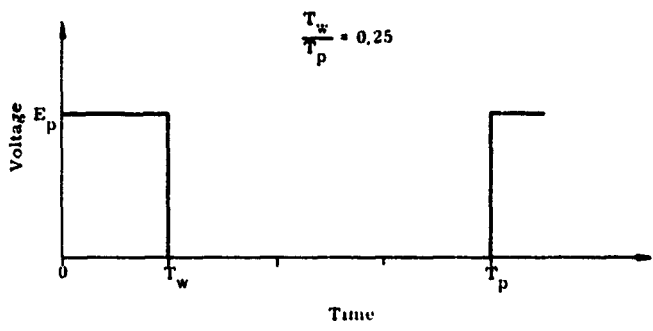


Fig. IV-42. Pulse Modulator

dead zone angle, the output must be zero. This is necessary to prevent noise from operating the pulse modulator. For signal inputs greater than the dead zone angle, the output should be proportional to the input. In addition, for signal inputs it is desirable to have a small signal output slightly less than or equal to the dead zone (to insure one pulse and one pulse only from the pulse modulator). Insurance of a single input pulse during the limit cycle reduces fuel consumption (since more than one pulse would cause a higher rate and therefore a shorter limit cycle period). Output versus input curve for such a device is shown in Fig. IV-43.

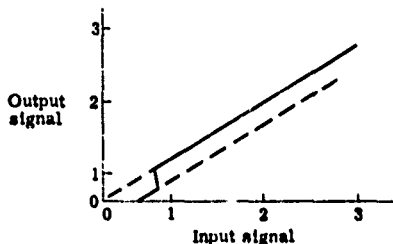


Fig. IV-43. Error Magnitude Detector Characteristics

Figure IV-44 shows a phase plant plot for a proportional control system using a jet thrust of 7 lb. The system is the same as that for Figs. IV-40 and 41, except that the thrust is proportional to the amount of error. The dotted line shows the limit cycle which has an average fuel consumption of  $5.01 \times 10^{-6}$  lb/sec, while the fuel demand for moving from point A into the limit cycle is  $8.5 \times 10^{-3}$  lb. At this thrust level, the period of the limit cycle is 169 sec and the maximum angular excursion of the satellite is 0.241 degrees.

The following (Table IV-4) summarizes and compares the three systems:

TABLE IV-4

System	Limit Cycle Fuel Economy		Approach Maneuver Fuel Economy (lb)*	Tightness of System
	(lb/sec)	(lb/yr)		
High thrust Bang-Bang	$1.70 \times 10^{-6}$	5440	$11.7 \times 10^{-3}$	Very tight, can correct for large disturbance quickly.

TABLE IV-4 (continued)

System	Limit Cycle Fuel Economy		Approach Maneuver Fuel Economy	Tightness of System
	(lb/sec)	(lb/yr)	(lb)*	
Low thrust	$3.78 \times 10^{-6}$	121	$9.7 \times 10^{-3}$	Loose control, relatively large errors can develop for short times.
Proportional control	$5.04 \times 10^{-6}$	161	$8.5 \times 10^{-3}$	Good control, compromise between the above two.

\*To re-establish limit cycle from  $\theta_0 = 50 \times 10^{-4}$  rad = 0.3 degrees;  
 $\dot{\theta} = 50 \times 10^{-4}$  rad/sec = 0.3 deg/sec.

## 2. Hardware Investigation

A program was undertaken to determine the degree to which the pulse modulated system described above could be realized in hardware.

The circuits have been designed, breadboarded, tested and packaged to demonstrate feasible design concepts for the pulse modulated system. Certain of the circuits are well established designs which have been used in various Martin missile applications and represent the result of considerable experience and testing. Other circuits have been developed and tested specifically for this application. All circuits utilize semiconductor application techniques, exclusively, to achieve a high degree of reliability with minimum space, weight and power requirements. The reaction control circuits have been constructed in breadboard form and have been tested and successfully married to an analog computer to demonstrate adequate characteristics relative to stability and accuracy.

An experimental autopilot has been packaged as shown in Fig. IV-45. This unit is designed to be pressurized to approximately one-half atmosphere to promote heat transfer and to avoid problems associated with operation in a vacuum. The internal construction of this unit is shown in Fig. IV-46. The circuits are developed on printed circuit cards, each of which is mounted on a cast aluminum frame. The frame serves both a structural function and as a heat sink mounting for power diodes and transistors. The primary heat flow path is through the frame, into

the base platf. and, from there, into the vehicle structure. Note that this construction permits ready access to the individual cards for in-flight troubleshooting and maintenance by crew members on manned mission. The volume of the unit is approximately 2500 in.<sup>3</sup> and the weight is 40 lb.

The reaction control circuits provide for roll, pitch and yaw stabilization during coasting flight. The reaction system provides proportional plus rate control for large errors and is also capable of operation in a limit cycle mode when the attitude errors are reduced. This dual capability is obtained from the pulse modulation system, used to control the reaction jets. The pulse modulator operates under a control law which is linear in average jet thrust, but limits both the pulse width and pulse repetition frequency to a useful minimum and maximum, respectively.

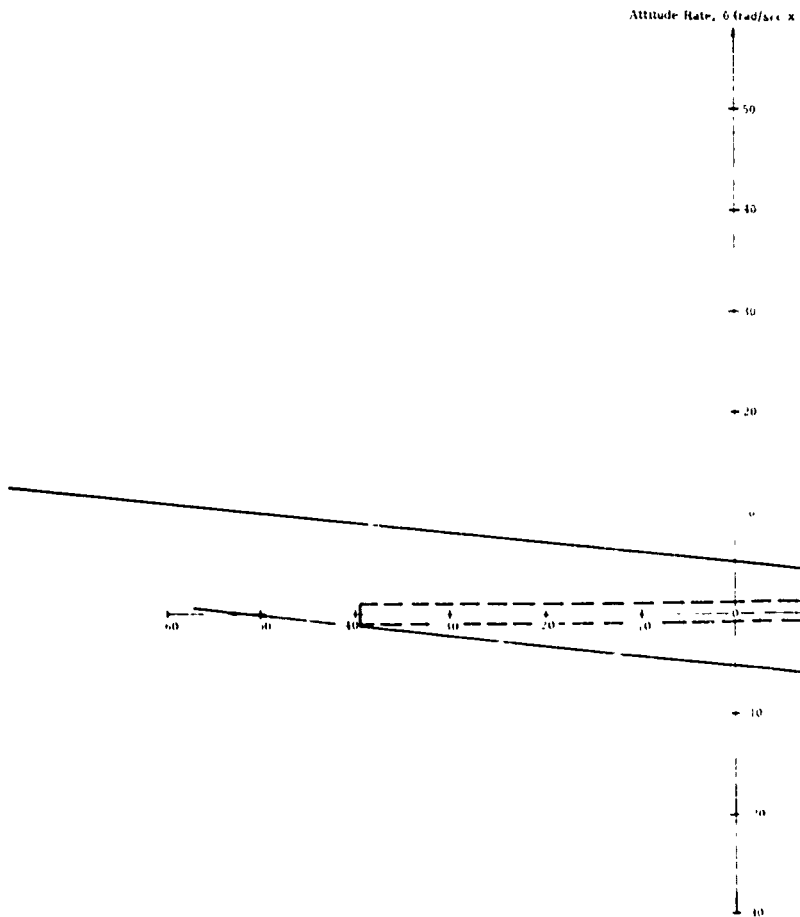
The reaction control system circuits produce signals which operate the vehicle reaction jets in response to attitude displacement and rate error signals. The output signals are modulated in such a manner that the average thrust produced by the jets is proportional to the attitude error signals. For errors equal to the system deadspot level, the circuits produce single pulses of a minimum duration to reduce fuel consumption.

A single axis block diagram of the control system hardware is given in Fig. IV-47. Each axis employs the same basic elements and the three axes are identical.

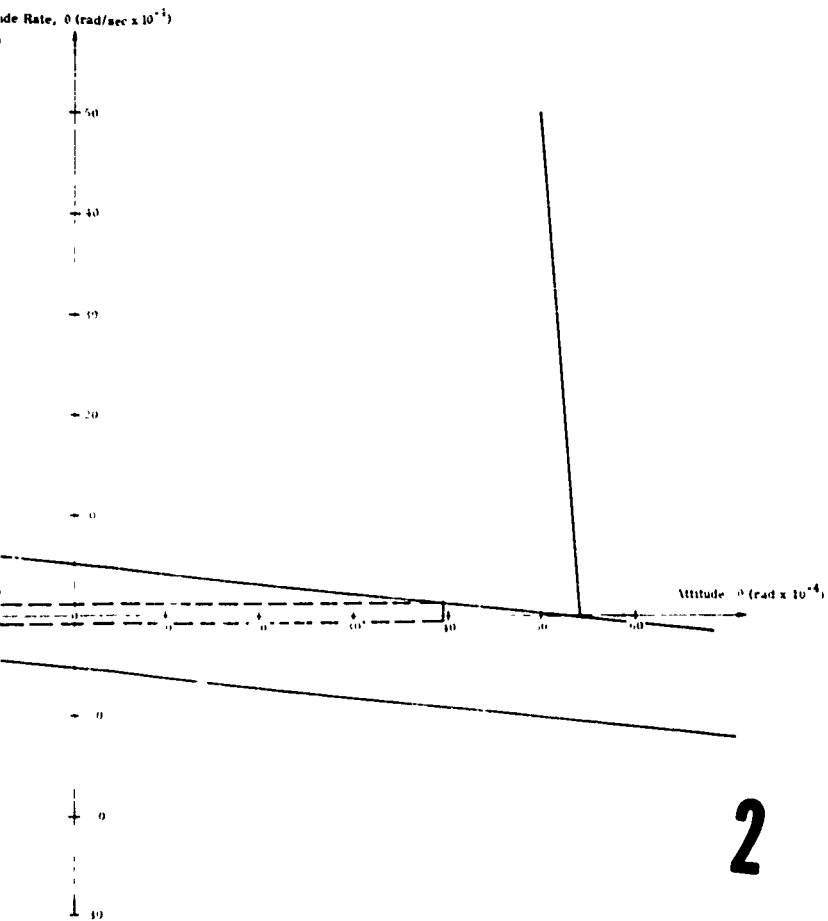
The key to the operation of this system lies in the pulse modulator. The function of the modulator is the production of a constant amplitude pulse train whose average value is linearly related to the modulator input signal. The pulse train average value is varied by control of the pulse width and the pulse repetition frequency. While the usual approach to such a modulator calls for variation of either pulse width or pulse frequency (while holding one or the other constant), this modulator will vary both the width and frequency. The width and frequency are varied in such a manner that the operation is always within the bounds of a certain minimum width and a certain maximum frequency. This is an advantage over the pure pulse width or pulse frequency modulation because jets do not respond efficiently to either very short pulses or very high frequencies. The modulator follows the operating laws

$$T_W = \frac{(T_W)_{\min}}{1-x} \quad f_p = f_p^{\max} (x) (1-x).$$

where  $T_W$  is the pulse width,  $(T_W)_{\min}$  is the minimum pulse width,  $f_p$  is the pulse repetition frequency,  $(f_p)_{\max}$  is the maximum pulse



1



2

Fig. IV-44. Phase Plane Trajectory Pulse Modulated Attitude Control System (7-lb thrust)



Fig. IV-45 Experimental Actopilot

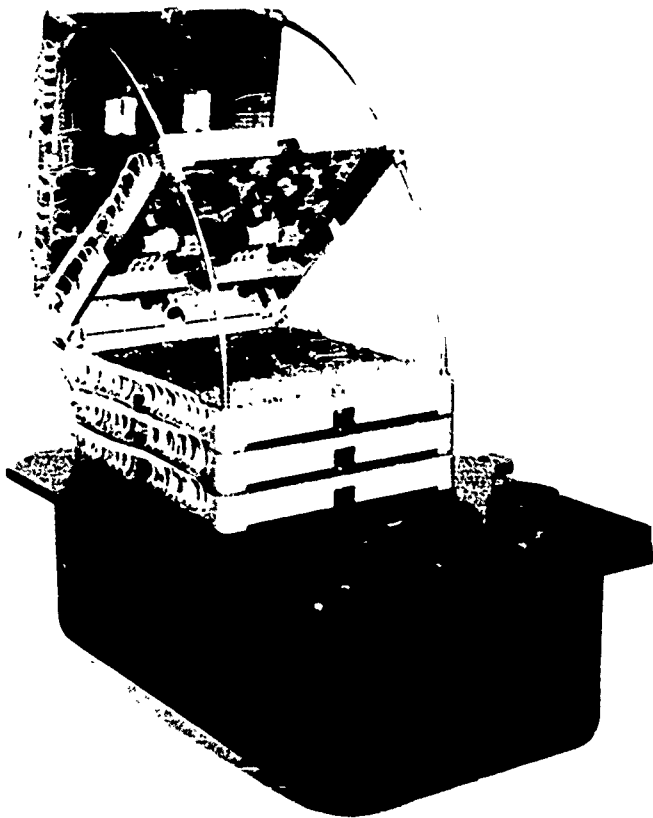


Fig IV-46 Internal Construction of Autopilot

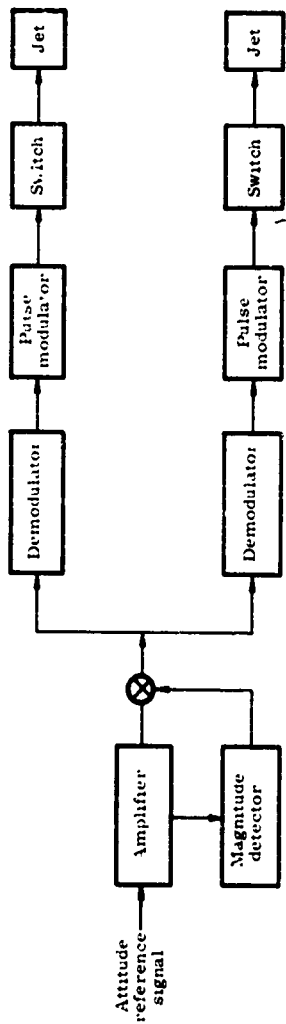


Fig. IV-47. Pulse-Modulated Control System

frequency, and  $x$  is the input signal normalized, the value of input error which produces a unity pulse train average value--(full on jets). The average value (or duty cycle) of the pulse train is equal to the product  $T_W f_p$  which is linear in  $x$ ,

$$T_W f_p = 4 (T_W)_{\min} (f_p)_{\max} (x)$$

For errors near the deadspot value, the pulse width is very nearly equal to  $(T_W)_{\min}$ .

### 3. Conclusion

The study indicates that the requirements of a control system for use with the attitude-occultation guidance system can be met with existing technology. A proportional pulse modulation attitude control system satisfies the accuracy requirements of the proposed guidance system. Under normal limit cycle operation, the vehicle on which the guidance system is placed may be kept within the required radar altimeter measurements (0.5 degree) and consequently within the 1 degree required for orbital corrections. The pulse modulated attitude control system minimizes fuel requirements. The major development problem in the control system is reliability; further design studies and a life test program are required to explore the potentialities of the dual propellant system herein described.

## V. ERROR ANALYSIS

### A. PROPAGATION OF LAUNCH ERRORS

In general, the satellite will be injected into the final orbit under conditions which deviate from those prescribed. If these deviations are excessive, the fuel required to make the corrections for the prescribed orbit would be intolerable. Therefore, remaining for assessment are the effects of deviations in velocity, altitude and flight path angle errors at the time of injection into the final orbit. An error in the inclination of the final orbit will also result from the injection deviation in azimuth, but velocity, altitude and flight path angle errors are normally the major sources of error. The effects of these errors are discussed below with reference to a circular orbit.

At the time of injection into the final orbit, two requirements must be satisfied if a circular orbit is to be achieved:

- (1) The velocity vector must be perpendicular to the local true vertical (i.e., the flight path angle = 90°)
- (2) The vehicle must be at the altitude corresponding to the magnitude of the circular velocity vector in (1) above.

In general, the above conditions will not be satisfied at injection, and an eccentric orbit will result. Silber\* has considered the variations from circularity as nonlinearized functions of the injection parameters. The eccentricity, as a result of altitude, velocity and flight path angle deviations, may be expressed as follows:

$$e \left( \frac{\Delta r}{r_c} \right) = \frac{\Delta r}{r_c} \quad (1)$$

$r_c$  = circular orbit radial distance

$\Delta r$  = deviation from correct radial distance.

$$e \left( \frac{\Delta V}{V_c} \right) = \left| \frac{\Delta V}{V_c} \right| \left( 2 + \frac{\Delta V}{V_c} \right) \quad (2)$$

$V_c$  = velocity for circularity

$\Delta V$  = velocity error.

---

\*Report No. DA TR 5-59, R. Silber, Aeroballistics Laboratory, April 1953.

$$e(\Delta\theta) = \frac{1}{\sin \Delta\theta} \quad (3)$$

$\Delta\theta$  = flight path angle error.

Combinations of these errors may be expressed as

$$e\left(\frac{\Delta r}{r_c}, \frac{\Delta V}{V_c}\right) = \frac{1}{1 - \left(1 + \frac{\Delta r}{r_c}\right)\left(1 + \frac{\Delta V}{V_c}\right)^2} \quad (4)$$

$$e\left(\frac{\Delta r}{r_c}, \Delta\theta\right) = \frac{1}{\sqrt{\sin^2 \Delta\theta + \left(\frac{\Delta r}{r_c}\right)^2 \cos^2 \Delta\theta}} \quad (5)$$

$$e\left(\frac{\Delta V}{V_c}, \Delta\theta\right) = \frac{1}{\sqrt{1 + \left\{ \left[ \left(1 + \frac{\Delta V}{V_c}\right)^2 - 1 \right] - 1 \right\} \cos^2 \Delta\theta}} \quad (6)$$

and

$$e\left(\frac{\Delta V}{V_c}, \frac{\Delta r}{r_c}, \Delta\theta\right) = \quad (7)$$

$$\frac{1}{\sqrt{1 - \left(1 + \frac{\Delta r}{r_c}\right)\left(1 + \frac{\Delta V}{V_c}\right)^2 \left[ 2 - \left(1 + \frac{\Delta r}{r_c}\right)\left(1 + \frac{\Delta V}{V_c}\right)^2 \right] \cos^2 \Delta\theta}}$$

In view of the fact that the radar will measure the altitude at injection, the radial distance error at injection should not be greater than 1 naut ml. The IR system should provide the proper flight path angle to approximately 0.10 degree. Therefore, if the velocity error can be held to 5 fps, the eccentricity should be 0.0019 according to Eqs (1) through (7) above. The assumed errors also introduce a slight rotation of the line of apsides; the direction of rotation being dependent on whether the errors are positive or negative.

The effects of this eccentricity on the apogee and perigee radii are:

$$\frac{\Delta r_A}{r_c} \left( \frac{\Delta r}{r_c}, \frac{\Delta V}{V_c}, \Delta\theta \right) = \frac{\left(1 + \frac{\Delta r}{r_c}\right)^2 \left(1 + \frac{\Delta V}{V_c}\right)^2 \cos^2 \Delta\theta}{1 + \sqrt{1 - \left(1 + \frac{\Delta r}{r_c}\right)\left(1 + \frac{\Delta V}{V_c}\right)^2 \left[ 2 - \left(1 + \frac{\Delta r}{r_c}\right)\left(1 + \frac{\Delta V}{V_c}\right)^2 \right] \cos^2 \Delta\theta}} \quad (8)$$

where

$r_A$  = apogee radius

and

$$\frac{\Delta r_p}{r_c} \left( \frac{\Delta r}{r_c} \cdot \frac{\Delta V}{V_c} \cdot \Delta \theta \right) = \frac{\left(1 + \frac{\Delta r}{r_c}\right)^2 \left(1 + \frac{\Delta V}{V_c}\right)^2 \cos^2 \Delta \theta}{1 - \sqrt{1 - \left(1 + \frac{\Delta r}{r_c}\right) \left(1 + \frac{\Delta V}{V_c}\right)^2} \left[ 2 - \left(1 + \frac{\Delta r}{r_c}\right) \left(1 + \frac{\Delta V}{V_c}\right)^2 \right] \cos^2 \Delta \theta} \quad (9)$$

where

$r_p$  = perigee radius

Substituting the above deviations in velocity, altitude and flight path angle into Eqs. (8) and (9) gives a ratio  $\frac{r_A}{r_p} = 1.0037$

where

$r_A$  = apogee radial distance.

$r_p$  = perigee radial distance.

This corresponds to an apogee-perigee difference of approximately 40 naut mi at the injection altitude in question.

The error coefficients for perturbations in the eccentricity and perigee-apogee radii are summarized in Table V-1.

TABLE V-1  
Error Coefficients

$\frac{\delta e}{\delta r_c}$	= 0.010/0.05% radial distance error at injection.
$\frac{\delta e}{\delta V_c}$	= 0.020/1% velocity error.
$\frac{\delta e}{\delta \theta}$	= 0.018/degree flight path angle error.
$\frac{\delta r_p}{\delta r_c}$	= 1% deviation in perigee radius/1% deviation in injection radius.
$\frac{\delta r_p}{\delta V_c}$	= 0 for $\Delta V > 0$ , -4% deviation in perigee/-1% deviation in velocity.
$\frac{\delta r_p}{\delta \theta}$	= 1.8% deviation in perigee radius/1% deviation in flight path angle.
$\frac{\delta r_A}{\delta r_c}$	= 3% deviation in apogee radius/1% deviation in injection radius.
$\frac{\delta r_A}{\delta V_c}$	= 4% deviation in apogee radius/1% deviation in injection velocity.
$\frac{\delta r_A}{\delta \theta}$	= 1.8% deviation in apogee radius/1% deviation in flight path angle.

## B. SYSTEM ERRORS

### 1. The Radar Altimeter

If the signal-to-noise ratio in the IF passband of the receiver can be maintained at a sufficiently high level ( $\frac{S}{N} > 12$  db), the radar range can be measured with a precision of from 0.10 to 0.20 mi. The radar altimeter section (IV-A) has shown that the signal-to-noise requirement can be satisfied with the system design. There are other sources of error, however, which will increase the above error estimate. Due to the method of tracking the local vertical, the radar will not, in general, be looking along the true vertical. In addition, the initial radar readings cannot be corrected for target latitude at the time these initial measurements are recorded, and a mean earth radius must be used to define the radial distance of the satellite from the center of the earth. When the orbital parameters have been established, the sum of the radar altitude readings and earth radius can be corrected for latitude.

A consideration of the geometry of the problem indicates that total error in defining the radial distance of the satellite from the center of the earth should be slightly under 1.0 mi in the initial calculations. This level of accuracy cannot be expected to hold for 1 yr of automatic operation, due to drifts in the vertical tracking system and the radar altimeter.

### 2. Infrared Vertical Tracker

The IR system provides the error signals for continuously erecting the vehicle to the local vertical. The accuracy of the IR system can be estimated from Fig. V-1.

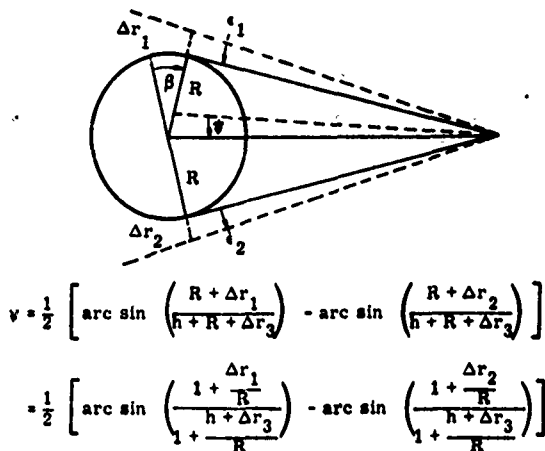


Fig. V-1. Accuracy of IR System

In an attempt to obtain the maximum value of  $\psi$  for a given altitude, one of the two radii of tangency is assumed to be at the pole, in which case  $\frac{\Delta r_1}{R}$  is maximum (-0.00225). The other two values of  $\Delta r$  are then functions of satellite latitude. However, for purposes of simplification, the altitude is assumed to be measured from the radius of a sphere of the same volume as that of the earth. Thus,  $\Delta r_3 = 0$ . With these simplifications, the error in the local vertical due to the earth's ellipticity is less than 0.122 degree above the 1000 statute miles. Thus, while this number represents only the inherent inaccuracy of such a vertical defining technique, it appears reasonable to assume that the local vertical can be known to within 0.1 degree at a 6000-mi altitude.

This accuracy seems to be sufficient, since the present studies indicate that errors in the direction of the thrust vector as large as 0.5 degree produce very slight errors in the orbital parameters.

It is not expected that a 0.10 degree precision could be maintained over a period of 1 year due to drifts in circuit components of the system.

### 3. Occultoscope-Star Tracker System

The overall effects of any errors in the occultoscope-star tracker system will be interpreted as "time of occultation" errors insofar as the orbit computation is concerned. These errors arise from meteorological fluctuations and instrument errors. Work\* completed on another phase of this effort shows that the expected error in the determination of the actual occultation time should be no greater than 0.10 sec. In the error analysis of the system contained in the following section (V-C), we have assumed the "time error equivalent" to be somewhat larger. The geometry used in the error analysis (as shown in Section V-C) and the "time equivalent error" at the upper limit of the occulting surface are taken as 1.5 mi (Fig. V-2).

Use of this estimate of error results in predicted position error within the 1 mi required if an excess of orbit computation data is available.

---

\*"Stellar Aberrascopes Study," Final Report, General Mills, Inc., December 1960.

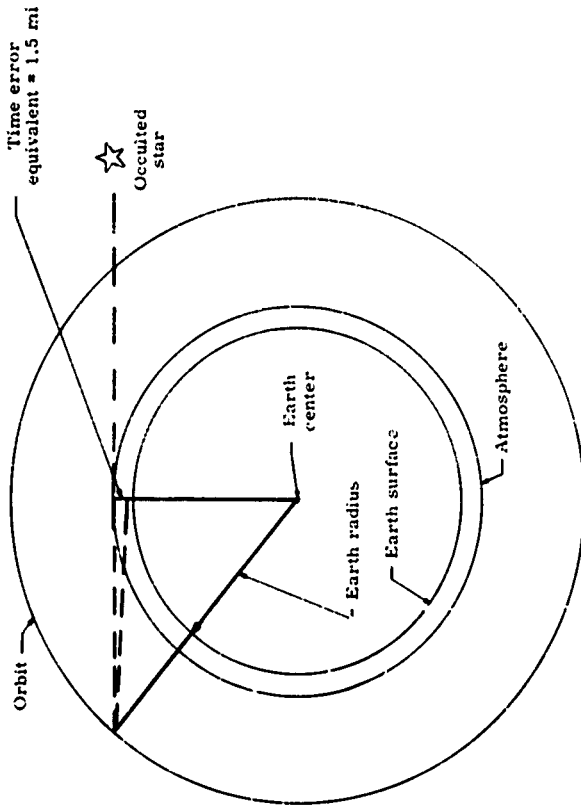


Fig V-2. Time Equivalent Error

### C. COMPOUNDED SYSTEM ERROR ANALYSIS

The problem of processing data to obtain a prediction is crucial to any position-predicting system. In this section we will consider:

- (1) Measurement of errors.
- (2) Handling of systematic instrument errors.
- (3) Errors in time.
- (4) Sources of errors.
- (5) Program for evaluating system.

#### 1. Measurement of Errors

Errors measurements have been considered as

$$\Delta m_i = \sum_{j=1}^6 \frac{\partial M_i}{\partial C_j} \Delta C_j \quad (1)$$

Measurements usually are given as range, an angle, a range rate, or angular rate, at some known certain time. A range measurement means that the object is some place on a sphere. Near the approximate position, the sphere can be considered by a plane. An error in range implies an error in the location of this plane. Let  $\vec{d}_i^0$  be a unit vector normal to the  $i^{\text{th}}$  range plane. The direction cosines of  $\vec{d}_i^0$  are  $\cos \alpha_i \cos \beta_i$  and  $\cos \gamma_i$ . An error in range causes an error in the positioning of the range plane along the normal. The positioning of this range plane for a given range error is

$$\Delta \gamma_i = \Delta x_i \cos \alpha_i + \Delta y_i \cos \beta_i + \Delta z_i \cos \gamma_i \quad (2)$$

If the approximate orbit is known then the direction cosines are known. We assume that a slight error in the direction cosines caused by errors in the approximate position are negligible. Since

$$\Delta x_i = \sum_{j=1}^6 x_{ij} (\dot{c}_j^0) \Delta C_j$$

$$\Delta y_i = \sum_{j=1}^6 y_{g_j} (\delta t_i) \Delta C_j \quad (3)$$

It is possible to write  $\Delta x_i = \sum_{j=1}^6 x_{g_j} (\delta t_i) \Delta C_j$

$$\Delta y_j = \sum \frac{\partial M_j}{\partial C_j} (\delta t_i) \Delta C_j \quad (4)$$

by combining Eq.(2) and (3). This is the form required for use in the least squares method.

An angle measurement also establishes a plane. A direction measurement is the intersection of two normal planes, each plane containing the line of sight. An error in direction is the error of the intersection of two planes whose position errors are independent of each other. An error in direction is written in the required form as two independent measurements of position planes which are normal to each other.

Error in range doppler can be written, where  $\frac{\partial \Delta r}{\partial t} = \Delta \dot{r}_j$

$$\Delta \dot{r} = \Delta \dot{x}_1 \cos \alpha_1 + \Delta \dot{y}_1 \cos \beta_1 + \Delta \dot{z}_1 \cos \gamma_1 \quad (5)$$

Using Eq (3)

$$\Delta \dot{x}_1 = \sum_{j=1}^6 x_{g_j} (\delta t_i) \Delta C_j$$

$$\Delta \dot{y}_1 = \sum_{j=1}^6 y_{g_j} (\delta t_i) \Delta C_j \quad (6)$$

$$\Delta \dot{z}_1 = \sum_{j=1}^6 z_{g_j} (\delta t_i) \Delta C_j$$

leads to

$$\Delta r = \sum \frac{\partial M_1}{\partial C_j} (c' t_1) \Delta C_j \quad (7)$$

which can be used with our formalism.

For angular rate measurement, similar reasoning leads to the required form with the two independent measurement planes in velocity space.

## 2. Handling of Systematic Instrument Errors

Instrument errors are usually classified as random and systematic. We have shown how to handle random errors, and until now we neglected the possibility of systematic errors which can be handled. To illustrate, we take a radar set range measurement. A radar measures the time interval between the sending and receiving of a radar signal. There are two possible systematic errors besides the random or noise errors. The range or the time interval is measured by starting and stopping of some timing device. The radar may consistently start or stop the timing device early or late. This means that the measured range, outside random errors, is off by a constant. The second error would be in the timing device. It may run fast or slow which introduces a linear error in the range measurement. A range measurement can then be considered as

$$r_{\text{measured}} = r_0 + \Delta r_1 + a + br_0 \quad (8)$$

where  $\Delta r_1$ , the random Gaussian error,  $r_0$  the actual range,  $a$ , a range error in stopping and starting of clock and  $br_0$ , the error caused by the timing device being fast or slow. Equation (8) can be written as

$$\Delta r_1 = r_{\text{measurement}} - r_0 - a - br_0 \quad (9)$$

Equation (3) becomes

$$\Delta r_1 = \sum_{j=1}^6 \frac{\partial M_1}{\partial C_j} (c' t_1) \Delta C_j - a - br_0 \quad (10)$$

The developed formalism can be used. The systematic errors are just treated as two additional constants of integration. Any systematic error which can be linearized can be counted for by considering it as an additional integration constant to be evaluated.

### 3. Errors in Time

Until now we have assumed that the basic time of the measurement was not in error (i. e., the clock was perfect). If there is systematic linear error in the clock, this error can be treated as another constant to be evaluated. The error in the clock would generate an error in the position of the reference orbit. The errors with respect to the reference orbit would be

$$\Delta m_1 = \sum_{j=1}^6 \frac{\partial M_1}{\partial C_j} \Delta C_j + \frac{\partial M_1}{\partial t} \cdot a t \quad (11)$$

where "a" is rate of linear time error. Note that a time error for elliptical orbits might be considered an error in the semimajor axis, or in the gravitational constant.

If the time of measurement itself is subject to a random error then

$$\Delta m_1 = \sum_{j=1}^6 \frac{\partial M_1}{\partial C_j} \Delta C_j + \frac{\partial M_1}{\partial t} \Delta t$$

or

$$\Delta m_1' = \Delta M_1 - \frac{\partial M_1}{\partial t} \Delta t = \sum_{j=1}^7 \frac{\partial M_1}{\partial C_j} \Delta C_j$$

where  $\Delta M_1'$  is new measurement error that includes random time error. The square of the standard deviation of  $\Delta M_1'$  is equal to the sum of the squares of the standard deviation of  $\Delta M_1$  and  $\frac{\partial M_1}{\partial t} \Delta t$ .

#### a. Nonindependent measurements

We have assumed that each measurement is independent. For the system that we shall evaluate, the occultation readings will not be completely independent. The variation in the atmosphere is really not Gaussian. It could be hoped that some sort of prediction method could be incorporated into the present position predicting system to improve it. This paper does not consider nonindependent measurements.

#### b. Evaluation of a functioning system

After a system is in operation, it should be evaluated. By using the "best" orbit, the  $\Delta m_1$  can be tabulated and the instrument standard

deviation can be evaluated statistically. If more than one type of measuring instrument is used, care must be taken in the evaluation of the individual instrument errors.

In the evaluation of the actual standard deviation of the instrument errors, the distribution of the samples should be Gaussian. Measurements taken in different directions and different parts of the orbit also should be subjected to analysis of variance to try to locate irregularities in the evaluation of the standard deviation. Any non-Gaussian effects could indicate that the instrument error is non-Gaussian or that there is a systematic error in the orbit, i. e., some significant physical effect is being neglected. Whether any non-Gaussian effect is the instrument or an error in the equations of motion will have to be left to the discretion of the person analyzing the statistics and available physical explanations. The existence of non-Gaussian effects should be investigated with all the tools of statistics and physics. An attempt should be made to construct some explanation for the existence of non-Gaussian effects exists.

### c. Probability ellipsoid

We want to know the size of the ellipsoid for different p (percentage) levels. First, find the eigenvectors and eigenvalues of the 3-dimensional positional probability ellipsoid. Reorient the axis and the distribution is in terms of  $\xi$ ,  $\zeta$  and  $\eta$  and the inverse square root of the

eigenvalue ( $\sigma_i = \sqrt{\lambda_i}$ )

$$f(\Delta x) = \frac{1}{(2\pi)^{3/2}} \sigma_\xi \sigma_\zeta \sigma_\eta e^{-1/2 \left[ \left(\frac{\xi}{\sigma_\xi}\right)^2 + \left(\frac{\zeta}{\sigma_\zeta}\right)^2 + \left(\frac{\eta}{\sigma_\eta}\right)^2 \right]} d\Delta \vec{x} \quad (12)$$

A linear change in variables,  $x = \frac{\xi}{\sigma_\xi}$ ,  $y = \frac{\zeta}{\sigma_\zeta}$  and  $z = \frac{\eta}{\sigma_\eta}$  make

the distribution spherical. Now change to spherical coordinates and the probability of the actual object being within a certain sphere R (i. e., a certain ellipsoid) is

$$P_3(R) = \frac{4\pi}{(2\pi)^{3/2}} \int_0^R e^{-1/2 r^2} r^2 dr$$

$$= \sqrt{\frac{2}{\pi}} \left[ \int_0^R e^{-1/2 r^2} dr - R e^{-1/2 R^2} \right] \quad (13)$$

For two dimensions, the equation is

$$P_2(R) = \frac{1}{2\pi} \int_0^R 2\pi r e^{-\frac{r^2}{2}} dr = 1 - e^{-\frac{R^2}{2}}$$

and for one dimension

$$P_1(R) = \frac{1}{2\pi} \int_{-R}^R e^{-\frac{r^2}{2}} dr \quad (14)$$

These are tabulated in the following order.

<u>R</u>	<u>P<sub>3</sub>(R)</u>	<u>P<sub>2</sub>(R)</u>	<u>P<sub>1</sub>(R)</u>
0.5	0.0113	0.1175	0.3829
1.0	0.1087	0.3935	0.6827
1.5	0.4779	0.6753	0.8664
2.0	0.7586	0.8647	0.9545
2.5	0.9000	0.3561	0.9876
3.0	0.9707	0.9880	0.9973
3.5	0.9934	0.9978	0.9999
4.0	0.9989	0.9997	1.0000
4.5	0.9998	1.0000	1.0000
5.0	1.0000	1.0000	1.0000

#### 4. Sources of Error

There are two major sources of error in the measurement of the time of egress or ingress of star by an occultation instrument. One source is the occultation instrument's inability to determine the exact time of occultation. The other is in our knowledge of the exact density profile of the refracting atmosphere at any specific time. The linear sum of both errors will be considered as variations in our knowledge of the radius of the earth. Both the occultation instrument time error and earth radius atmospheric errors for this analysis are assumed to be Gaussian, independent and with fixed standard deviations, so that their linear combination has a normal distribution.

##### a. Effect of errors

When an egress or ingress of a star occurs, the satellite is somewhere on the occultation cylinder (see Fig. V-3).

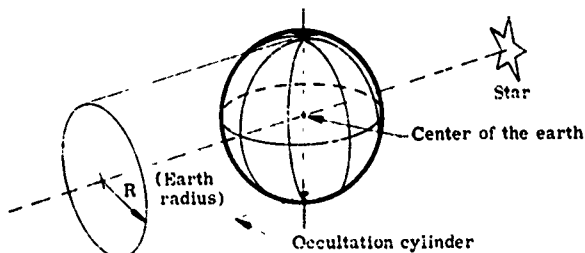


Fig. V-3

When the approximate position of a satellite is known, the occultation cylinder can be approximated by an occultation plane. The satellite is in some "sample" plane which is parallel to this occultation plane when the occultation instrument indicates an occultation. Since both sources of error are Gaussian, the distribution of distances of the sample plane from the occultation plane is therefore Gaussian.

#### b. Coordinate system

The intersection of the satellite orbit and the occultation plane will be the origin of right-handed Cartesian coordinates  $(\Delta x, \Delta y, \Delta z)$ . The  $\Delta z$  axis is established by drawing a line through the origin and the center of the earth with the positive direction being away from the earth. The  $\Delta x$  axis is in the satellite orbital plane with positive direction in the direction of the velocity vector of the satellite.

The distance between the occultation plane and the  $i^{\text{th}}$  sample plane is  $\Delta d_i = \Delta d_i^* \cdot P_i$ , where  $\Delta d_i^*$  is unit vector normal to occultation plane and  $P_i$  is any position  $(\Delta x_i, \Delta y_i, \Delta z_i)$  on the sample plane. The direction cosines of  $\Delta d_i^*$  are  $\cos \alpha_i$ ,  $\cos \beta_i$  and  $\cos \gamma_i$ .

$$\Delta d = \Delta x_i \cos \alpha_i + \Delta y_i \cos \beta_i + \Delta z_i \cos \gamma_i \quad (15)$$

#### c. Calculation of occultation plane

Because our primary interest is in errors in circular orbits, the orbit will be assumed circular about a spherical earth (Fig. V-4). The position of the star of the  $i^{\text{th}}$  occultation will be given by its right ascension  $(\alpha_i)$ , and its declination  $(\delta_i)$ , where the right ascension is

measured in the orbit plane from the x-axis. For a specific star and a specific orbit the relative  $\alpha_1$  and  $\delta_1$  can be calculated from the celestial right ascension and declination and knowledge of the specific orbit.

In a right-hand Cartesian coordinate system (x, y, z) whose origin is the center of the earth, the satellite orbit defines the x-y plane where the arbitrarily chosen perigee defines the x-direction. Using usual Eulerian angles (see Goldstein, Classical Mechanics, Section IV-4), rotate by an angle  $\alpha_1 - \frac{\pi}{2}$  about the z-axis (see Fig. V-4). Then rotate by an angle  $\delta_1$  about new x'-axis. This points the new y'' axis at the star.

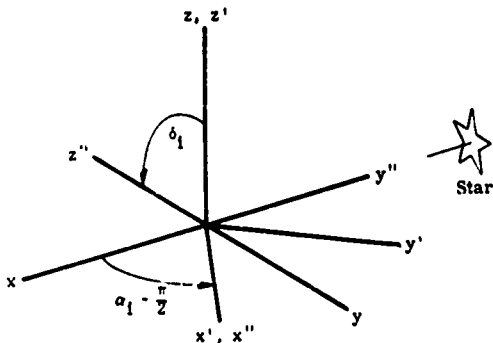


Fig. V-4

The equation of the occultation cylinder will be  $x''^2 + z''^2 = R^2$ .

The intersection of the orbit and the occultation cylinder will occur at

$$r^2 - y''^2 = R^2 \quad (16)$$

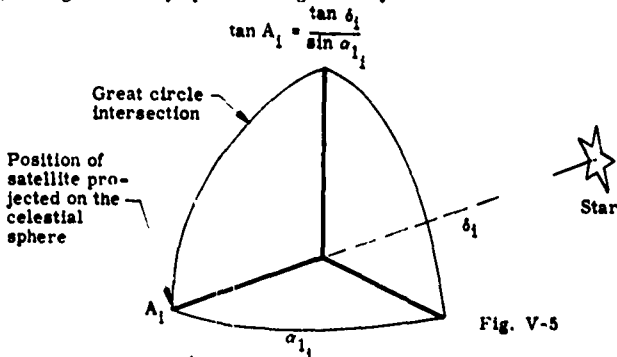
where  $r$  is the distance the satellite is from the center of the earth. Let  $\theta$  be the angle from the x axis to the satellite's position. It can be shown that the satellite crosses the occultation cylinder when (use Eq (16))

$$[1 - \cos^2 \delta_1 \cos^2 (\theta - \alpha_1)] = \frac{R^2}{r^2} \quad (17)$$

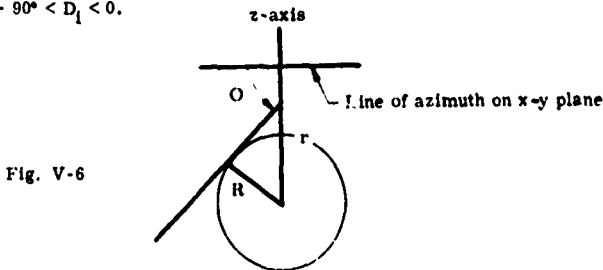
Given  $r$  of the specific circular orbit, there are four values of  $\alpha_{M_1}$   $\equiv \theta - \alpha_1$  which satisfy Eq (17). Occultation can occur only where  $\cos(\theta - \alpha_1) = \cos(\alpha_{M_1}) < 0$ .

d. Direction of errors

When the plane is through the center of the earth, the satellite and reference star, this plane intersects the earth forming a great circle (see Fig. V-5). By spherical trigonometry:



The angle  $A_1$  is the  $i^{\text{th}}$  star's azimuth in the satellite's,  $(\Delta x, \Delta y, \Delta z)$ , coordinate system at the time of occultation. From Fig. V-6, the  $i^{\text{th}}$  star's declination  $D_1$  at the time of occultation is  $\cos D_1 = \frac{R}{r}$  where  $-90^\circ < D_1 < 0$ .



The direction cosines of the line joining the satellite and the star are:

$$\begin{aligned}\cos \alpha_{s_1} &= \cos D_1 \cos A_1 \\ \cos \beta_{s_1} &= \cos D_1 \sin A_1 \\ \cos \gamma_{s_1} &= \sin D_1\end{aligned}\quad (18)$$

The azimuth of  $\Delta \vec{d}^*$  is obviously equal to  $A_1$  and its declination is equal to  $D + \frac{\pi}{2}$ . The direction cosines of the normal are:

$$\begin{aligned}\cos \alpha_1 &= -\sin D_1 \cos A_1 \\ \cos \beta_1 &= -\sin D_1 \sin A_1 \\ \cos \gamma_1 &= \cos D_1\end{aligned}\quad (19)$$

For the radar readings, the direction cosines of the sample plane are fixed  $\cos \alpha_1 = \beta_1 = 0$  and  $\cos \gamma_1 = 1$ .

### 3. Program for Evaluating System

#### a. Program

To obtain Eq (4) we use  $\Delta z = \Delta r_0 \cos \phi + \Delta_1 r \sin \phi$ ; ( $\eta = 0$   $i = 0$ )

$$\Delta r = 2\Delta r_0 + 2r \frac{\Delta V_n}{V} - \cos M (\Delta r_0 + 2 \frac{\Delta V_n}{V}) + \sin M (r \frac{\Delta V}{V})$$

$$\Delta \phi = -3M \left( \frac{\Delta r_0}{r} + \frac{\Delta V_n}{V} \right) + \Delta w + 2 \sin M \left[ \frac{\Delta r_0}{r} + 2r \frac{\Delta V_n}{V} \right] -$$

$$2 [1 - \cos M] \frac{\Delta V}{V} \text{ and Eq (19) to construct}$$

matrices  $(\cos \alpha_1, \cos \beta_1, \cos \gamma_1)$ . (20)

$$\begin{pmatrix} 0 & 0 & 1 & -2 + 2 \cos M_1 & -3 M_1 + 2 \sin M_1 & -3 M_1 + 4 \sin M_1 \\ \sin M_1 & \cos M_1 & 0 & 0 & 0 & 0 \\ 0 & 0 & 0 & \sin M_1 & 2 - \cos M_1 & 2 - 2 \cos M_1 \end{pmatrix} \quad 1$$

The product of these two is defined as  $m_i$  which is equivalent to Eq (5). Each  $m_i$  is then divided by its specific  $\sigma_i$ . The  $n$  readings and resulting  $\frac{m_i}{\sigma_i}$  are combined to form matrix

$$N = \begin{pmatrix} \frac{m_1}{\sigma_1} \\ \dots \\ \dots \\ \dots \\ \frac{m_r}{\sigma_r} \end{pmatrix} \quad (21)$$

which is multiplied by its transposed,

$$N N^T = M \quad (22)$$

$$\text{where } M = E \left[ \Delta M_p \Delta M_p \right] = \sum_{i=1}^n \left( \frac{1}{\sigma_i} \frac{\partial M_i}{\partial C_p} \right) \left( \frac{1}{\sigma_i} \frac{\partial M_i}{\partial C_j} \right) = \mu_{pj} = M_{pj}$$

The first piece of data to be obtained from the  $M$  is the quality of the evaluations of  $\Delta a$ . This is obtained by matrix multiplication,

$$(000022) M^{-1} \begin{pmatrix} 0 \\ 0 \\ 0 \\ 2 \\ 2 \end{pmatrix} = \sigma_{\Delta a}^2 \quad (23)$$

If a different set of parameters were used, the  $\sigma_{\Delta a}$  could have been taken directly from the  $M$  matrix.

For prediction, the matrix of the required linear transformation is equal,

$$P(t) = \begin{pmatrix} 0 & 0 & 1 & -2 + 2 \cos M_T & -3M_T + 2 \sin M_T & -3M_T + 4 \sin M_T \\ \sin M_T & \cos M_T & 0 & 0 & 0 & 0 \\ 0 & 0 & 0 & \sin M_T & 2 - \cos M_T & 2 - 2 \cos M_T \end{pmatrix} \quad (24)$$

The characteristic function of the 3-dimensional probability ellipsoid is obtained by matrix multiplication.

$$\psi(\vec{r}_{\Delta x}) = e^{-\frac{1}{2} \vec{r}_{\Delta x}^T P(t) \vec{r}_{\Delta x}} \quad (25)$$

The eigenvectors of this matrix are the eigenvectors of the positional probability ellipsoid and the square root of the eigenvalues are equal to the standard deviation along that axis in the positional probability ellipsoid.

To find the inplane probability ellipsoid, Eq (24) is redefined

$$P(t) = \begin{pmatrix} 0 & 0 & 1 & -2 + 2 \cos M_T & -3M_T + 2 \sin M_T & -3M_T + 4 \sin M_T \\ 0 & 0 & 0 & 0 & 0 & 0 \\ 0 & 0 & 0 & \sin M_T & 2 - \cos M_T & 2 - 2 \cos M_T \end{pmatrix} \quad (26)$$

and Eq (25) becomes

$$\psi(\vec{r}_{\Delta x}) = e^{-\frac{1}{2} \vec{r}_{\Delta x}^T \begin{pmatrix} \sigma_x^2 & 0 & \sigma_{xz}^2 \\ 0 & 0 & 0 \\ \sigma_{xz}^2 & 0 & \sigma_z^2 \end{pmatrix} \vec{r}_{\Delta x}}$$

which yields 2-dimensional inplane ellipsoid.

#### b. Evaluation of the system

A computer study was conducted to determine the quality of prediction that can be obtained by a satellite borne occultation-instrument radar-altimeter system. The study was not exhaustive but the general accuracy of the system was determined. We shall present some sample results to illustrate our general conclusions.

For the sample predictions we assume that the vehicle is in a six-hour circular orbit ( $r = 5.5 \times 10^7$  ft) and that occultation (ingression and egression) are taken from four stars whose location is given in Fig. V-7 and Table V-2. The  $\alpha_1$  and  $\delta_1$  were defined in Fig. V-4.

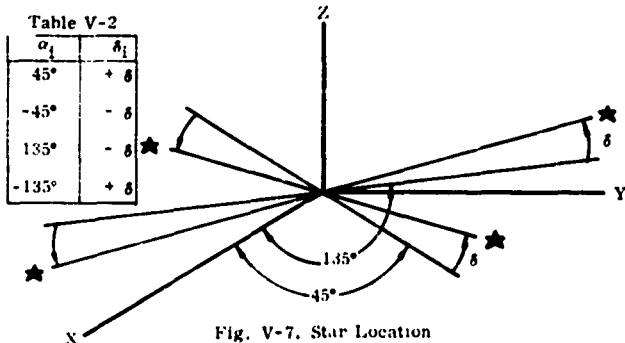


Fig. V-7. Star Location

The  $\delta_1$ 's were varied, but the absolute value  $\delta$  of the stars was the same for each prediction.

A  $3\sigma$  value (see Table 1) of the occultation readings was taken as 1.5 m which seems to be a reasonably representative value when considering the statistics of the atmospheric variation. If another  $3\sigma$  value were chosen, the results of the examples would only need to be linearly scaled. The  $3\sigma$  value may be pessimistic because the occultation readings are not completely independent and some sort of predictor method might reduce the inaccuracy. It should be noted that a constant bias should at least be assumed for the actual prediction. This bias would be treated as just another constant of integration (see Eq (10)).

In one orbit, 8 occultation readings can be taken (4 ingress and 4 egress). For the six-hour orbit, the elevation of an occulting star in the satellite coordinate system ( $\Delta x$ ,  $\Delta y$ ,  $\Delta z$ ) is  $-67.9^\circ$  (see Fig. V-6). The basic  $A_1$  and  $\alpha_1$  for  $\delta_1$  is given in Table V-3 (see Fig. V-5).

TABLE V-3

$\delta_i$	$A_i$	$\delta M_i$
5°	13.4°	158.4°
10°	27.5°	160.2°
15°	43.5°	163.6°

The quality of prediction is represented by a  $3\sigma$ , 3-dimensional ellipsoid (see Fig. V-8) which would contain 97% of the orbits if 8 occultation readings are taken, for  $360^\circ < M_i < 0$ ,  $\delta_i = 10^\circ$ ,  $3\sigma = 1.5$  mi. The prediction ellipsoids are for  $M_i = 0^\circ$ ,  $30^\circ$  and  $60^\circ$  (Fig. V-8).

In general, the tri-axial ellipsoid has axes which can be designated as the  $\Delta x$ ,  $\Delta y$  and  $\Delta z$  axes because the ellipsoid does not tumble as  $M_i$  varies. It oscillates and pulsates, but it does not tumble. In general, the  $\Delta x$ -axis is greater than the  $\Delta z$ -axis. As the declination of the stars is increased, the  $\Delta y$ -axis of the probability ellipsoid decreased rapidly while the  $\Delta x$ - and  $\Delta z$ -axes increased slowly.

Figures V-9 and V-10 represents the length of the  $\Delta y$ - and  $\Delta x$ - axis as a function of the  $M_i$  of prediction. The  $\Delta z$ -axis was not plotted because it is always less than the  $\Delta x$ -axis. The  $\Delta y$ -axis is cyclic as is the  $\Delta z$ -axis, but the  $\Delta x$ -axis increases as the time of prediction increases. By inspection of Eq. (20), it can be seen that the non-cyclic part of  $\Delta x$  comes from an error in  $\Delta a$  (i.e. an error in the evaluation of the period). For the runs of Figures V-9 and V-10 the  $3\sigma$  values of  $\Delta a$  are tabulated in Table V-4.

TABLE V-4

$\delta_i$	$\sigma_{\Delta a}$
5°	0.483 miles
10°	0.554 miles
15°	0.721 miles

The  $\Delta a$  increases with increasing  $\delta_i$ .

Although we are primarily interested in the 6-hr orbit, the altitude varies. The major effect of the lower altitude is an increase in the  $\Delta x$  error and a decrease in the  $\Delta z$  error.

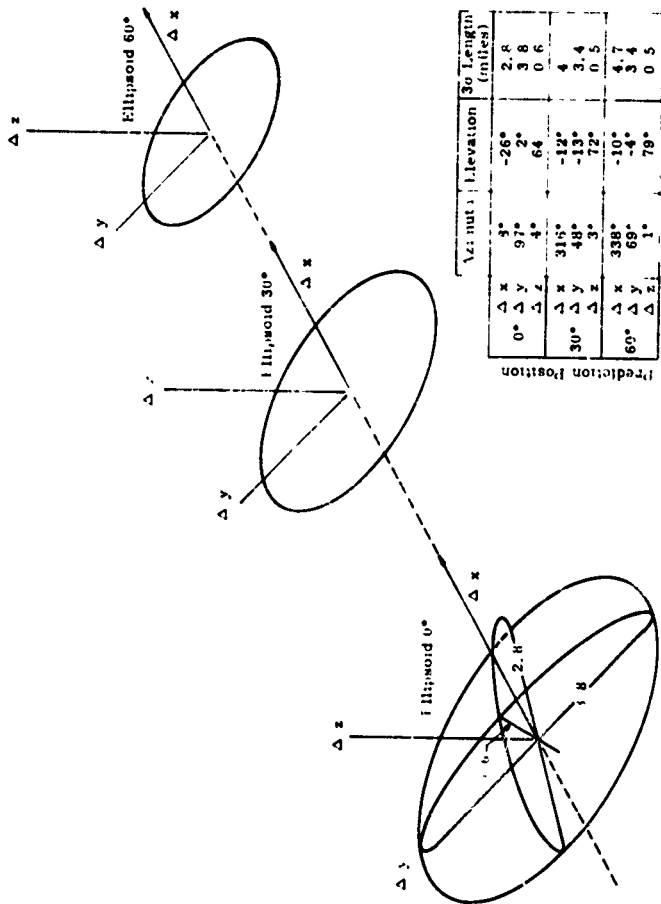


Fig. V-8. Three-Dimensional Ellipsoid

Because of the cyclic nature of the  $\Delta y$ -axis and its relative independence of  $\Delta x$ - and  $\Delta z$ -axes with respect to the perturbations of drag and oblateness, it is assumed that the  $\Delta y$ -axis may be smoothed over many orbits while the  $\Delta x$ - $\Delta z$  plane can only be smoothed over many fewer orbits. Because of this our interest is now focused on the projection of the ellipsoid onto the  $\Delta x$ - $\Delta z$  plane (see Eq 26)

Of vital importance is the effect of smoothing over several orbits.

Going back to the original 8 occultation readings in one orbit, radar readings are now added. Prediction is made where 4 or 12 additional radar readings are evenly spaced in one orbit where the radar  $3\sigma$  values are taken as 1.5, 0.7 and 0.3 mi.

The  $\Delta x$ -axis is plotted in Fig. V-12 for 1 radar readings and Fig. V-13 for 12 radar readings. In general, after several radar readings, additional radar readings do not improve the accuracy very much. The improvement is strongly affected by the  $\sigma$  of the individual radar readings (Figs. V-12 and V-13).

The radar readings primarily decrease the marginal  $\Delta z$  distribution of the probability ellipsoid. If the  $\Delta x$ -axis of the probability ellipsoid makes a relatively large angle with the  $\Delta z$  coordinate axis, the radar readings help a great deal. When the marginal  $\Delta z$  distribution is smaller than the  $\sigma$  of a radar reading, the radar reading does very little in improving the  $\Delta x$ -axis of the probability ellipsoid (i.e., the important error).

The radar, in general, helps to establish accurate prediction more quickly. If establishing accuracy in a few orbits is not necessary, the occultation measurements will eventually yield the required accuracy (Fig. V-11).

We shall consider the projection of the probability ellipsoid in the  $\Delta x$ - $\Delta z$  plane. For these predictions, 24 occultations readings were taken with  $\delta_1 = 5^\circ$

On the first of these runs, the 24 readings occurred in one orbit at the places specified in Table V-2. For the second run, the 24 readings were taken in 3 orbits; and for the third run, in 5 orbits. The resulting  $\Delta x$ -axis of the ellipsoid is plotted in Fig. V-11.

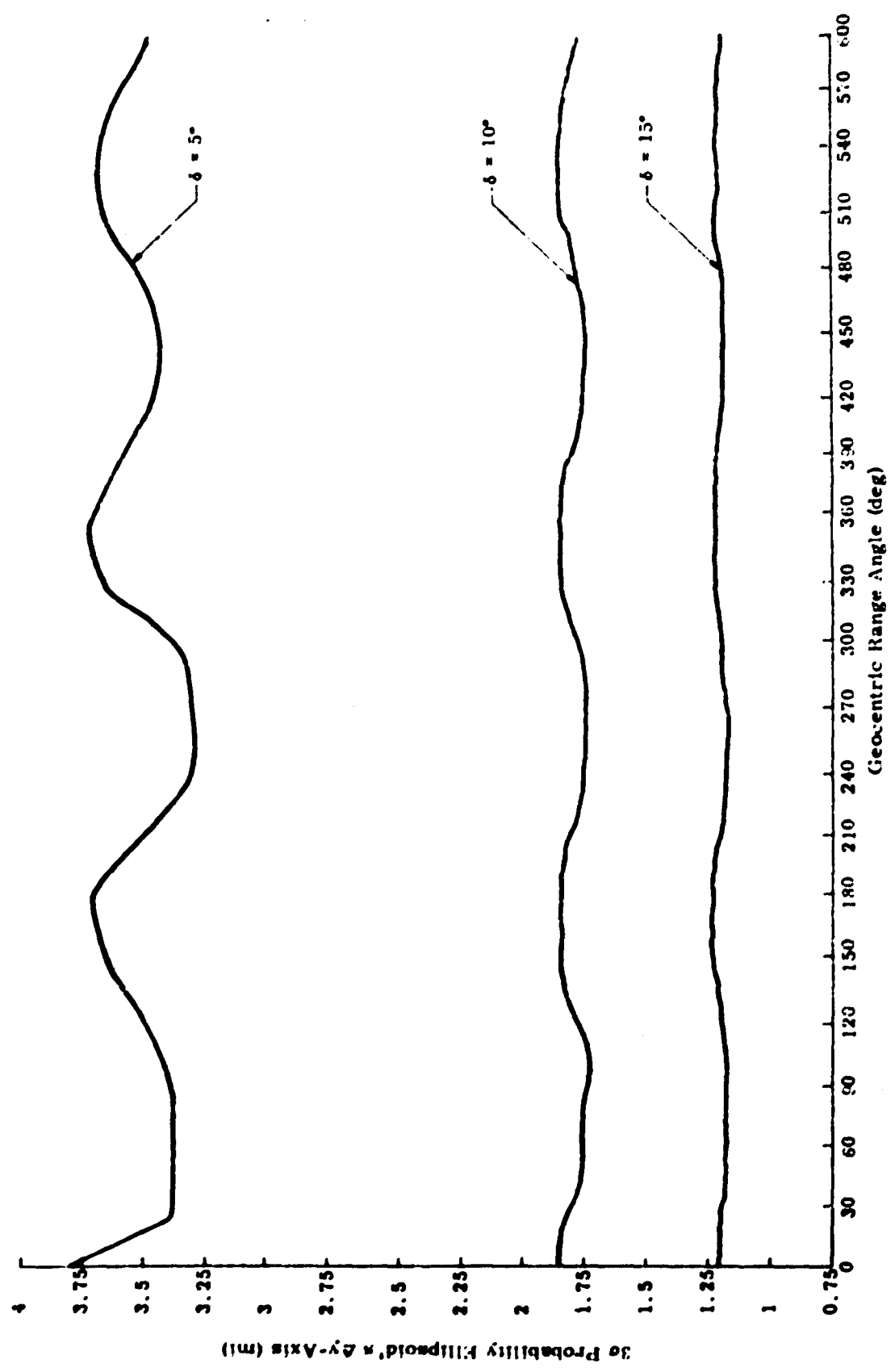
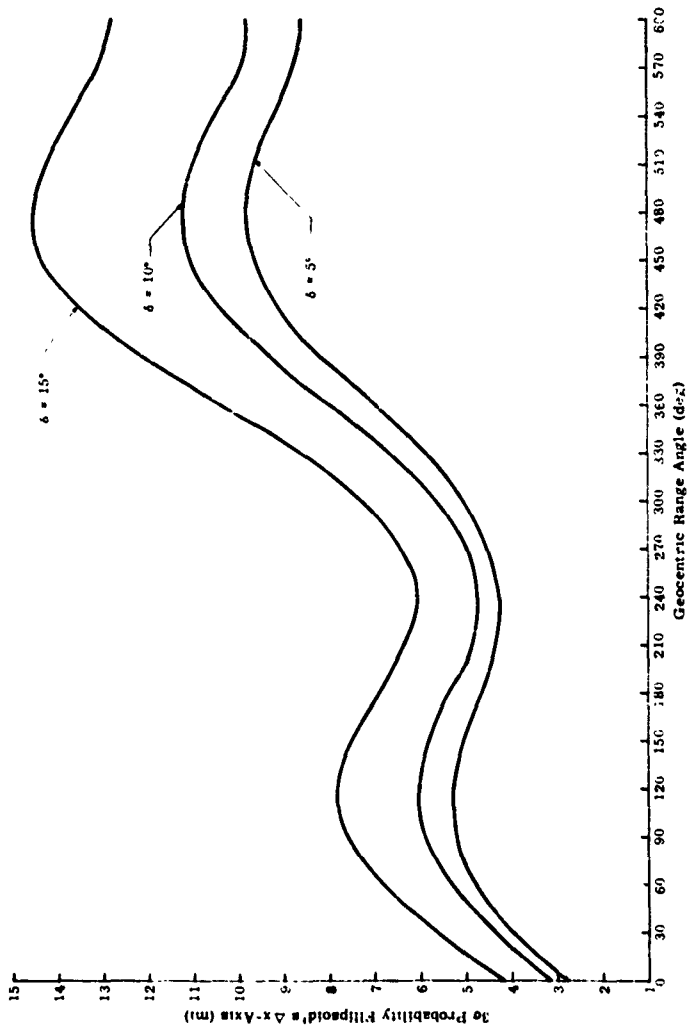


Fig. V-9. Effect of Occulting Star's Declination,  $\delta$

Fig. V-10. Effect of Occulting Star's Declination,  $\delta$

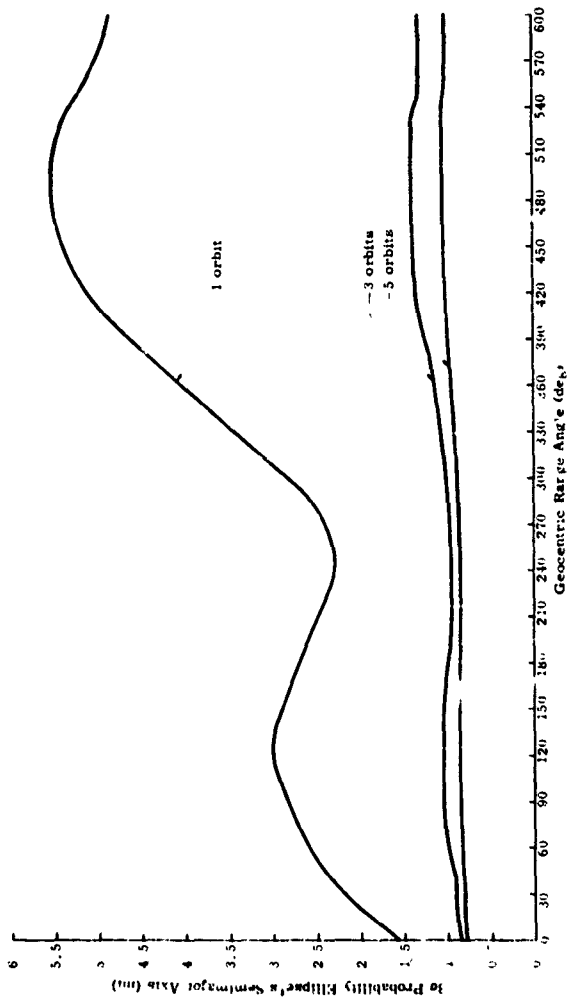


Fig. V-11. Effects of Smoothing Occultation Data (24 readings)

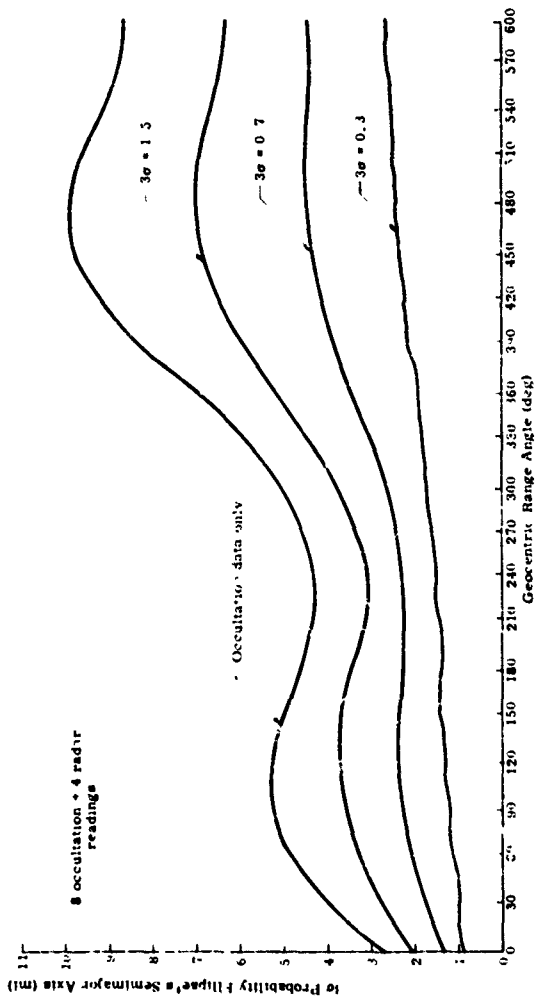


Fig. V-12. Effect of Additional Radar Readings with Varying Sigmas on Occultation Data

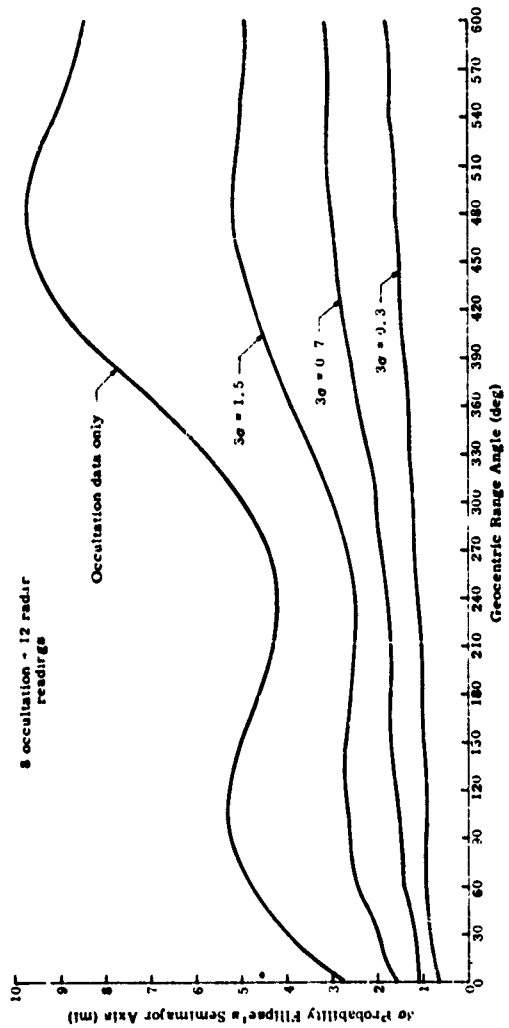


Fig. V-13. Effect of Additional Radar Readings with Varying Sigmas on Occultation Data

## VI. RELIABILITY ANALYSIS

In a study of this type, attention to reliability is an important means of determining the limits of mission length and complexity of equipment. Elaborate analyses of highly hypothetical equipment, environment and functions are better reserved for the time when an actual hardware program is closer to reality. The analysis below is an elementary estimate based on a favorable solution to the environmental control problem and also on a successful solution to all design problems. As an example of what is not considered, the horizon sensor used in Tiros I was useless because of certain technical features that were incorrectly specified. The horizon sensor did not "fail", apparently. The material presented in this section does not deal with such difficulties.

The reliabilities of various subsystems are offered as probably the best that could be achieved with component parts available in the next several years. Reliability comparisons of various alternative system concepts have not been made, since accuracy dictated the proposed configuration.

The most obvious conclusion is that a 1-yr mission seems out of the question.

### A. RADAR

The radar, used for measuring the earth-satellite distance, is a vital element of the guidance and control system. Cessation of range data would make it impossible for the satellite to determine and correct its orbit.

The recommended subsystem is a pulsed-magnetron timed-echo radar, unusual only in its extremely low pulse repetition frequency (15 pps) and its intermittent operation. The low prf does not appear to create any reliability problem. The on-off operation is a cycle of 90-sec warmup, 10 sec of pulse radiation and power off for 58 min. Total radiating time in 1 yr is then 24 hr, which is well below the minimum radiating life (250 hr) of the magnetron contemplated (Ref. VI-1). To be conservative, however, the operating time of the radar is taken to include warmup time, then, total time is 243 hr.

The estimated part count and probable failure rates are listed below. Before discussing these, it is well to note that the environmental parameters are quite uncertain and would remain so until a packaging concept is defined.

Environmental control in a satellite can make a very important difference in reliability. While shock and vibration protection for the initial boost are absolutely essential, the temperature control features for the 1-yr mission will determine the eventual life of the radar. In a vacuum, convection would depend on a locally contained atmosphere coupled to an external heat radiator. It seems certain that the requirement of 1-yr service dictates a nuclear reactor of rather low efficiency. Such a power source is quite likely to require dissipation of more than 1000 watts/sq m of satellite surface. That is a rule-of-thumb threshold beyond which an active cooling system is required. Thus a pressurized atmosphere for convection, with the attendant circulation system and pressure-gas reservoir, appears to be required.

Under these conditions, a comfortably high ambient should reduce the thermal stresses of intermittent radar operation.

In Table VI-1 below, estimated use of various parts in the radar is listed. Also shown are probable failure rates.

TABLE VI-1  
Radar Altimeter Reliability

<u>Component</u>	<u>Maximum Quantity</u>	<u>Failure Rate (failures/10<sup>6</sup> hr)</u>
Capacitors, LV	130	0.01
Capacitors, HV	4	1.32
Diodes, silicon	8	0.2
Diodes, zener	2	0.03
Diodes, rectifier	32	0.2
Diodes, miscellaneous	10	0.2
Coils, r-f	14	0.01
Coils, filter choke	1	0.03
Inductors	26	0.02
Resistor	100	0.03

TAEI 1, 1-1 (continued)

<u>Component</u>	<u>Maximum Quantity</u>	<u>Failure Rate (per year <math>\times 10^6</math> hr)</u>
Resistor	1	0.028
Transformer, power	1	0.4
Transformer, pulse	1	0.15
Transformer, 1F	13	0.1
Transistors	20	0.5
Klystron	1	3.0
Magnetron	1	150.0
Pentode	2	1.6
Thyratron	1	6.5
Blower	2	2.4
Fuses	2	0.5
Relays	10	0.04
Relay, thermal	1	0.4
Rectifier	1	0.6
Wave guide switch	2	0.5
Directional coupler	1	1.64
TR tube	1	5.0
Total failure rate		$20.109 \times 10^{-6}/hr$
Total operating time		<u>243</u>
Total expected failures (1 yr)		0.0506
Correction for orbital environment		$0.0506 \times 2 = 0.1012$
Reliability for one year		$= e^{-0.10} = 0.90$

The failure rates in the above table are taken from ref. VI-2. The correction for orbital magnetron was taken from proprietary data of Martin's Baltimore Division.

Some consideration of the total magnetron "radiating" time is in order. That is the time during which pulses are actually being transmitted. Although the rated life of the magnetron is 250 hr, there is evidence that many magnetrons will fail sooner. If it is desired to restrict total radiating time to 100 hr during a year, or 41 sec/hr, a 5-hr orbit should not involve any more than 246 sec of altimeter radiating time. Thus, six altimeter measurements per orbit should be restricted to below 41 sec each to be conservative of magnetron life. That allowance seems very generous, as just a few seconds, or only less than 10 at a rate of 15 pps, are needed for altitude measurement.

## B. IR SYSTEM

The horizon scanner used to establish the vertical is a group of horizon sensors and associated electrical circuitry. Barnes Engineering Company has a contract with ARPA which may result in the development of a long life, high reliability device. In this development program, Barnes has tested a breadboard vibrating-mirror type of sensor for over 2000 hr without failure. It is expected to have an operating life of over 1 yr. Older Barnes models (13-130) operated successfully in the first manned Mercury flight.

The recommended configuration is four sensors mounted along the edges of a four-sided pyramid, the diagonally opposite sensors being paired to provide detection of two vertical planes whose intersection is the vertical.

Based on data supplied for a similar three-sensor configuration, the reliability of the four-sensor system is quite low, 0.045 1-yr operation. Since the four-sensor system could be operated with one sensor out of commission, with certain fail-safe provisions, it is of interest to consider the probability of "any three of the four" working. That probability, computed by the binomial probability law, is 0.250, still quite low but a substantial enough improvement to motivate further study of the fail-safe feature.

Fail-safe devices would include:

- (1) Sensing the malfunction of one of the sensors.
- (2) Switching the outputs of the three good sensors from satellite attitude control amplifiers to an intermediate computer.

- (3) . Providing either a simple analog computer or a program for the satellite navigation computer, which could determine the vertical from three sensors

Given in Table VI-2 are the components of a single sensor and expected failure rates.

**TABLE VI-2**  
Reliability of a Single Horizon Sensor

<u>Part Type</u>	<u>Quantity</u>	<u>Total Failures/10<sup>6</sup> hr</u>
Resistor, 10%	94	4.0
Resistor, 1%	5	0.3
Capacitor, ceramic	4	0.2
Capacitor, electrolytic	9	0.3
Capacitor, tantalum	28	2.8
Capacitor, mylar	6	0.1
Diode, silicon	40	8.0
Diode, zener	1	0.2
Transistor, germanium	3	2.7
Transistor, silicon	39	19.5
Potentiometer	2	2.4
Multivibrator	1	1.2
Transformer	2	0.6
Trimpot	1	0.1
Motor	1	0.3

TABLE VI-2 (continued)

<u>Part Type</u>	<u>Quantity</u>	<u>Total Failures/10<sup>6</sup> hr</u>
Thermister bolometer	1	0.6
Vibrating-mirror assembly	1	<u>0.1</u>
Total		43.4 x 10 <sup>-6</sup>
Environmental factor		2
Operating time		8760 hr
Expected number of failures		0.76

Reliability of a single sensor for one year is  $R_s = e^{-0.76} = 0.468$

Given in Table VI-3 are the components of the Barnes Model 13-160 summer circuit, which combines the data from the individual sensors.

TABLE VI-3  
Reliability of Barnes Summer Circuit

<u>Part Type</u>	<u>Quantity</u>	<u>Total Failure/10<sup>6</sup> hr</u>
Resistor, 1%	3	0.2
Capacitor, ceramic	1	0.1
Capacitor, tantalum	3	0.3
Transistor, silicon	3	1.5
Diode, zener	1	0.2
Trimpot	2	0.2
Relay	3	<u>0.8</u>
Total failure rate		3.3 x 10 <sup>-6</sup>
Environmental factor		2
Operating time		8760 hr

Expected number of failures 0.0578

Reliability of summer circuit for one year is  $R_c = e^{-0.0578} = 0.942$

The reliability of the Earnes 13-150 with three sensors is

$$R_R^3 R_c = (0.463)^3 (0.942) = 0.0966$$

The reliability of a similar device with four sensors is approximately

$$R_S^4 R_c = (0.463)^4 (0.942) = 0.0452$$

The reliability of a device which uses four sensors if available, or three if one fails, is

$$R_c \left[ R_S^4 + 4R_S^3 (1 - R_S) \right] = R_c R_S^3 \left[ 4 - 3R_S \right] = 0.250$$

It would appear that the value of a four-head system lies largely in its providing a form of redundancy. Thus the additional fail-safe features mentioned above should be considered.

### C. OCCULTOSCOPE-STAR TRACKER

This sensor consists of five telescopes mounted on a stable platform, which maintains its orientation with respect to stars by a servodrive closing a loop with the telescopes. The control components are shown in Table VI-4.

Of the five telescopes, two are used for orbital tracking, and if either fails, the other provides sufficient data. Of the three remaining telescopes (which observe the orbital plane) any may fail, however, the remainder will provide sufficient data.

Calling the reliability of the control components  $R_1$  and the reliability of a single telescope and its associated hardware  $R_2$  (Table VI-4), the reliability of the occultoscope-star tracker is

$$\begin{aligned} R &= R_1 \left[ 1 - (1 - R_2)^2 \right] \left[ R_2^3 + 3R_2^2 (1 - R_2) \right] \\ &= R_1 R_2^3 (2 - R_2) (3 - 2R_2) \end{aligned}$$

TABLE VI-4

## Reliability of Occultoscope-Star Tracker

<u>Components</u>	<u>Quantity</u>	<u>Failure Rate/ 10<sup>6</sup> hr</u>	<u>Expected No. of Failures/10<sup>6</sup> hr</u>
<b>(Control)</b>			
Servo motor	3	0.23	0.69
Synchro	3	0.35	1.05
Worm gear assembly	3	0.9	2.7
Slip ring assembly	1	0.2	0.2
Gimbal assembly	1	7.5	7.5
Transistor, silicon	15	0.5	7.5
Power supply	1	6.5	6.5
<b>(Single telescope)</b>			
Lens	1	6.9	6.9
Vibrating slit assembly	1	0.6	0.6
Photomultiplier tube	1	20.0	20.0
Resistor	5	0.03	0.15
Capacitor	2	0.1	0.2
Photocell	1	4.7	4.7
Transistor, silicon	2	0.5	1.0
Relay DPDT	1	1.0/actuation	10.0

(Assume 10 actuations because this relay operates sun-protection cover, which should never be needed)

Total failure rate, controls  $26.14 \times 10^{-6}/\text{hr}$

Total failure rate, one telescope  $43.55 \times 10^{-6}/\text{hr}$

To account for orbit environment, we use an environmental factor of 2. Then

$$R_1 = e^{-52 \times 10^{-6} t}$$

$$R_2 = e^{-87 \times 10^{-6} t}$$

$$R = e^{-313 \times 10^{-6} t} (2 - e^{-87 \times 10^{-6} t}) (3 - 2e^{-87 \times 10^{-6} t})$$

For one year ( $t = 8760 \text{ hr}$ )

$$R = 0.0650 (1.532) (2.064)$$

$$= 0.206$$

#### D. POWER SYSTEM

Of the possible sources of power, the use of an isotope-fueled thermoelectric generator is recommended. The Martin Company has proposed, designed and built a variety of such generators, and the reliability estimate below is based on one such proprietary design (Ref. VI-4). A short discussion of the conceivable modes of failure is given below, followed by a reliability estimate of a power source suitable for the Synchronized Satellite.

The two vital functions to be performed by the power unit are:

Maintenance of the required Seebeck voltage.

(2) Control of the internal resistance.

The Seebeck voltage coefficient of the materials considered appears on the basis of tests to be only insignificantly degraded through time. If a mechanical failure in the structure of the power unit or an insulation failure occurs, an adverse effect on the Seebeck voltage may result. A fracture which results in leakage of the gas in the generator housing would cause chemical changes of active elements, resulting in increase of internal resistance. Insulation degrades with time, under elevated temperatures. The corresponding reduction in temperature gradient reduces generator efficiency.

Internal resistance and load resistance must be matched to allow operation of the generator at maximum output power. Also, an increased internal resistance lowers the maximum available power. Various metal bonds, spring contacts and thermoelectric elements may crack or fracture under vibration and shock. The attendant loss in circuit continuity causes partial or complete failure of the generator output.

Contact resistivity is considered the greatest contributor to increased internal resistance of the generator for long periods of time. The band between the heat source and the thermoelectric element, being maintained at a high temperature, sublimates significantly over a long period of time, resulting in increased internal resistance and reduced power output.

The various conceivable sources of failure are listed in Table VI-5 with estimated numbers of failures over the 1-yr period.

**TABLE VI-5**  
**Thermoelectric Generator Reliability Estimate**

<u>Source</u>	<u>Expected Number of Failures/1 yr</u>
<b>Seebeck voltage</b>	
(1) Thermoelectric units	
Degradation of element	0.000000
Element selection and installation	0.000000
(2) Temperature gradient	
Structure and loss of gas	0.000009
Thermal control	0.000196
Insulation	0.001000
<b>Internal resistance</b>	
(1) Mechanical failures	0.009240
(2) Degradation of contact and element resistivity	<u>0.000000</u>
Total expected number of failures	0.010445
Reliability for one year $e^{-0.010445} = 0.99$	

The extreme reliability of the thermoelectric units is borne out by tests of duration up to 315 days, with no significant change in the Seebeck voltage-temperature coefficient.

The structural reliability is based on a material strength safety factor of 1.5 and a material strength control to within 7.5% of nominal (1 $\sigma$ ). The probability of an overstress on this basis is 0.000009.

The thermal control reliability is based on two independent systems in active redundancy. Each system consists of linkages, hinges, support and spring, bellows, lines and a temperature sensing bulb, with a total failure rate of 1.6/million hr in the space environment. Excluding prelaunch difficulties, the expected number of failures for 1 hr is  $1.6 \times 10^{-6}$ , and the probability of survival is

$$R_t = 2e^{-1.6 \times 10^{-6} t} = e^{-3.2 \times 10^{-6} t}$$

For 1 yr,  $R_t = 0.999804$ , with an equivalent expected number of failures of 0.000196.

Insulation deteriorates slightly with age, and there is a small probability of sufficient degradation to cause generator output to drop below minimum power required. The calculations below were worked out based on an older power generator and would be more favorable with newer designs. It is estimated that the thermal conductivity of the insulation increases by about 1.7%/mo with a standard deviation of 0.05%/mo. Nominal heat loss through insulation is 15.5%, and if this exceeds 18.3%, power output will be below rated (minimum). Thus the safety margin is  $18.3\% - 15.5\% = 2.8\%$ , and the 15.5% will increase by  $0.017(15.5) = 0.263\%/mo$ . The standard deviation of the degradation of power loss is 0.49%; thus, the safety margin would start out at  $\frac{2.8\%}{0.49\%} = 5.7$  standard deviations, and this "normalized" safety margin would decrease by  $\frac{0.263\%}{0.49\%} = 0.537$  standard deviations per month. The probabilities of successful performance, by month, are shown in Table VI-6.

TABLE VI-6  
Insulation Reliability

<u>Month</u>	<u>Normalized Safety Margin</u>	<u>Reliability</u>
0	5.70	0.9999+
1	5.16	0.9998+
2	4.63	0.9998+
3	4.09	0.9999+
4	3.55	0.9998
5	3.02	0.9987
6	2.48	0.9934
7	1.94	0.9738
8	1.40	0.9192
9	0.87	0.8079

TABLE VI-6 (continued)

<u>Month</u>	<u>Normalized Safety Margin</u>	<u>Reliability</u>
10	0.33	0.62%
11	-0.21	0.11%
12	-0.74	0.00077%

It would seem obvious that a larger safety factor, either by insulation or a higher power generator, could improve these figures. Both means would be reflected as more weight, but it would be necessary to raise this particular reliability to at least 0.999 for 1 yr. Working backward in Table VI-6, it would take a normalized safety margin of 3.55 (shown for 4 mo) and that would have to be increased to  $3.55 + 12 (0.537) = 9.99$  for a new article. The stated 2.8% safety margin in power output loss due to insulation degradation then goes up to  $0.49\% (9.99) = 4.9\%$  and, finally, either:

- (1) Heat loss through insulation would have to be reduced from 15.5% estimated for a previous design to  $18.3 - 4.9 = 13.4\%$ .
- (2) Minimum allowable generator output would have to be decreased from 100 - 18.3 = 81.7% of rated to  $100 - (15.5 + 4.9) = 79.6\%$ . This could be accomplished by increasing the rated generator output by a factor of 1.027 or 2.7%.
- (3) Same combination of the above.

It is concluded that insulation reliability could be made better than 0.999 for 1 yr or an equivalent expected number of failures of 0.001, which is the number used in Table VI-5.

Mechanical failures which cause an increase in internal resistance have been discussed above. Reference VI-4 contains analysis leading to the conclusion that the expected number of failures per month would be 0.00077, due to bonds, elements and interconnections. Contact and element resistivity growth is fairly constant with time. A reasonable assumption appears to be that power output loss would be limited to a maximum of 10%, with a design-apportioned loss from this cause allowed to be 20%. Control of the internal resistance loss to a coefficient of variation of 0.025 would result in a reliability corresponding to

$$\frac{1.20 - 1.10}{0.025} = 4 \text{ standard deviations}$$

or

$$R = 0.9999+$$

The expected number of failures in Table VI-5 is taken to be 0.000000.

In summary (see Table VI-5), it is anticipated that with some improvements in design of presently existing or proposed isotope-powered thermoelectric generators, a reliability of approximately 0.99 can be achieved.

A solar power generator was also considered. This would consist of 7500 solar cells connected in a variety of series-parallel paths so that circuit continuity would be highly redundant. Approximately 2500 cells could fail without causing reduction in power output sufficient to degrade satellite equipment performance. It is believed that cell failures could occur only by damage from meteors, with an extremely low probability.

There would be three diodes for current control and a storage battery. The only other possible source of failure would be some of the 1500 cell-to-all solder connections. The total failure rate of the items in series is:

Diodes	$3 \times 0.2 \times 10^{-6}$	=	$0.6 \times 10^{-6}$
Battery	$1 \times 1.4 \times 10^{-6}$	=	$1.4 \times 10^{-6}$
	Total	=	$2.0 \times 10^{-6}/\text{hr}$
	Operating time		6760 hours
	Expected number of failures		0.017520

The failure rate of a solder connection is not at all agreed upon, but an extremely high figure is  $1 \times 10^{-6}/\text{hr}$ . The probability of failure of a single connection in 1 yr is, on that assumption, 0.0876, and the expected number of connection failures is  $1500 \times 0.0876 = 132$  failures. The standard deviation of the observed number of failures is

$(132 \times 0.9124)^{1/2} = 11$ ; thus, the probability of 500 failures corresponds to the probability of a normal deviate  $\frac{500 - 132}{11} = 33$  standard deviations from the mean. This probability is of the order of  $10^{-7}$  and thus can be neglected.

Finally, the reliability of the solar power generator is  $e^{-0.0175} = 0.9825$  for 1 yr. This is quite close to the reliability calculated for the isotope thermoelectric power generator, which was used in the system summary.

### E. CONTROL AND STABILIZATION SYSTEM

This consists of a set of thrust engines and an electromechanical programmer.

The thrust engines include the propellant plumbing and thrust chambers, reliability of which are taken from Ref. VI-3. There is considerable uncertainty as to the reliability of a thrust chamber, as it has not been possible to obtain a relationship between life, thrust energy, temperature of the propellant and chemical types of degradation of the nozzles. However, it is believed that a low temperature, low pressure monopropellant will allow practically infinite nozzle and chamber life, so that the failure rate has been taken as zero. Since the thrust chambers are the only redundant features, the remaining devices are all in series, as shown in Table VI-7. It will be noted that only attitude control features are listed. This is because velocity control for orbital corrections is expected to consist of only 100C thrusts, which is negligible for reliability purposes.

TABLE VI-7  
Reliability of Propulsion Subsystem

<u>Part</u>	<u>Quantity</u>	<u>Failure Rate</u>	<u>Usage (hr)</u>	<u>Expected Number of Failures</u>
Propellant pressure tank	1	$5 \times 10^{-6}/\text{hr}$	8,760	0,044
Propellant filter	1	$5 \times 10^{-6}/\text{hr}$	8,760	0,044
Thermal relief valve	1	$40 \times 10^{-6}/\text{hr}$	8,760	0,350

TABLE VI-7 (continued)

<u>Part</u>	<u>Quantity</u>	<u>Failure Rate</u>	<u>Usage (hr)</u>	<u>Expected Number of Failures</u>
Lines and fittings	--	$10 \times 10^{-6}/\text{hr}$	8,760	0,088
Pressure regulator	1	$7 \times 10^{-6}$ per thrust	70,000	0,490
Control solenoid and valve	6	$20 \times 10^{-6}$ per actuation	70,000	1,400
Thrust chamber assembly	12	0	140,000	--

Total expected number of failures in 1 yr 2,416

Reliability for 1 yr =  $e^{-2,416} = 0,0893$

Reliability function for t hr =  $e^{-276 \times 10^{-6} t}$

(propulsion only)

The programmer reliability is as follows:

Two synchronous timer motors, 1 rpm, one rotation every 24 hr, 12,2-hr total operating time. The failure rate is  $0,37 \times 10^{-6}$  and the expected number of failures is  $4,5 \times 10^{-6}/\text{yr}$ .

One-way clutch, 6,1-hr operating time, failure rate  $1,3 \times 10^{-6}$ ,  $1,3 \times 10^{-6}$  failures expected/yr.

Gear strain external to motors, 6,1-hr operating time, failure rate  $0,9 \times 10^{-6}$ ,  $5,4 \times 10^{-6}$  failures expected.

Ten microswitches operated by cams, each 24 times/day, in a total of 88,000 actuations. The failure rate is  $0,25 \times 10^{-6}$  and

expected number of failures is  $22,000 \times 10^{-6}$ . This item dominates.

Reliability for 1 yr,  $e^{-0.022} = 0.978$

Reliability function for t hr,  $e^{-3 \times 10^{-6} t}$

In conclusion, the reliability of the stabilization and control system is  $e^{-279 \times 10^{-6} t}$ , which for 1 yr is 0.9870. The propulsion system appears to be the outstanding weakness in a 1-yr mission. It is possible to obtain a more pleasing reliability prediction by hypothesizing more optimistic failure rates, but since other subsystems appear not much better, it is believed that such efforts are beyond the scope of this study.

## F. COMPUTER

The recommended computer has a number of reliability features, among which are:

- (1) Several types of redundancy in checking of arithmetic and ability to repeat computations in the event of discrepancy. This is valuable, because of the few errors made by computers, a large part are transitory and will not be repeated. This is especially true in space, where radiation causes errors.
- (2) Evaporated-film silicon connections for the memory, which eliminates the connections found in core-type memories.
- (3) Special advances in connector reliability by use of plated conductors and welded joints instead of soldered joints.
- (4) In the last analysis, the presence of humans who can repair computers is a valuable feature that should be considered further.

It must be recognized that no satellite has to this date been equipped with a digital computer. Therefore, all estimates are based on theoretical data. These are credible because the various component parts have mostly seen space duty successfully and because the Minuteman reliability program gives evidence of exceeding recently experienced reliabilities by orders of magnitude. A summary of the analysis (Ref. VI-5) is contained in Table VI-8.

TABLE VI-8  
Estimated Computer Reliability

<u>Component</u>	<u>Quantity</u>	<u>Failure Rate/ 10<sup>6</sup> hr</u>	<u>Total Failure Rate</u>
Resistor	1141	0.004	4.6
Diode, silicon	2305	0.002	4.6
Silicon memory	16	0.25	1.0
Capacitor	252	0.01	2.5
Transistor	355	0.01	3.6
Transformer	116	0.01	1.2
Welded joints	9116	0.00001	0.1
Case memory	1	1.0	1.0
Total failure rate			21.6 x 10 <sup>-6</sup> /hr
Environmental factor			2
Failure rate in orbit			43.2 x 10 <sup>-6</sup> /hr
For 1 yr, reliability is 0.687.			

It should be noted that most of the failure rates in Table VI-8 are taken from specifications in the Minuteman Program, as suggested by a leading computer manufacturer. For other subsystems, failure rates were used as recommended by authoritative sources, or according to Ref. VI-2, where not otherwise supplied.

The time standard is included with the computer and Table VI-9 shows its estimated components and reliability.

TABLE VI-9  
Reliability of Time Standard

<u>Component</u>	<u>Quantity</u>	<u>Total Failure Rate/ 10<sup>-6</sup> hr</u>
Quartz crystal	1	0.30
Crystal oven	1	0.05
Transistors	20	10.00
Resistors	50	1.50
Capacitors	20	2.00
Connectors	2,10 pin	4.00
Total failure rate		17.85 x 10 <sup>-6</sup>
Environmental factor		2
Failure rate in orbit		36 x 10 <sup>-6</sup>
Reliability for 1 yr		0.732

### G. PREDICTED SYSTEM RELIABILITY

The satellite has only a slight chance of operating for 1 yr successfully. The outstanding difficulties are the horizon scanner, the occultoscope-star tracker and the control-stabilization subsystems. The reason appears to be that these subsystems are required to operate continuously.

For a satellite to perform the required functions for 8760 hr with a 90% probability, the total failure rate allowable for continuous operation is about  $11 \times 10^{-6}$  failures/hr. This is the equivalent of one neon glow tube or about 22 silicon transistors operated carefully in the laboratory.

A much shorter mission time, or highly intermittent operation as allowed by lower accuracy requirements, would provide a more favorable possibility.

Summarized in Table VI-10 are the estimated reliability functions of the various subsystems, for  $t$  calendar hours.

**TABLE VI-10**  
Subsystem Reliability Functions

Radar	$e^{-12 \times 10^{-6} t}$
Infrared system	$e^{-267 \times 10^{-6} t} (4 - 3e^{-87 \times 10^{-6} t})$
Occultoscope-star tracker	$e^{-118 \times 10^{-6} t} (2 - e^{-22 \times 10^{-6} t})$
	$(3 - 2e^{-22 \times 10^{-6} t})$
Power system	$e^{-1.2 \times 10^{-6} t}$
Control-stabilization and programmer	$e^{-279 \times 10^{-6} t}$
Computer-time standard	$e^{-79 \times 10^{-6} t}$
Total system	$e^{-736 \times 10^{-6} t} (4 - 3e^{-87 \times 10^{-6} t})$
	$(2 - e^{-22 \times 10^{-6} t}) (3 - 2e^{-22 \times 10^{-6} t})$

The total system reliability for 1 yr is 0.0054.

In order to explore possibilities of shorter missions, the reliability functions were evaluated for various shorter times at 1-mo intervals. These results are presented in Table VI-11 and are shown graphically in Figs. VI-1 and VI-2.

**TABLE VI-11**  
**Estimated System Reliabilities**

<u>Time (mo)</u>	<u>Radar</u>	<u>Infrared</u>	<u>Occultoscope-Star Tracker</u>	<u>Power</u>	<u>Control Stabilization and Programmer</u>	<u>Computer-Time Standard</u>	<u>Total System</u>
1	0.991	0.981	0.959	0.999	0.816	0.944	0.717
2	0.982	0.926	0.926	0.998	0.665	0.891	0.498
3	0.974	0.852	0.887	0.997	0.543	0.841	0.335
4	0.965	0.767	0.854	0.996	0.443	0.794	0.221
5	0.956	0.684	0.816	0.995	0.361	0.749	0.144
6	0.947	0.604	0.780	0.994	0.295	0.707	0.0925
7	0.939	0.528	0.746	0.994	0.240	0.668	0.0591
8	0.930	0.459	0.718	0.993	0.196	0.630	0.0376
9	0.921	0.398	0.666	0.992	0.160	0.595	0.0231
10	0.912	0.342	0.634	0.991	0.130	0.562	0.0143
11	0.904	0.293	0.597	0.990	0.106	0.530	0.0088
12	0.895	0.250	0.563	0.989	0.087	0.501	0.0054

Figure VI-2 indicates the level of system reliability improvement which may be realized for the type of mission discussed in Section VIII. This figure is based on greatly reduced use of the attitude control system and the infrared system, with no reduction in use of the other subsystems.

Since the station keeping system is to be used rather infrequently, the reliability of this system, therefore, is not expected to present a problem.

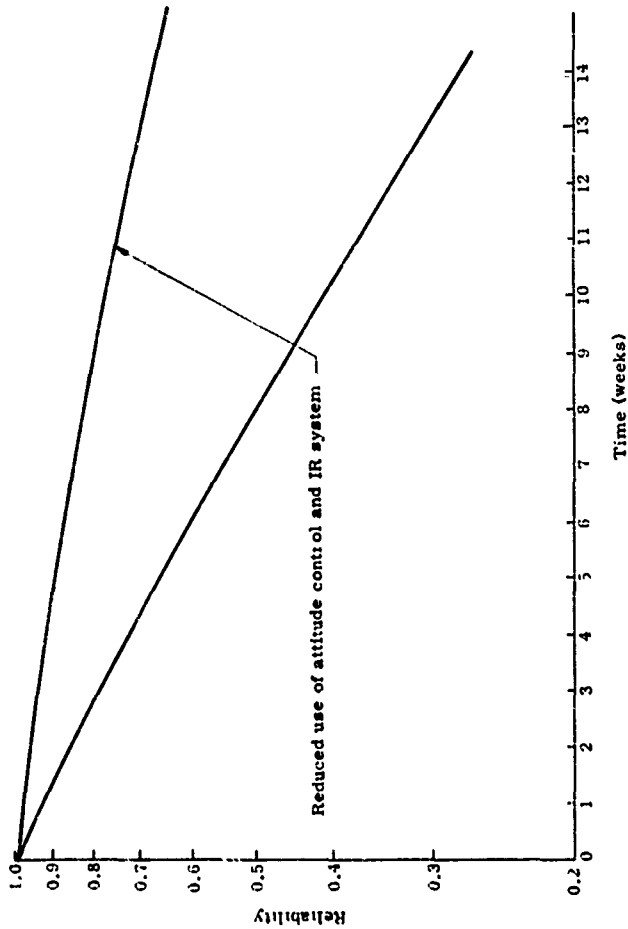


Fig. VI-1. Total System Reliability

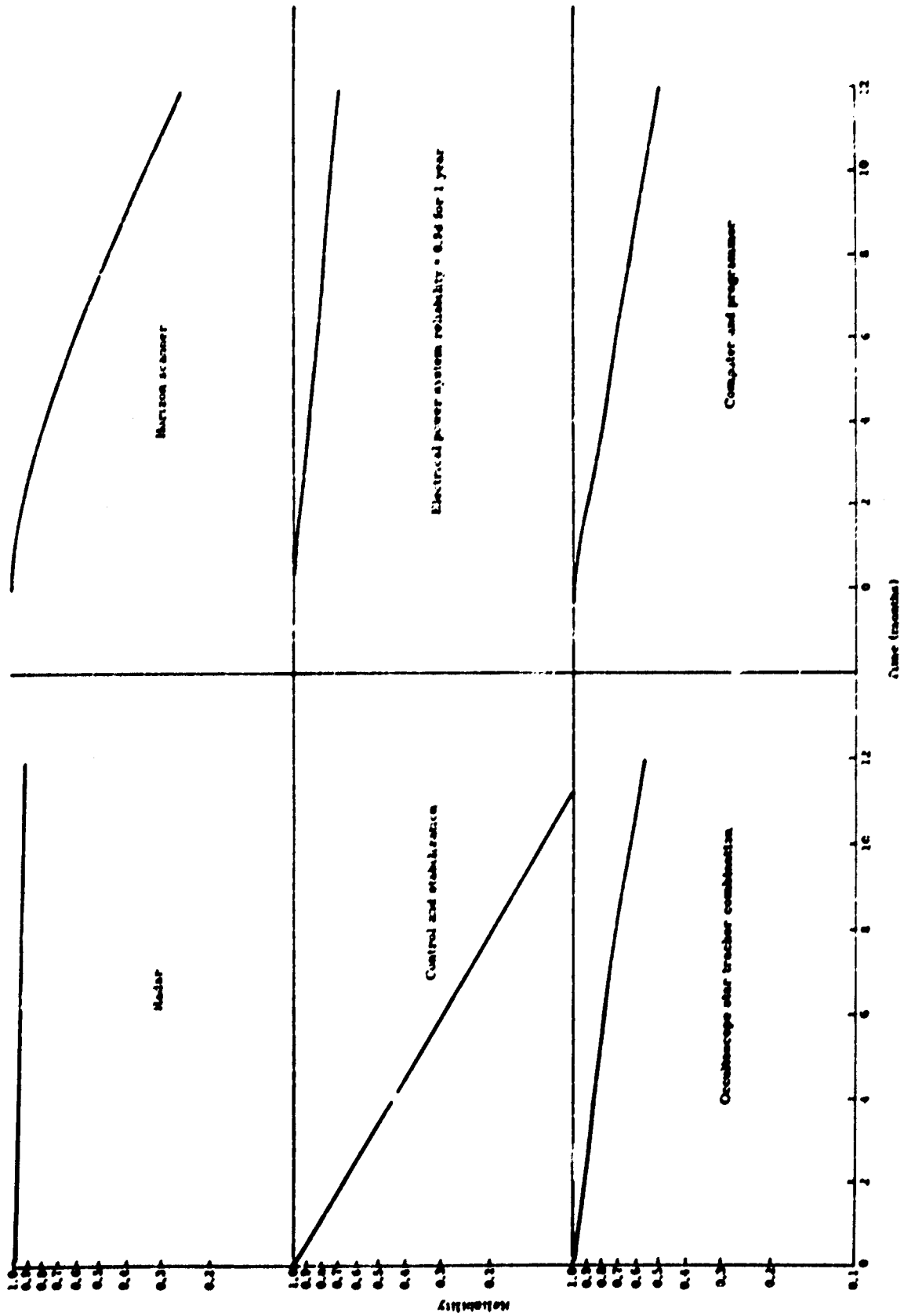


Fig. VI-2. Subsystem Reliability

## VII. SATELLITE SYNCHRONIZATION STUDY DEVELOPMENT PLAN

In order to determine how the altitude-occultation guidance system compares to the present state of the art of building and successfully operating such equipment, the steps needed to build a prototype system have been studied. The results of this study will be presented in this section of the report as a development time table (Fig. VII-1). Very little technical data is given in this section, since each of the subsystems is described in detail in other sections of the report.

The purpose of the study has been to determine the earliest date at which two flyable prototype systems (one as the primary flight article and the second as backup in case the first launch fails) can be completed. For planning purposes only, we have assumed that follow-on production consists of 16 operational systems. In order to provide for incorporating changes deemed advisable on the basis of the experimental launch a 6-month lapse between development and operational firings is assumed.

One further guideline has been that state-of-the-art hardware will be used wherever possible; research and development into new concepts are kept to a minimum. A go-ahead date of 1 January 1962 has been assumed. The significance of this assumption is that it provides a reference (with respect to other development programs) in order to evaluate the extent to which related programs can be used (directly or with modification) in this system.

The development plan, summarized in Fig. VII-1, shows that 30 months are required to have a flyable prototype ready for the experimental launch. Before the experimental launch is attempted, this time span will include a 3-month period of ground testing (during which the various subsystems will be integrated in a series of "marriage" tests) to substantiate the performance of the entire system.

The development plan for components of the guidance system is discussed as follows.

### A. RADAR ALTIMETER

A detailed technical description of the altimeter is given elsewhere in this report, suffice it to say here that the techniques to be used in this instrument are well established, although the specific instrument

does not exist. Our design concept for the altimeter has been shown to be extremely simple so that it can be engineered well within the framework of today's state of the art. In addition to being utilized as an altimeter in this system, it can also be used with only slight modifications and great effectiveness as a part of a satellite rendezvous guidance system.

Figure VII-1 shows our plan for bringing the altimeter into being. The RF plumbing and the magnetron are components which can be purchased from today's catalogs. However, the antenna IF strips, AFC circuitry, and modulator must be designed (Fig. VII-1) so that basic engineering of the altimeter can be completed in 8 months. As pointed out previously, the mission time of 1 year makes high reliability one of the pivotal issues in determining the system design. Therefore, in engineering the altimeter, an extensive life testing program utilizing altimeter breadboard elements, built as closely as possible to the final design of the altimeter, is planned (this program spans 6 months). Construction of the flyable prototype will begin in the latter portion of the life testing program but obviously cannot be finished until after the lifetest program is completed. Thus we estimate that a flyable prototype can be available at the end of 18 months.

## B. COMPUTER

Digital computers of the type needed in this guidance system are currently being engineered on several programs. Of course, the logical design of these computers must be rearranged to fit this particular problem, but this presents no great difficulty. In the computer, it is desirable to avoid using rotating magnetic drum memories, therefore, solid-state memory techniques will be used to enhance reliability and minimize unwanted torques on the satellite. Several computer developments are now under way which, with some modifications, will fulfill our needs. Since the development of this computer is already under way, modifying it to suit his application should shorten the computer lead time by approximately 6 months. Therefore, in formulating this development plan, a span time of 21 months is assumed for the computer.

## C. IR HORIZON SCANNER

The IR (infrared) horizon scanners are available from several sources in this country, practically on an "off-the-shelf" basis. For instance, the IR horizon scanner described in Section IV-B is available within 4 to 4-1/2 months after placement of an order. In order to provide time for possible minor design changes, 6 months are allowed in this development plan for the IR horizon scanner.

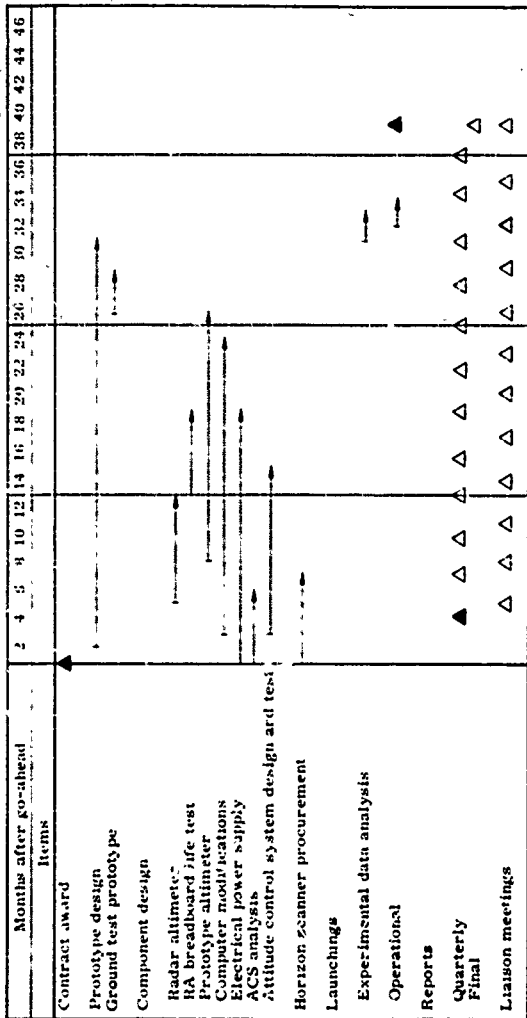


Fig. VII-1. Satellite Synchronization Development Plan

#### D. ELECTRICAL POWER SUPPLY

As described previously in Section IV, either a solar cell system or an isotopic power supply is recommended for this satellite guidance system. Of the two systems considered, the solar cell system is most attractive because of its immediate availability and good performance. Therefore, since a minimum of time is required to incorporate such a system, no development of components will be required.

The isotopic power supply uses the heat output of an isotope block to heat the hot junction of a thermoelectric material (such as lead telluride) which in turn converts the applied heat to electrical power. On the basis of the previous experience of The Martin Company in designing, building and testing isotopic power supplies, a power supply using a Strontium-90 heat source and lead telluride thermoelectric elements is characterized by a weight of 1 to 1-1/2 watts/lb and can be made available in approximately 1-1/2 years. Once this type of power supply is loaded with the radioactive isotope, it is necessary to shield against the high energy gamma radiation emitted due to the bremsstrahlung effect.

Other man-made elements are becoming available which will minimize the radiation problem. For example, the power supply could be designed around Curium-242, which emits alpha radiation and is much easier to shield against. By the time Curium-242 becomes available in the next 2 or 3 years, additional progress can be expected from current research in thermoelectric materials. Therefore, a power supply could be designed (weighing about 2 to 3 watts/lb) without presenting too difficult a radiation shielding problem.

If, in the final engineering of this guidance system, the recommended solar cell system is used, only a nominal time of 18 months (Fig. VII-1) will be required to select, procure and test the proper cells. On the other hand, if the isotopic power system is used, then a lead time of approximately 24 months would be considered necessary.

#### E. ATTITUDE CONTROL SYSTEM

The pulse-modulated attitude control system recommended in this report is an extension of many years of missile and space vehicle autopilot development work at The Martin Company. Hardware work is already under way on the electronic components which can be used in this system; therefore, the major problems in the control system are easily spotlighted.

The foremost of these problems is high reliability and closely related is minimization of the fuel required to execute the commands of the various sensors.

The attack of the reliability problem requires a two-pronged engineering effort. A detailed system stability analysis should be undertaken to minimize the number of operations of the control system. It is hoped that this can be accomplished by operating the attitude control system only during the period just prior to and during the taking of the altitude measurements rather than attempting to operate continuously for the 1-year mission.

Secondly, the effect of our concept of designing a fuel system to be used as a hypergolic bipropellant system for orbital corrections and also as a monopropellant catalytic system for attitude controls should be investigated both analytically and experimentally.

A 4- to 5-month analysis program is required for the system analysis work described above, and the design and test work necessary to evaluate the thrust-producing system will probably span 9 to 12 months. The bulk of this period is required to experimentally evaluate the performance of presently available nozzles in such a system and incorporate possible changes. This phase of the program may uncover unforeseen problems since, by way of comparison, we are talking of a system which will be called on for upward of 800 vacuum starts and, in today's state of the art, the only available restartable engine is designed for two altitude starts. Therefore, this development plan includes an allowance of 18 months to fully develop and build the prototype attitude control system.



## VIII. MISSION ANALYSIS

Previous sections of this report have shown that a hypothetical mission of one year, for the type of guidance and control system being considered, would be difficult to achieve, largely due to problems of a reliability nature. It is apparent, however, that this system could be utilized to great advantage on other missions. Consider a manned satellite system in which the ultimate objective may be to: (a) recover the man from orbit, (b) recover reconnaissance data (such as exposed film) from orbit and (c) conduct bombardment from an orbital position. A central problem in all of these missions is the maintenance of very accurate orbital exit conditions. In particular, the attitude control problems at the time of exit from orbit are severe. Figures VIII-1 through VIII-9, taken from work previously completed under this contract (Ref. VIII-1), illustrate the errors incurred on an orbital exit maneuver to 300,000 ft as a result of errors in attitude, velocity and altitude at the time of orbit exit. Attitude errors at the time of exit from orbit are seen to be a potential source of large dispersions in impact range.

The error coefficients shown apply only to deorbit flight paths resulting in very small re-entry flight path angles. Relatively small re-entry flight path angles are compatible with the requirements for reasonable values of heating and g loading of a typical, manned, re-entry vehicle.

The definitions and symbols used in Figs. VIII-1 through VIII-9, Errors in Re-entry Parameters, are as follows:

All orbital departures = assumed to start from circular orbit and  $0^\circ$  flight path angle

Thrust-to-weight ratio = constant = 0.5

$t_{sp}$  = 300 sec

$\Delta V$  = retrorocket thrust, contained in orbital plane and rotated clockwise with respect to velocity vector by  $180^\circ$  ( $\delta = 180^\circ$ )

$h_1$  = initial altitude

$v_1$  = initial velocity

$S$  = retrorocket mass ratio.

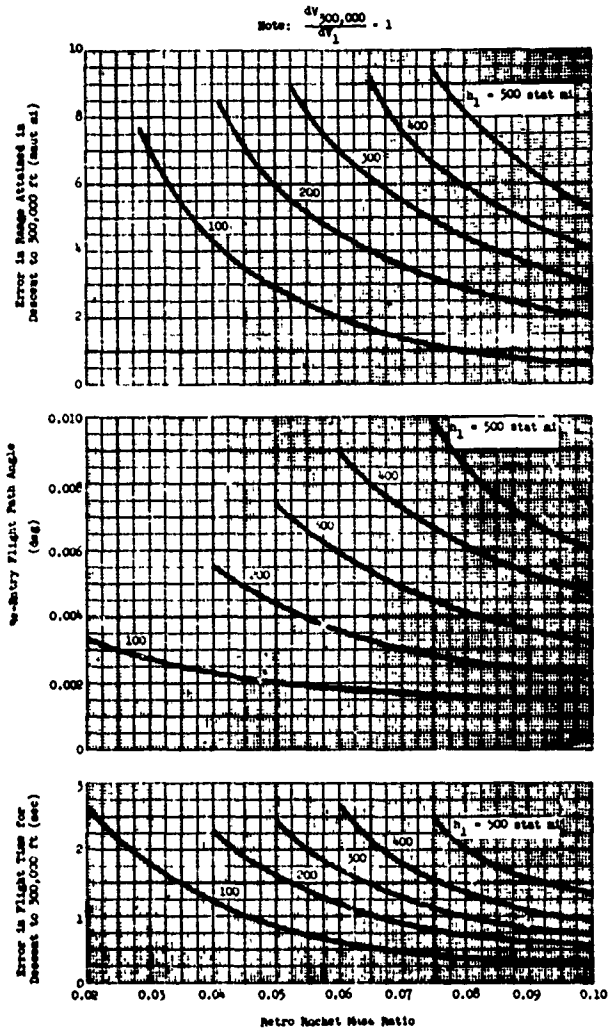


Fig. VIII-1. Errors in Re-Entry Parameters due to a 1-fps Error in Vehicle Velocity Prior to Firing a Retro Rocket ( $\delta = 180^\circ$ ,  $\gamma_1 = 0^\circ$ ,  $T/W_0 = 0.5$ ,  $I_{sp} = 300$  sec)

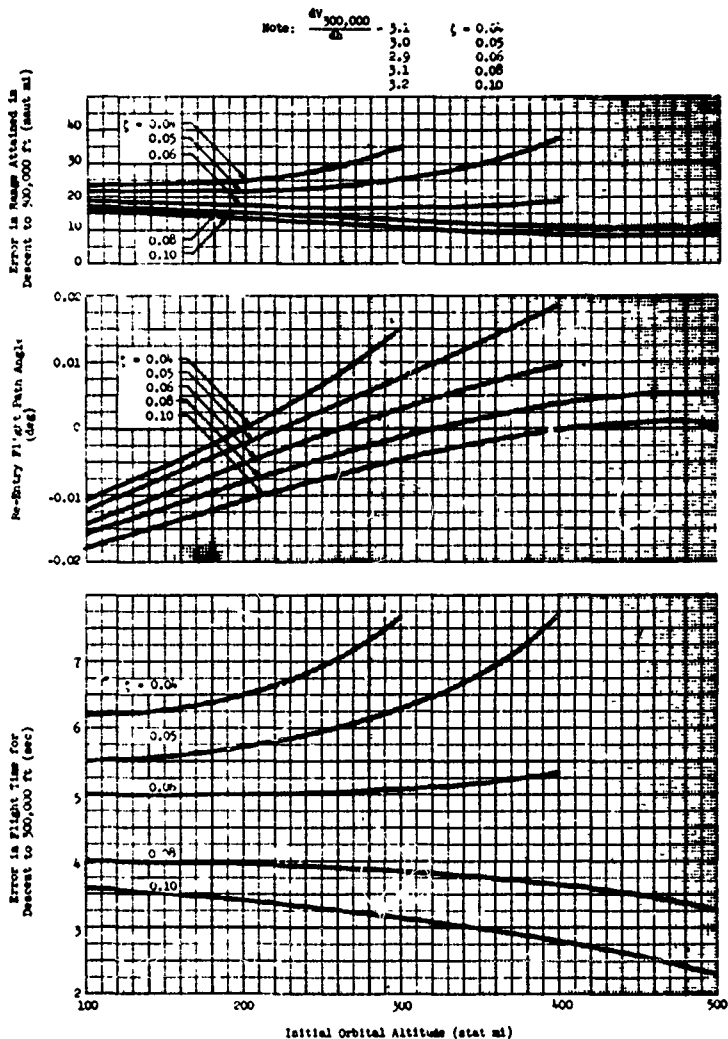


Fig. VIII-2. Errors in Re-Entry Parameters due to a 1-stat mi Error in Altitude Prior to Firing a Retro Rocket ( $V_1 = V_C$ ,  $\delta = 180^\circ$ ,  $\gamma_1 = 0^\circ$ ,  $T/W_0 = 0.5$ ,  $I_{a1} = 300$  sec)

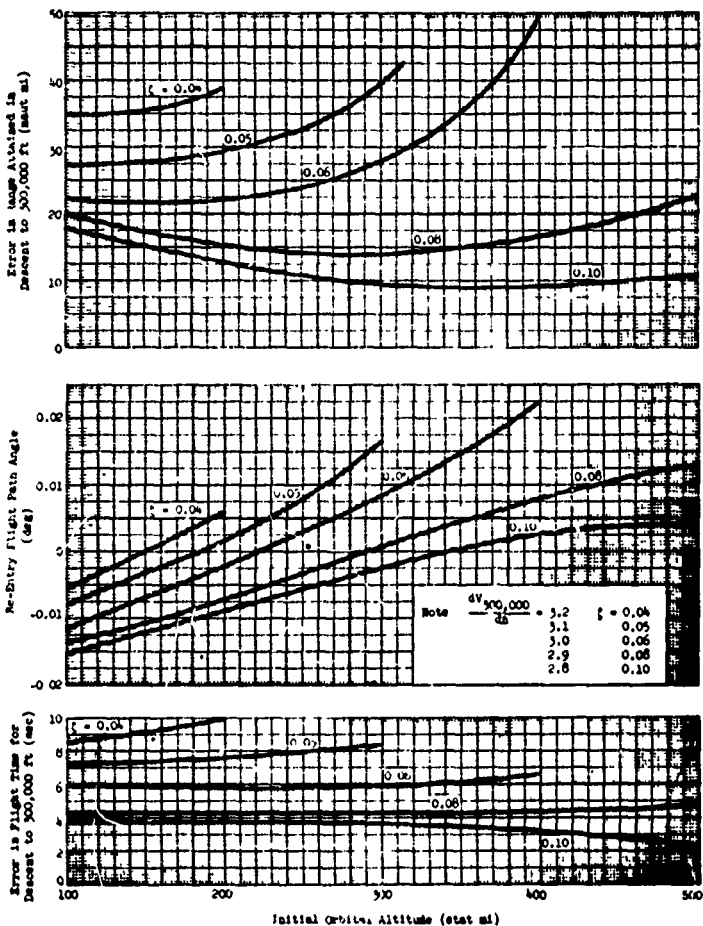


Fig. VIII-3. Errors in Re-Entry Parameters due to a 1-stat mi Error in Altitude Prior to Firing a Retro Rocket ( $V_1 = V_C + 100$  fps,  $\delta = 180^\circ$ ,  $\gamma_1 = 0^\circ$ ,  $T/W_0 = 0.5$ ,  $t_{sp} = 300$  sec)

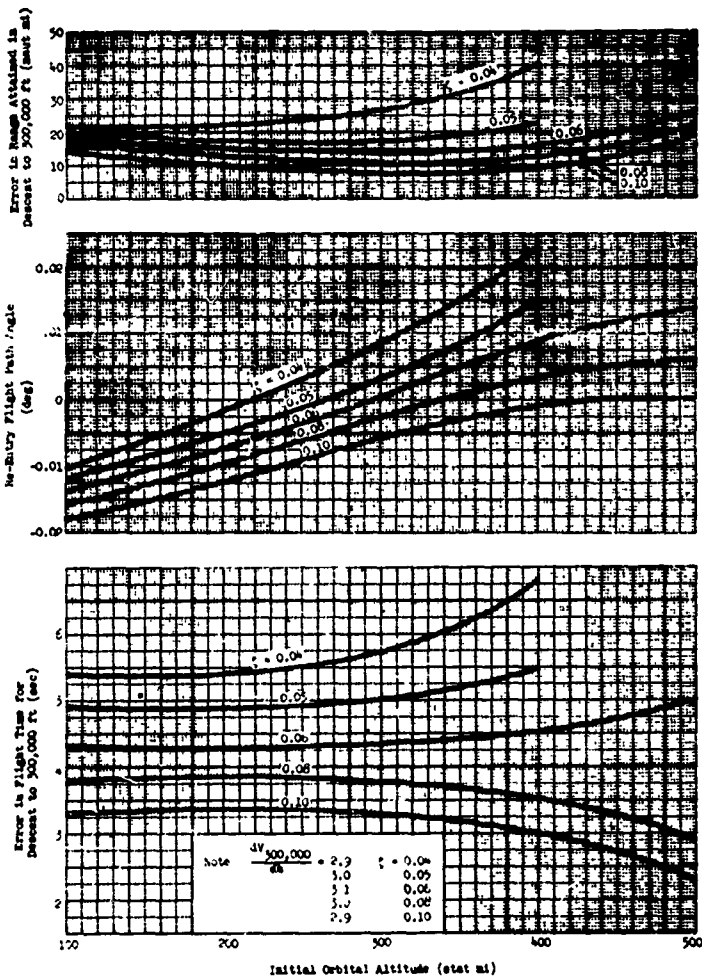


Fig. VIII-4. Errors in Re-Entry Parameters due to a 1-stat mi Error in the Altitude Prior to Firing a Retro Rocket ( $V_1 = V_C - 100$  fps,  $\delta = 180^\circ$ ,  $\gamma_1 = 0^\circ$ ,  $T/W_0 = 0.5$ ,  $t_{sp} = 300$  sec)

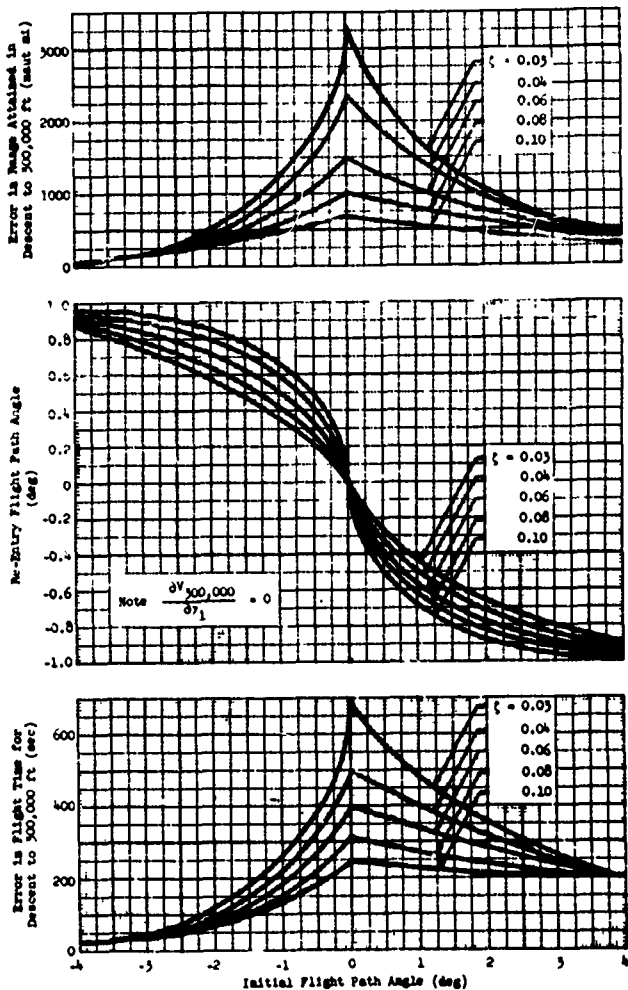


Fig. VIII-5. Errors in Re-Entry Parameters due to a 1-deg Error in Initial Flight Path Angle ( $h_1 = 100$  stat mi,  $\delta = 180^\circ$ ,  $T/W_0 = 0.5$ ,  $I_{sp} = 300$  sec,  $V_1 = V_C$ )

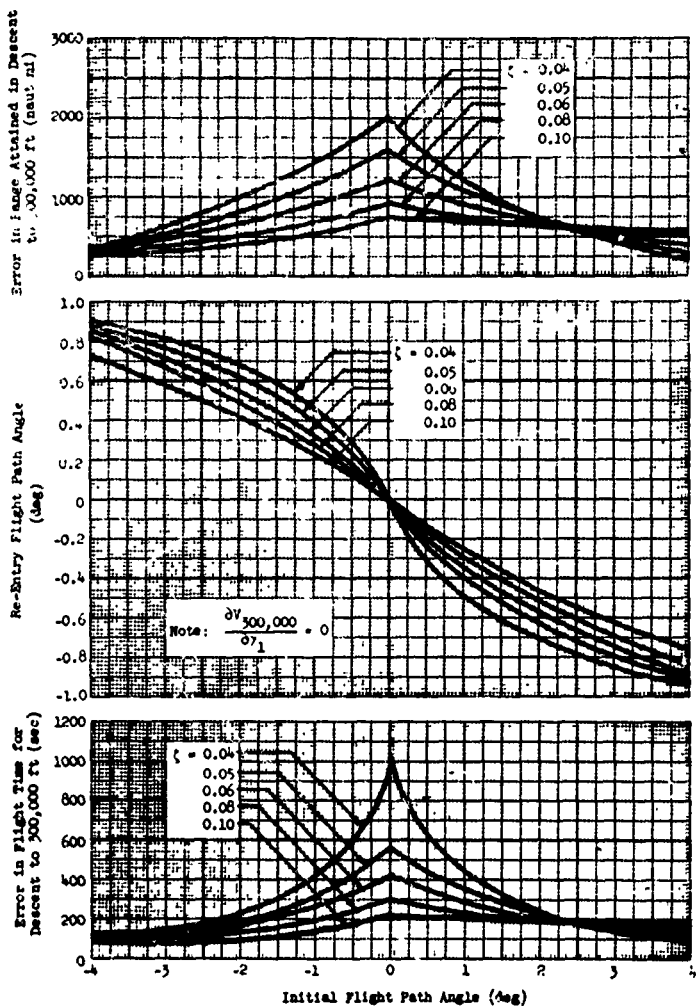


Fig. VIII-6. Errors in Re-Entry Parameters due to a 1-deg Error in Initial Flight Path Angle ( $h_1 = 200$  stat mi,  $\delta = 180^\circ$ ,  $T/W_0 = 0.5$ ,  $I_{sp} = 300$  sec,  $V_1 = V_C$ )

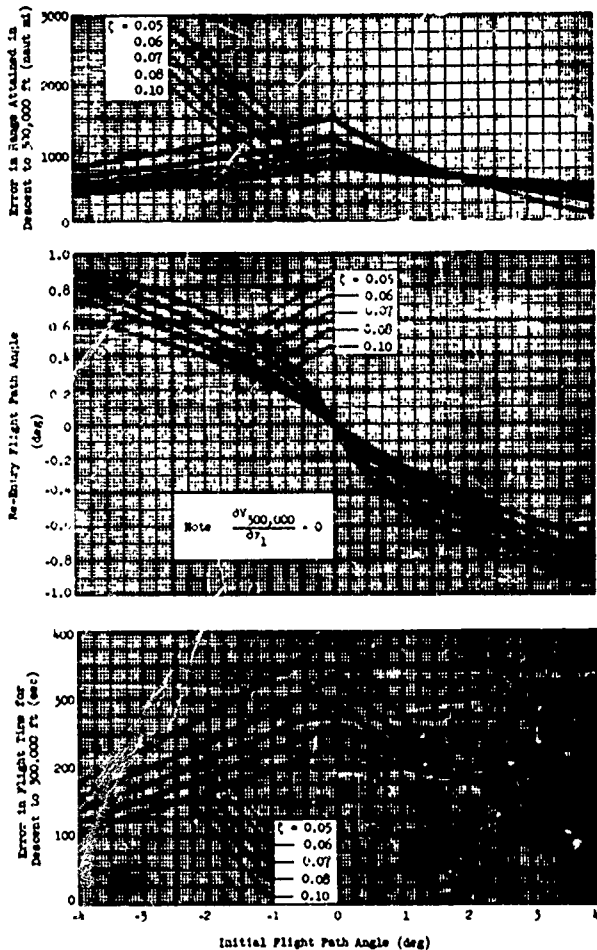


Fig. VIII-7. Errors in Re-Entry Parameters due to a 1-deg Error in Initial Flight Path Angle ( $h_1 = 300$  stat mi,  $\delta = 180^\circ$ ,  $T/W_0 = 0.5$ ,  $I_{sp} = 300$  sec,  $V_1 = V_C$ )

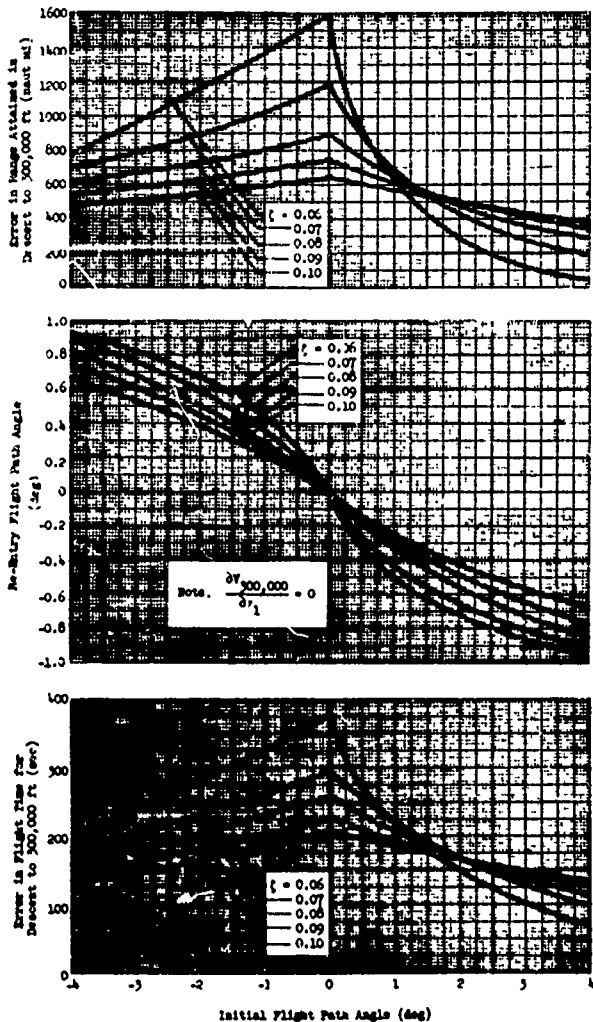


Fig. VIII-8. Errors in Re-Entry Parameters due to a 1-deg Error in Initial Flight Path Angle ( $h_1 = 400$  stat mi,  $\delta = 180^\circ$ ,  $T/W_0 = 0.5$ ,  $I_{sp} = 300$  sec,  $V_1 = V_C$ )

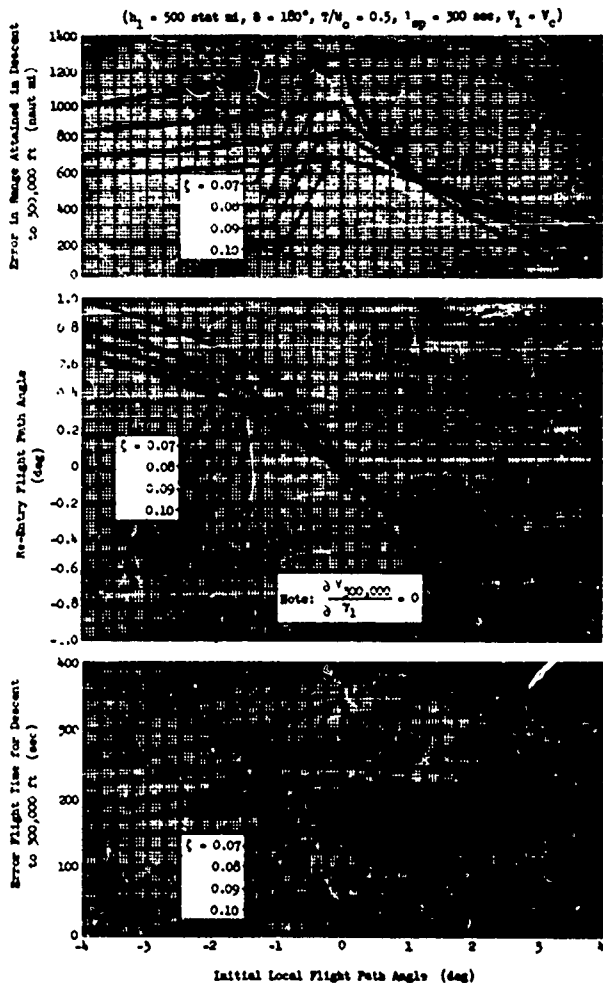


Fig. VIII-9. Errors in Re-Entry Parameters due to a 1-deg Error in Initial Flight Path Angle ( $h_1 = 500$  stat mi,  $\delta = 180^\circ$ ,  $T/W_0 = 0.5$ ,

$$t_{sp} = 300 \text{ sec, } V_1 = V_C)$$

A completely self-contained guidance and control system offers numerous advantages in missions of the type (a), (b) and (c) mentioned previously. With manned supervision of the system available, it should be possible to greatly improve the overall system reliability because of the following.

- (1) Reliability considerations for those subsystems which must be continuously used in the unmanned, automatic system are greatly modified. Continuous tracking of certain stars, for example, would not be necessary, since these target stars could be acquired at any time they are needed.
- (2) The useful life of these systems which must remain on during the entire mission can be greatly extended by the application of very simple concepts of "preventive" maintenance (Ref. VIII-2).

The self-contained guidance and control system error analysis presented earlier indicates that more precise control of orbital exit conditions is possible for type (a), (b) and (c) missions. In particular, the direction of the local vertical could be established with more precision than is presently possible using infrared techniques to establish this direction. The geometry of the problem is shown in Fig. VIII-10 for a simple two-dimensional case and at some projected instant of time of departure from the orbit. Prior to this time, the orbital elements have been computed so that the radius vector direction angles can be established with respect to the orthogonal inertial coordinate system. Referring to Fig. VIII-10:

- (1) The  $\theta_1$  is known in advance and is equal to the angle between the equatorial plane and the star line of position. The value of  $\theta_1$  is available from a star catalog.
- (2) The  $\theta_2$ ,  $\theta_3$  and  $\theta_4$  can be predicted in advance to an accuracy which depends on future predicted position accuracy (i.e.,  $\Delta b$ ). If the predicted position error is, for example, 2 naut mi, then  $\Delta \theta$  is  $\frac{2}{3441 + 500}$  rad for an orbit altitude of 500 naut mi. Therefore  $\theta_2$ ,  $\theta_3$  and  $\theta_4$  may be predicted quite accurately. The flight path angle,  $\alpha$ , will be small if the orbit is near circular. The maximum value of  $\alpha$  occurs between apogee and perigee at the position shown in Fig. VIII-11. Maximum flight path angle as a function of orbit eccentricity is also shown.

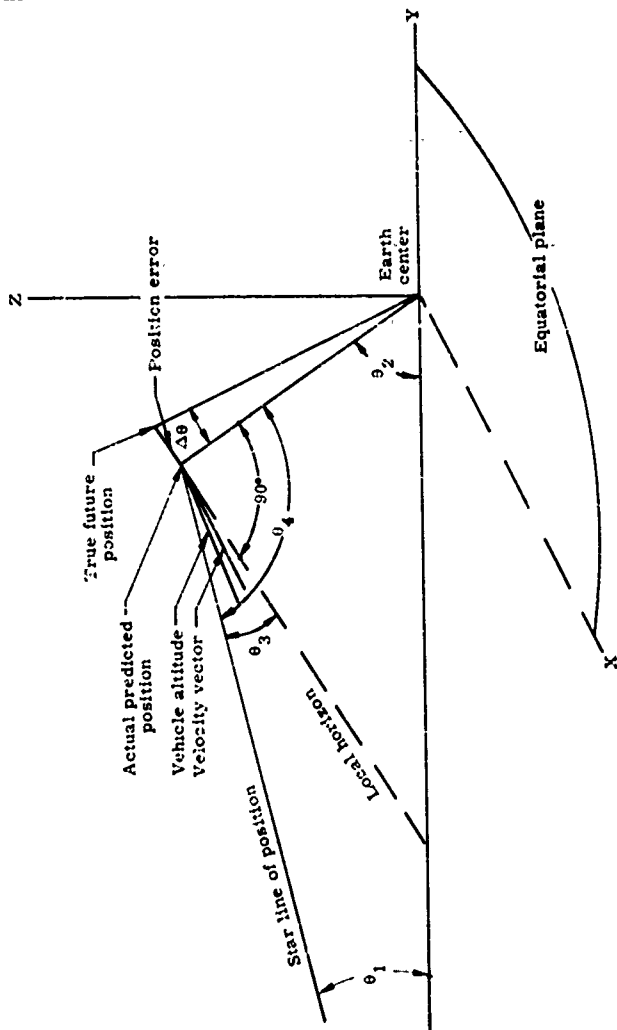


Fig. VIII-10. Prediction of Direction of the Vertical

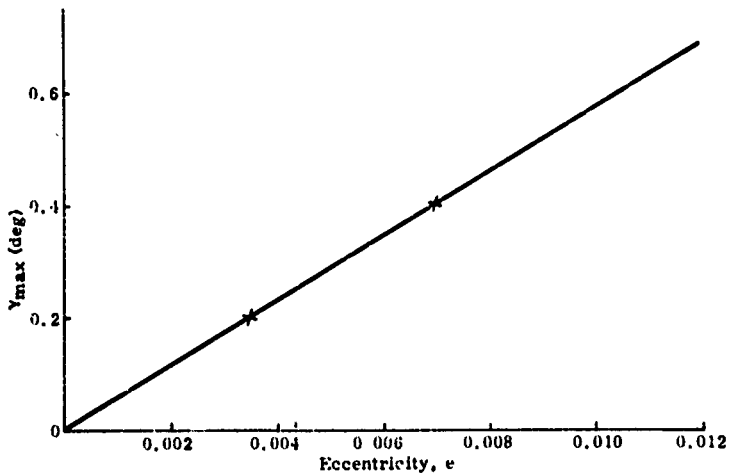
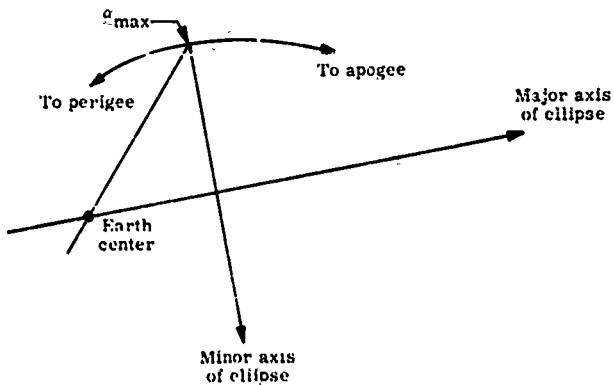


Fig. VIII-11. Flight Path Angle Relations

To summarize, then, a typical mission might be executed as follows:

- (1) The orbital elements have been computed and some future time has been established as the time to depart from the completed orbit. The departure is for the purpose of rendezvous with some preselected impact point at the 300,000 ft altitude level. The location of this point determines the time of exit from orbit, hence, in general, the departure will not occur at apogee or perigee ( $\alpha \neq 0^\circ$  at apogee and perigee). The value of  $\alpha$  at orbital exit is given by.

$$\tan \alpha = \pm \frac{e \sin \delta}{1 - e \cos \delta}$$

where

- e = orbit eccentricity
  - $\delta$  = angular distance from apogee at the time of exit
  - $\pm$  = clockwise or counterclockwise motion, respectively
- (2) If prior orbital maneuvering has resulted in a near circular orbit, then e is very small. For an apogee and perigee difference of 50 naut mi, for example, the eccentricity is given by:

$$e = \frac{A - P}{A + P} = 0.0053$$

where

- A = radial distance from earth center at apogee, e.g., 3991 naut mi
  - P = radial distance from earth center at perigee, e.g., 3941 naut mi.
- (3) The vehicle is rotated in the pitch plane so that the pitch axis and the local horizon (Fig. VIII-10) are colinear at the time orbital exit is to be initiated. In addition, and prior to

initiation of orbital exit, a radial thrust adjusts the velocity vector (from knowledge of the predicted flight path angle at orbital exit) so that the velocity vector is along the local horizontal at the time the retrorocket is fired (i.e., the velocity at the point of exit from orbit is adjusted for the characteristic velocity of a circular orbit at the orbital exit altitude). Let Fig. VIII-12 represent the position of the vehicle sometime after the star line of position has been acquired. As in the previous considerations,  $\theta_1$  is known from the star catalog and  $\theta_2$  and  $\theta_4$  can be predicted with a precision of a few hundredths of a second of arc. As shown in Fig. VIII-12, the angle  $\theta_6$  can also be predicted with this same precision. With respect to the inertial reference frame, the flight path angle can be expressed as

$$\alpha = \tan^{-1} \frac{\dot{Z}}{\dot{Y}} = \frac{V_T \cos \alpha \cos \theta_6}{V_T \sin \alpha \sin \theta_6}$$

$$\tan \alpha = \cot \alpha \cot \theta_6$$

and

$$\tan \alpha = (\cot \theta_6)^{1/2}$$

To first order the error in  $\alpha$  due to error in  $\theta_6$  is then given by

$$\Delta \alpha = \frac{\cos^2 \alpha \Delta \theta_6}{2 (\cot \alpha)^{1/2}}$$

and for a near circular orbit (i.e., small  $\alpha$ ), this error is quite small.

This brief analysis has shown that it is possible to align the vehicle pitch axis and the velocity vector to the local horizontal with considerable precision in preparation for an orbital exit maneuver. It is to be understood, however, that such orbital exit conditions are not optimum from an accuracy viewpoint. The reader is referred to earlier work completed (Ref. VIII-1) under this contract for a thorough treatment of this problem.

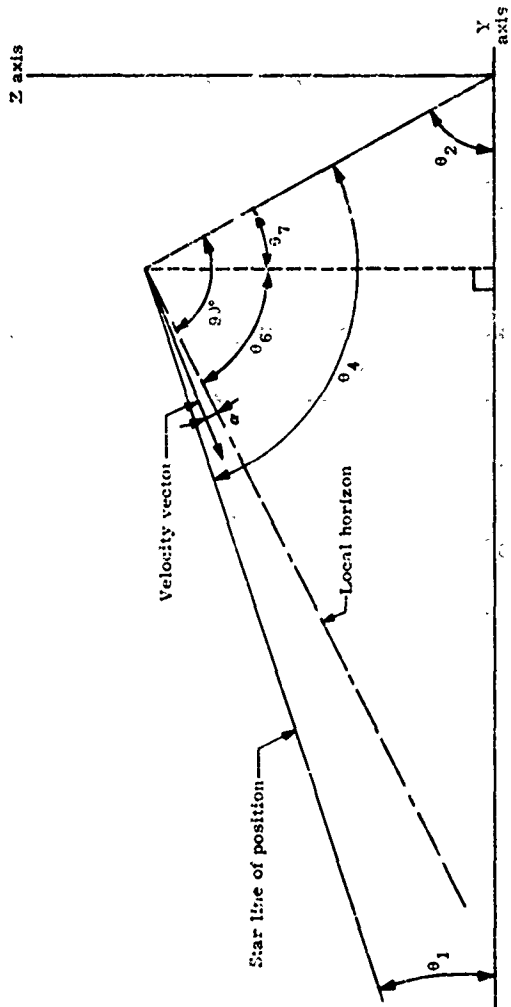


Fig. VIII-12. Flight Path Angle Computation Geometry

## IX. CONCLUSIONS AND RECOMMENDATIONS

The findings of this final report indicate that it is feasible to implement the design of a completely self-contained guidance and control system using state-of-the-art hardware. The accuracy of such a system would be such as to permit predicting future position of the vehicle to approximately 1 naut mi neglecting perturbations on the orbit due to earth model effects. The reliability of the system has been found unacceptable (with reference to a one-year hypothetical mission in which system operation is completely automatic), and it is concluded that the hypothetical mission and the system are incompatible (however, the system can be used to advantage on alternate missions).

It is recommended that the present effort be amended to include a detailed study of the following:

- (1) Application of the self-contained guidance and control system to manned, earth satellite weapon systems currently in the R&D phase of Air Force development. It is expected that manned supervision of the system will greatly enhance overall system operation.
- (2) Prototype development of actual hardware, consistent in time with current R&D programs in the Air Force, should be initiated as early as possible.
- (3) The mathematical model used to evaluate the system accuracy should be modified to include:
  - (a) A more accurate earth model.
  - (b) The statistical implications of atmospheric anomalies.

With reference to (1) above and Section VIII concerning mission analysis, it appears that the system would have an important application in orbital exit missions. Precise attitude control at the time of exit from orbit, for example, will have important applications in manned space flight in the years to come. It is recommended that this system be explored for possible application on such missions as early as possible.

## X. REFERENCES

All references contained in this study are listed according to chapter designation.

- I. (none)
- II. (none)
- III. (none)
- IV-1. Atmospheric Absorption of 10 to 100 kmc Radiation; Summary, and Bibliography to 1961 by E. S. Rosenblum, The Microwave Journal, March 1961.
- IV-2. Back-Scattering from Water and Land at Centimeter and Millimeter Wave Lengths by C. R. Grant and B. S. Yaplee, Proceedings of the IRE, July 1957.
- IV-3. Back-Scattering Characteristics of the Sea in the Region from 10 to 50 kmc by J. C. Wiltse, S. P. Schleinger and C. M. Johnson, Proceedings of the IRE, February 1957.
- IV-4. Pulse Generators by G. N. Glasoe and J. V. Lebacqz, MIT Radiation Lab Series 5, McGraw-Hill Book Company, 1948.
- IV-5. Solid State Modulator for a Two-Repetition-Rate, Two-Pulse-Width Surveillance Radar by Dr. B. M. Wolfram, Proceedings of the Sixth Symposium on Hydrogen Thyatrons and Modulators, May 17, 18 and 19, 1960.
- IV-6. Microwave Receivers, S. Van Voorheis, MIT Radiation Lab Series, Vol. 23, McGraw-Hill Book Company, 1948.
- IV-7. Microwave Mixers, R. V. Pound and E. Durand, MIT Radiation Lab Series, Vol. 16.
- IV-8. Reconnaissance Satellite Antennas, R. B. MacAskill, Hallicrafters Corp., Electronic Industries, April 1961.
- IV-9. Automatic Gain Control of Transistor Amplifiers, W. F. Chow and A. P. Stern, Proc. IRE, Vol. 43, p 1119, September 1955.
- IV-10. A Review of the Current Status of Satellite Attitude Control, Roberson. Paper to IAS-ARS at San Diego, California, 5 August 1958.

- IV-11. Comparison of Some Actuation Methods for Attitude Control, W. Haeussermann. Paper presented at Manned Space Station Symposium, IAS, Los Angeles, California, April 20-22, 1960.
- IV-12. Satellite Synchronization Study, Final Report No. ER 11018-3, The Martin Company.
- IV-13. Rocket Systems for Attitude Control, Willard D. Sancrainte and David C. Scheavone. Paper--ARS Controllable Satellite Conference, MIT, April 30 - May 1, 1959.
- IV-14. Orbital Guidance Systems Study, ER 11430-3 dated November 1960; The Martin Company. (Confidential)
- IV-15. Attitude Control Rocket Requirements for Space Vehicles, Charles N. Tripp and Warren P. Boardman.
- IV-16. Minimizing Reaction Mass Expenditure During Limit Cycling in a Space Vehicle On-Off Attitude Control System, E. Crum and O. Kaste, The Martin Company, Baltimore, February 1960.
- IV-17. On-Off Control System for Attitude Stabilization of a Space Vehicle, Josef S. Pistiner, ARS Journal, April 1959.
- V. (none)
- VI-1. Verbal information from Sylvania Sales Representative re Tube 5789.
- VI-2. Component Part Failure Rates Associated with Installation Environment, Pub. No. M-60-47, The Martin Company (Denver).
- VI-3. Hydrogen/Fluorine Propulsion System, Report S-128023, Bell Aerosystems Company, 31 January 1961.
- VI-4. The Martin Company Nuclear Division Internal Report MND-2570, 12 May 1961.
- VI-5. Advanced Guidance System for Earth Satellite Weapon System, Internal Report, The Martin Company, Denver Space Technology Section.
- VII. (none)
- VIII-1. Dynamic Analysis and Design Performance Requirements for Satellite Vehicle Guidance Systems, ER 10470-6, The Martin Company, dated 31 January 1959.

VIII-2. Global Surveillance System Final Report, Phase II, Volume 2,  
Human Factors, 61 WWR-1672, ASD-TR-No. 61-19(2), ER 11649-2,  
The Martin Company, dated 31 June 1961.

IX. (none)

## DISTRIBUTION LIST

Commander  
Wright Air Development Division  
Wright-Patterson Air Force Base  
Ohio

Attn: WWRNGC-2 Captain May  
(3 copies)

Attn: WWRNGE-2 Mr. Coombs  
Attn: WWRNGC-3 Mr. Moothart  
Attn: WWRMCM Mr. Woodcock  
Attn: WWRPSG Mr. Xenakis  
Attn: WWDSI Library

Goodyear Aircraft Corporation  
1210 Massillon Road  
Akron 15, Ohio  
Attn: Mr. W. Steiner  
Dept 475G

Radiation, Inc.  
P. O. Box 6904  
Orlando, Florida  
Attn: Mr. P. Button

Mass. Institute of Technology  
Instrumentation Laboratory  
68 Albany Street  
Cambridge, Massachusetts  
Attn: Mr. N. Sears

Institute of Technology  
Wright-Patterson Air Force Base  
Ohio  
Attn: Library

Commander  
ARDC Office, USAF  
Naval Research Laboratory  
Washington, D. C.

Air Technical Intelligence Center  
Wright-Patterson AFB, Ohio  
Attn: AFCIN-4E1B

Commander  
Headquarters ARDC  
Andrews Air Force Base  
Washington 25, D. C.  
Attn: RDRWGG, Capt. Speuker

Commander  
Air Force Ballistic Missile Division  
Air Force Unit Post Office  
Los Angeles 45, California  
Attn: WDTG Lt. Col. F. M. Box  
Attn: WDWWS Lt. Col. J. Brigham

Commander  
Wright Air Development Division  
Los Angeles Office  
Los Angeles 45, California  
Attn: WWDML Capt. Stephenson

Commander  
Air Force Missile Development Center  
Holloman AFB, New Mexico  
Attn: MDWG, Mr. Guenther

Commander  
Air Force Command and Control  
Development Division  
Laurence G. Hanscom Field  
Bedford, Massachusetts  
Attn: Library

Aeronautical Research Laboratory  
AF Research Division  
Attn: RRIO Mr. Callan  
Wright-Patterson AFB, Ohio

Commander  
Rome Air Development Center  
Griffiss AFB, New York  
Attn: RCKNN

The Rand Corporation  
1700 Main Street  
Santa Monica, California

NASA  
1520 H Street, N.W.  
Washington 25, D. C.  
Attn: J. Crocker, Code DA

**DISTRIBUTION LIST (continued)**

**NASA  
Lewis Research Center  
2100 Brookpark Road  
Cleveland, Ohio  
Attn: H. Heppler**

**Jet Propulsion Laboratory  
4800 Oak Grove Drive  
Pasadena, California  
Attn: H. A. Curtis**

**Commander (all remaining copies)  
ASTIA  
Arlington Hall Station  
Arlington 12, Virginia**

